Technische Universität München
Fakultät für Maschinenwesen
Institut für Luft- und Raumfahrt
Lehrstuhl für Leichtbau

Design optimization of lightweight space-frame structures considering crashworthiness and parameter uncertainty

Erich Josef Wehrle

Vollständiger Abdruck der von der Fakultät für Maschinenwesen der Technischen Universität München zur Erlangung des akademischen Grades eines

Doktor-Ingenieurs

genehmigten Dissertation.

Vorsitzender:		Univ.-Prof. Dr. Phaedon-Stelios Koutsourelakis
Prüfer der Dissertation:	1.	Univ.-Prof. Dr.-Ing. Horst Baier
	2.	Univ.-Prof. Dr.-Ing. habil. Fabian Duddeck

Die Dissertation wurde am 18. März 2015 bei der Technischen Universität München eingereicht und durch die Fakultät für Maschinenwesen am 29. Juni 2015 angenommen.

ABSTRACT

Mechanical structures undergoing crashworthiness loads can behave very sensitive with respect to uncertainty of loading, geometry and material parameters. In this work, techniques are presented and investigated for design optimization of lightweight space-frame structures considering structural mechanics, including crashworthiness and uncertainty using fuzzy methods. Complementary to the developed optimization approaches, shadow uncertainties and shadow uncertainty prices—based on the idea of Lagrangian multipliers as shadow prices—are derived and applied to post-process results of both uncertainty analyses and optimizations under uncertainty. Through these measures, the effect of uncertain parameters can be estimated on system responses and the optimization objective. As a demonstrator for the methods developed here, a space-frame body-in-white, the Lightweight Extruded Aluminum Frame (LEAF), and its design philosophy will be introduced. An efficient fuzzy analysis method based on α-level optimization was developed and implemented. Further, the feasibility of analytical design sensitivities with respect to uncertain and design variables of transient, nonlinear structural-mechanical analysis is investigated on an academic example. The ability to use surrogate modeling in optimization under uncertainty of crash structures with fuzzy methods to increase computational efficiency is also shown.

KURZFASSUNG

Mechanische Strukturen unter Aufpralllasten können sich sehr empfindlich gegenüber Unsicherheiten von Last-, Geometrie-, und Werkstoffparametern verhalten. Im Rahmen dieser Arbeit werden Techniken zur Entwurfsoptimierung leichter Rohrrahmenstrukturen unter Betrachtung von Strukturmechanik einschließlich Aufprallsicherheit und Unsicherheiten mittels unscharfer Methoden vorgestellt und untersucht. Ergänzend zu den entwickelten Optimierungsansätzen werden Schattenunsicherheiten und Schattenunsicherheitspreise – basierend auf der Idee der Lagrange'schen Multiplikatoren als Schattenpreise – hergeleitet und auf Ergebnisse aus Unsicherheitsanalysen und aus Optimierungen unter Unsicherheit angewandt. Hierdurch wird der Einfluss unsicherer Parameter auf Systemantworten und das Optimierungsziel abgeschätzt. Als Demonstrator für die entwickelten Methoden wird die Rohrrahmenkarosserie, der Leichte Extrudierte Aluminium-Fahrzeugrahmen (LEAF) und dessen Konstruktionsphilosophie präsentiert. Eine effiziente Methode für unscharfe Analyse wurde beruhend auf der α-Niveau-Optimierung entwickelt und implementiert. Des Weiteren wurde die Machbarkeit analytischer Entwurfssensitivitäten bezüglich Unsicherheits- und Entwurfsvariablen in transienten nichtlinearen strukturmechanischen Analysen anhand eines akademischen Beispieles untersucht. Um die Recheneffizienz zu erhöhen wird zudem die Anwendung von Ersatzmodellen bei der Optimierung von Aufprallstrukturen unter Unsicherheiten mithilfe unscharfer Methoden aufgezeigt.

ACKNOWLEDGMENTS

The present dissertation and the research within were conducted during my time as Research Assistant at the Institute for Lightweight Structures of the Technical University of Munich from October 13, 2008 until October 12, 2014.

First, I would like to thank Prof. Dr. Horst Baier for the opportunity to carry out research at his chair and his patience to allow my research to go in new directions. I would also like to thank the members of my examination committee: the chair Prof. Dr. Phaedon-Stelios Koutsourelakis and the second examiner Prof. Dr. Fabian Duddeck.

For the fruitful cooperation, I would like to express my gratitude to all my colleagues at the Institute of Lightweight Structures. Through their insights and support, I was able to further my knowledge greatly. Especially my appreciation goes to Dr. Martin Huber for his advisement of my semester and master's theses as well as his recommendation that allowed me to continue my research at the chair; Dr. Qian Xu for her assistance in teaching as well as cooperation in approximation models in optimization; Alexander Morasch for support in his material modeling and testing; Dr. Jan Both for project cooperation and insights on composite materials and design; Dr. Max Wedekind for his constant readiness to explain and discuss structural-mechanical aspects, Ögmundur Petersson for discussions in the theoretical side of optimization as well as cooperation in teaching; Markus Schatz for discussion in optimization and research cooperation in algorithm-based material selection; Gunar Reinicke for his assistance in dynamical aspects and for the coffee; Luiz da Rocha-Schmidt for his hardware and software assistance as well as his work for me as a student; and Dr. Leri Datashvili for technical discussions, often late into the evening.

The workshop at the Institute for Lightweight Structures assisted by prototype construction and testing, especially Bernhard Lerch und Josip Stokic. The tests that were performed with their support contributed to my structural-mechanical understanding greatly.

To my many students that I had the honor to advise: I hope they were able to learn as much from me as I did from them. Especially, I would like to thank Michael Tischer, Florian Wachter, Simon Rudolph, Georg Siroky, Mohammad Iqbal, David Binder, Florian Urban, and Franz Fellner for their extraordinary dedication, long hours and hard work.

My friends and family I thank for their support, despite my neglect over the last years during this research. Above all, I would like to thank my parents for their continued support throughout my education, for they taught me that learning did not start or end with school.

Lastly, I would also like to thank Dr. Jan Both, Alexander Morasch, Markus Schatz, Prof. Dr. Evelyn Walters, and my brother, Cpt. (ret.) Adam Wehrle for proofreading this document, though none of the errors, omissions, solecisms that should remain are their responsibility.

Munich, Winter 2014–15 Erich Wehrle

Indem wir vom Wahrscheinlichen sprechen, ist ja das Unwahrscheinliche immer schon inbegriffen und zwar als Grenzfall des Möglichen, und wenn es einmal eintritt, das Unwahrscheinliche, so besteht für unsereinen keinerlei Grund zur Verwunderung, zur Erschütterung, zur Mystifikation.

Max Frisch in *Homo Faber*

CONTENTS

LIST OF FIGURES

LIST OF TABLES

LIST OF LISTINGS

NOMENCLATURE

$\mathcal{A}$	Fuzzy uncertainty, i.e. area of fuzzy number
$\hat{\mathcal{A}}$	Normalized fuzzy uncertainty, i.e. normalized area of fuzzy number
$\boldsymbol{B}$	Strain-displacement operator matrix
$\boldsymbol{C}$	Material matrix
$\boldsymbol{D}$	Damping matrix
E	Young's modulus
$\boldsymbol{K}$	Stiffness matrix
L	Lagrangian function value
$\boldsymbol{M}$	Mass operator matrix
P_f	Probability of failure
$\mathcal{R}$	Fuzzy robustness
$\mathbf{X}$	Design domain matrix
c	State limit
f	Force
$\boldsymbol{f}$	Force vector
f^{crush}	Crushing force
$\boldsymbol{f}^{\text{ext}}$	External force vector
$\boldsymbol{f}^{\text{int}}$	Internal force vector
f^{res}	Resulting force
f	Objective function
f^0	Initial objective function
f^*	Optimal objective function
g	Inequality constraint function

$\mathbf{g}$	Inequality constraint function vector
$\mathbf{g}^0$	Initial inequality constraint function vector
$\mathbf{g}^*$	Optimal inequality constraint function vector
h	Equality constraint function
$\mathbf{h}$	Equality constraint function vector
$\mathbf{h}^0$	Initial equality constraint function vector
$\mathbf{h}^*$	Optimal equality constraint function vector
m	Mass
p	System parameter
$\tilde{p}$	Uncertain system parameter
$\tilde{\boldsymbol{p}}$	Uncertain system parameter vector
r	System response
$\tilde{r}$	Uncertain system response
$\tilde{\boldsymbol{r}}$	Uncertain system response vector
t	Time
u	Nodal displacement
$\boldsymbol{u}$	Nodal displacement vector
$\dot{u}$	Nodal velocity
$\dot{\boldsymbol{u}}$	Nodal velocity vector
$\ddot{u}$	Nodal acceleration
$\ddot{\boldsymbol{u}}$	Nodal acceleration vector
x	Design variable
$\mathbf{x}$	Design variable vector
x^L	Lower bounded design variable
$\mathbf{x}^L$	Lower bounded design variable vector
x^U	Upper bounded design variable

$\mathbf{x}^U$	Upper bounded design variable vector
$\mathbf{x}^*$	Optimal design variable vector
$\mathbf{x}^0$	Initial design variable vector
Π	Kinetic energy
Π_f	Possibility of failure
μ	Possibility level
$\boldsymbol{\lambda}$	Lagrangian multiplier vector
λ	Lagrangian multiplier
Δt	Time step
ε	Strain
$\boldsymbol{\varepsilon}$	Strain vector
$\dot{\varepsilon}$	Strain rate
ν	Poisson's ratio
ρ	Material density
σ	Stress
$\boldsymbol{\sigma}$	Stress vector
σ_e	Equivalent stress
σ_{pl}	Plastic stress
σ_u	Ultimate stress
σ_y	Yield stress
$\tilde{\square}$	Uncertain measure
∇	Nabla operator, here: gradient with respect to design variables
KKT	Karush–Kuhn–Tucker optimality criteria

The nomenclature is defined as the following: vectors and matrices are in bold and lower case and upper case, respectively. In the case of scalars lower and upper case has no meaning other than differentiation. Optimization symbols are written in sans serif font and those for structural mechanics are written with serif font.

1 INTRODUCTION

There is no more sense in having extra weight in an article than there is in the cockade on a coachman's hat. In fact, there is not as much. For the cockade may help the coachman to identify his hat while the extra weight means only a waste of strength. I cannot imagine where the delusion that weight means strength came from. It is all well enough in a pile-driver, but why move a heavy weight if we are not going to hit anything with it? In transportation why put extra weight in a machine? Why not add it to the load that the machine is designed to carry? Fat men cannot run as fast as thin men but we build most of our vehicles as though dead-weight fat increased speed! A deal of poverty grows out of the carriage of excess weight. Some day we shall discover how further to eliminate weight.

Henry Ford in *My life and work* (1922)

1.1 MOTIVATION

Light-weight frame structures are important, efficient structural elements in engineering design. This is especially the case in transportation vehicles, i.e. automotive, nautical, aeronautical and astronautical vehicles, which rely on such frames to provide structural integrity, stiffness and crashworthiness, amongst other criteria. While providing the structural function, they shall be as lightweight as possible. The lighter such structures are, the more economical they are; often in all facets of the life cycle of such structures: Lighter means (a) less use of material in the production, (b) less use of fuel in operation, (c) lower loads in operation, which lessen structural requirements, (d) less of which to recycle and dispose. This is, therefore, twofold of importance: cost and environmental, both of which are driving aspects in the design of modern products.

To achieve the lightest possible structures, structural design optimization is used, which is a mathematical algorithm-based approach used to find the *optimal* or best structure based upon one or more objectives being limited by constraints of geometrical, mechanical and manufacturing nature. Minimal mass is the most common objective, as the field of design optimization finds its origins in the budding American astronautical program. The reduction of mass was paramount to capacitate space exploration, as well as to allow larger payloads. Other objectives can be used including, but not limited to cost, manufacturability and other structural performance measure (e.g. stress or energy absorption).

Of special interest in the present work is the expansion of the design problem to include crashworthiness aspects of vehicles and vehicular components under uncertainty. Both of these topics represent numerical, computational and design challenges in structural design optimization. A space-frame structure will be used as a demonstrator, being developed in a decomposed design development philosophy.

Crashworthiness is ascertained numerically using computationally costly transient nonlinear finite-element method with explicit time integration. In the past, consideration of such structural responses in design optimization was not possible due to restrictive analysis time. The increase in computational power as well as parallelism in structural analysis have reduced computation times from days to minutes for the investigation of large, transient, nonlinear calculations, as is the case with vehicular crash simulations.

Structural analyses of transient and nonlinear nature are susceptible to uncertainty in loading, material and geometry. Engineering information is never complete and without uncertainty; meaning deviated, imperfect, erroneous and imprecise. Even low levels of uncertainty may lead to drastic deviations of the structural response. Uncertainty in engineering design can be found in the geometric model, load model, material model or from the requirements set. These areas of uncertainty have a number of different sources, which include manufacturing errors and deficient load assumptions. Uncertainties result from either inherent variation or from the lack of information at the time of designing. The models used to analyze mechanical behavior themselves can be uncertain or imprecise due to their abstraction from reality. Constantly improving manufacturing techniques can reduce both resulting material as well as geometrical uncertainty. Better knowledge of loading and the behavior of our models allows further refinement. Yet, both parameters as well as models are inherently imprecise and, thus, the resulting structural response. Structures, especially those responsible for human safety as is the case with crashworthiness, must perform as designed even with such uncertainty and, therefore, consideration of uncertainty in the design process is indispensable. In this work possibilistic and interval methods to describe this uncertainty are investigated and compared. These uncertainty analyses are integrated into the design optimization procedure.

1.2 STATE OF THE ART

The state of the art will be described of structural design optimization of light-weight frame structures with crashworthiness requirements under uncertainty. The literature survey is split into three sections: uncertainty in design and analysis in § 1.2.1, possibilistic modeling of uncertainty in § 1.2.2 and design optimization of structures with crashworthiness requirements in § 1.2.3.

1.2.1 *Uncertainty in structural-mechanical analysis and design*

Engineering information is neither complete nor fully understood; instead it is uncertain, deviated, imperfect, erroneous and imprecise. The known documentation of uncertainty and its consequences in engineering goes back to birth of civilization to the 18th century B.C. and the Code of Hammurabi, which describes the liability of the builder (engineer) for reliability problems:

> *If a builder builds a house for some one, and does not construct it properly, and the house which he built fall in and kill its owner, then that builder shall be put to death* (Hammurabi 1750 BC).

Understandably within this context, an overbuilding paradigm to accommodate the unknowns resulted and remains a tried method in engineering design. This simplest form of dealing with uncertainty, including lack of knowledge, known as safety factors, are detailed—especially in relation to reliability—by Elishakoff (2004), in which this pragmatic, yet possibly overly conservative method is discussed. Safety factors, being of implicit nature, ignore the actual source of the uncertainty with a blanket method and have, therefore, been referred to as an *ignorance factor*. Further safety factors are unable to afford proper handling in all structural-mechanical problems, especially when decoupled from the thought of reliability. In one such example where safety factors have little currency is that of Koiter (1945) in which it is shown that the lack of consideration of geometrical imperfections in previous work by Flügge and Donnell show a much higher critical buckling load factor (stability) than was found empirically.

Using the probability theory, which reached maturity in the 19th century with works by Laplace, engineers began to look at the uncertainty in structural mechanics at the beginning of the 20th century. The explicit consideration of structures of uncertainty with probability theory goes back to Mayer (1926). This early work treating structures as non-deterministic (i.e. uncertain) is dominated by civil engineers, e.g. Freudenthal (1947), but quickly moved to aeronautical engineers with Hilton and Feigen (1960) and Switzky (1964).

With the era of digital computation, came advancement with the finite-element method and structural design optimization and with it numerical routines for uncertainty analysis. In concert with structural-mechanical analysis, Monte Carlo simulations were used on one hand and on the other, more efficient methods of first- and second-order reliability theory, which are based on local sensitivities. Schuëller (2006, 2007) provides a contemporary overview of structural mechanics with stochastic uncertainty as do Lemaire (2014) and Bucher (2009), while the latter highlights especially the Monte Carlo methods.

Although, a probabilistic approach to uncertainty has dominated, non-probabilistic methods have also been put forward. In addition to a fuzzy or possibilistic approach (cf. § 1.2.2) other non-probabilistic methods include convex modeling, proposed by

Ben-Haim (1994), and anti-optimization by Elishakoff et al. (1994) and Qiu and Elishakoff (1998). The author of the present work considers both of these methods to be special cases of fuzzy uncertainty (cf. § 1.2.2). Hybrid methods have also been put forth, notably by Tonon et al. (2001).

The inclusion of uncertainty in structural design optimization is the natural next step. The first use of uncertainty (known to the author) in numerical optimization is put forth by Dantzig (1955) with applications to linear programming in operations research. Shortly after the application of numerical optimization to structural design by Schmit (1960) (cf. Barnett (1966) for a survey of early structural design optimization), uncertainty was integrated into the process. This was carried out in the form of reliability as posed by Switzky (1964).

Increased computational capabilities at the turn of the last millennium has allowed for further research in this field and interest from practitioners, evident in the number of books published: i.a. Ayyub and Klir (2006), Banichuk and Neittaanmäki (2010), Barlow (1998), Ben-Tal et al. (2009), Bernardini and Tonon (2010), Bucher (2009), Choi et al. (2006), Elishakoff (2004), Elishakoff and Ohsaki (2010) as well as Möller and Beer (2004).

1.2.2 *Describing engineering uncertainty with possibilistic methods*

Uncertainty can be categorized in two general types: aleatoric uncertainty due to randomness and epistemic uncertainty due to lack of information or imprecision. Epistemic uncertainty is nonreducible and is a common hurdle in the early design phase of structures. Interval methods and their extention in possibilistic or *fuzzy* methods are well suited for describing epistemic uncertainty. The origins of fuzziness can be traced back to the term *vagueness* used by Russell (1923) and Black (1937) and later *ensembles flou* (fuzzy or vague sets) by Menger (1951). Zadeh (1965) formalizes and coins the term *fuzziness*, which is further expanded to possibility theory by Zadeh (1978) as well as Dubois and Prade (1988).

Blockley (1979) makes (to the knowledge of the author) the first usage of the ideas put forth with fuzzy modeling of human and system uncertainty in structural design. The author uses a mixed approach of fuzziness and probability, foreshadowing the later work in fuzzy randomness of Möller and Beer (2004). Brown and Yao (1983) summarize the early use of fuzzy methods in structural engineering. These ideas of fuzziness have also been applied for nonlinear material behavior: Klisinski (1988) introduces a plastic theory based on fuzzy sets. Seising (2005, 2007) describes the broad practical usages of fuzzy uncertainty in the decision making process from fuzzy control theory to medical diagnoses.

Rao and Sawyer (1995) introduce the fuzzy counterpart to the stochastic finite-element method (cf. Ghanem and Spanos 1991, Panayirci 2010, Sudret et al. 2003, 2006 as well as Sudret and Der Kiureghian 2000) for structural-mecahnical analysis,

applying elastostatic analysis to a simple bar and beam example. This is furthered to elastodynamic problems including eigenvalue analysis and frequency response by Moens et al. (1998), comparing the results with Monte Carlo simulation. Crash analysis has been considered as presented by Thiele et al. (2005), Turrin et al. (2006), Turrin and Hanss (2007) as well as Beer and Liebscher (2008).

Muhanna and Mullen (1999) increase the complexity of applications and introduce a method of fuzzy analysis based on intervals at defined levels of uncertainty using optimization and antioptimization, thus defining an interval as a special (or a sub-) case of fuzzy theory. Möller et al. (2000), in advancing this using a modified evolutionary strategy, refer to this method as *α-level optimization*, as found in the present work. Moens and Hanss (2011) provide a summary of non-probabilistic methods of the finite-element method, including the interval finite-element method (cf. Köylüoglu and Elishakoff 1998, Modarezadeh 2005, Muhanna et al. 2004, Muhanna et al. 2007 and Rama Rao et al. 2011).

Huber (2010) extends modeling of engineering data with type-II fuzzy, originally introduced by Zadeh (1975a,b,c) to incorporate an uncertainty in the membership function, for fuzzy knowledge of manufacturing aspects.

Nikolaidis et al. (2004) compare the use of fuzzy and probabilistic methods, finding merit in both approaches, depending on the nature of the design problem. In a further comparison by Chen (2000), possibilistic methods are found to be more conservative than their probabilistic counterparts and the strength of possibilistic methods lies when little information is available in regards to the uncertainty.

1.2.3 *Design optimization of crashworthiness structures*

The foundation of structural design optimization considering crashworthiness is the structural-mechanical analysis of such, usually automotive, structures. Initially this was done using analytical methods, greatly simplifying the structural-mechanical problem, only on a component-level. Such components include the crushing of longitudinal sections in the so-called crumple zone in the front of a vehicle. Alexander (1960) derives a simple set of functions to serve in the design of thin-walled cylindrical shells under axial loading as energy-absorbing devices in nuclear reactors. Here an ideal rigid-plastic material model is used and it is limited to the unisymmetrical concertina collapse (or crush) mode. Johnson et al. (1977) extend this to consider different collapse modes based on geometric relationships. Abramowicz and Jones (1984a,b, 1986) build upon the early models to better represent the plastic hinges and their lobes, further expanding to square cross-sectional geometries. A summary of these findings and developments is found in Jones (1989).

Structural-mechanical analysis made great strides in the late 1970s and early 1980s with the advancement in transient nonlinear finite-element codes, especially LS-DYNA (including its predecessor DYNA3D) and Pam-Crash. These developments led to the

first automotive body-in-white crash, discussed by Haug et al. (1986), in which a small car was analyzed using 5555 shell elements and 106 beam elements. This calculation was able to meet the desired computational duration, completing overnight.

Although computational technology of the nonlinear finite-element method has progressed a long way since these initial investigations (cf. Belytschko et al. 2000, Crisfield 1996a,b, and de Borst et al. 2012), Belytschko and Mish 2001 outline the boundaries of computability including material models, smoothness of structural response, geometrical and material instabilities as well as uncertainty. The authors further point out that these challenges cannot be solved via increased computational effort and instead need fundamental advances.

Alternative methods of structural-mechanical analysis in crashworthiness are outside the scope of this work and include superfolding elements and equivalent mechanism. Super-folding elements, introduced by Abramowicz (2003, 2004) as well as Takada and Abramowicz (2004, 2007), allow for the analysis of complex assemblies of thin-walled sections. In the equivalent-mechanism approach, the complex structure of e.g. an automotive body-in-white is modeled with nonlinear spring elements as shown by Kim et al. (1996), Hamza and Saitou (2005), Liu (2005, 2010), Liu and Day (2006, 2007c,a,b), Fender (2013) and Fender et al. (2014). Both methods save the great computational expense of transient nonlinear finite-element analysis of full models, yet do this at the expense of less exact structural behavior.

Optimization being carried out with finite-element analysis is challenged by noisy and bifurcated structural-mechanical responses with respect to the design variables, as discussed by Duddeck (2008). These challenges are in addition to those posed for nonlinear finite-element analysis (cf. above, Belytschko and Mish 2001). To alleviate these challenges, structural optimization of crash structures has been handled by three general approaches: surrogate-based methods, utilization of simplified modeling and use of efficient optimization algorithms.

An overview of surrogating techniques in design optimitation is provided by Forrester et al. (2008). This method has been used extensively with crash optimization. Blumhardt (2001) introduces a surrogate-based optimization approach utilizing regressions for the design optimization using large-scale crash simulations. Sobieszczanski-Sobieski et al. (2001) carry out a multidisciplinary optimization of an automotive body-in-white including crash using different approximation techniques for each discipline. Kurtaran et al. (2002) discusses a sequential and adaptive technique, dividing the design domain into subdomains, which is applied to rather simple structures. Forsberg and Nilsson (2005) compare polynomial regression with Kriging for use in design optimization for crashworthiness. Xu (2014) uses an extended surrogate-based modeling approach for the design optimization of a front-crash system with adaptive, knowledge-enhanced Kriging to reduce the number of samples needed, yet still increases the resolution.

Structural optimization utilizing simplified models follows either the approach of equivalent mechanism or analytical modeling (c.f. above). In this way, the high computational effort of full finite-element analysis can be foregone. This is discussed thoroughly by Kim et al. (2001), Hamza and Saitou (2005), Halgrin et al. (2008), Fender (2013) and Fender et al. (2014).

New efficient optimization algorithms utilize local gradient information and do not necessitate design sensitivities as such. Examples of these algorithms are hybrid cellular automaton introduced by Tovar (2004) and expanded by Patel (2007) as well as (bidirectional) evolutionary structural optimization discussed by Huang et al. (2007), though poorly named as it has nothing to do with evolutionary algorithms. The current application of these algorithms are in topology optimization, which is out of the scope of this work.

1.3 CASE EXAMPLES OF TUBULAR SPACE FRAMES

The case examples in this dissertation are tubular space frames and components thereof. Tubular space frames are structural-mechanically efficient and are especially suitable for manufacturing in small series. Applications of space frames include architectural, aerospace and automotive structures. Space frames trace their lineage back to the early days of aviation and Alexander Graham Bell. Though more famous for his use of space frames in geodesic domes, Buckminister Fuller first made use of a space frame for automotive with his design of the DYMAXION (fig. 1.1a[1]). Other landmark automotive space frame designs include the "birdcage" of the 1959 MASERATI TIPO 61. This lineage continues today with the hybrid space-frame–integral-body structure AUDI SPACE FRAME (Paefgen and Leitermann 1994, Christlein and Schüler 2000, Leitermann and Christlein 2000 and Mayer et al. 2002, fig. 1.1b) and Lotus aluminum platforms. Further, tubular structures have shown to be effective in the absorption of impact loads (i.a. The Aluminum Association 1998 as well as Abramowicz and Jones 1984a,b, 1986).

(a) Space frame of Buckminster Fuller's DYMAXION[1]

(b) The AUDI SPACE FRAME (Mayer et al. 2002)

Figure 1.1: Examples of automotive space frames

1 www.classicdriver.com/de/article/norman-foster-lässt-buckminster-fullers-dymaxion-auferstehen

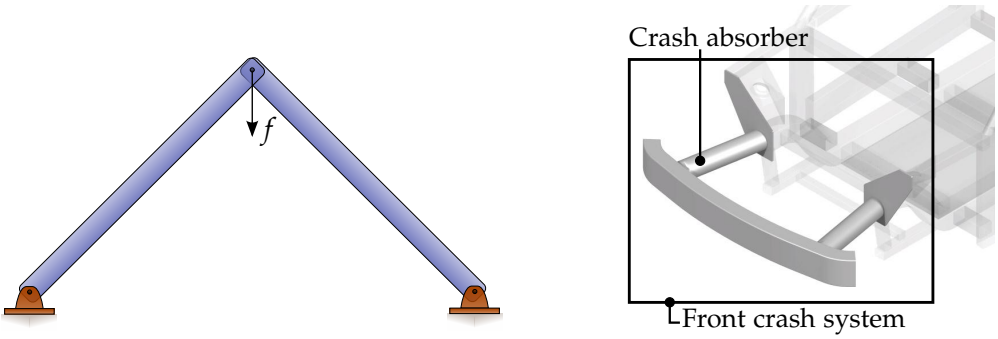

(a) Two-bar truss

(b) Crash absorber and front crash system from LEAF

Figure 1.2: Benchmark examples used here

The examples used in this work as benchmarks for the methods developed are introduced in the following sections. The second two examples are taken from the LIGHTWEIGHT EXTRUDED ALUMINUM FRAME (LEAF), which is introduced in § 6.

Two-bar truss

The cross-sectional area of the truss is to be dimensioned for lowest possible mass, while limiting the displacement, which allows for some displacement but does not allow for a loss of stability (snap through). Material uncertainty will be investigated. Further, the use of analytical design sensitivity with nonlinear structural-mechanical analysis will be shown.

Crash absorber

Extruded aluminum profiles are simple, yet effective structures to absorb energy of an impact. They are oriented so that the impact causes axial "crushing" of the section. This crushing is a complex, highly dynamic process, which is extremely sensitive to uncertainties if not properly designed. In the optimal design of this structure, attention will be paid to simplified modeling as well as uncertainty in the parameters.

Automotive front crash system

The space-frame front crash system is constructed of two longitudinal members (the crash absorbers above) and a transverse member (bumper). The structure, modeled with finite elements, will be optimized using a surrogate-based method. Again an uncertain material model will be considered.

1.4 ORGANIZATION

This dissertation is broken down into four columns in which a decomposed multi-level development of a vehicular space frame is used as a demonstrator: introduction, theory, numerical examples and conclusion. The flow of this dissertation is within the realm of a decomposed design philosophy (fig. 1.3). Following the introduction, the models used in the structural design optimization will be theoretically introduced. Thereafter, these models are implemented in numerical examples. Here, the structural design requirements are given for the concept of a vehicular space frame, LIGHTWEIGHT EXTRUDED ALUMINUM FRAME. As a last step, a verification of the optimization of the components is carried out using a full body-in-white finite-element analysis considering variation of material parameters.

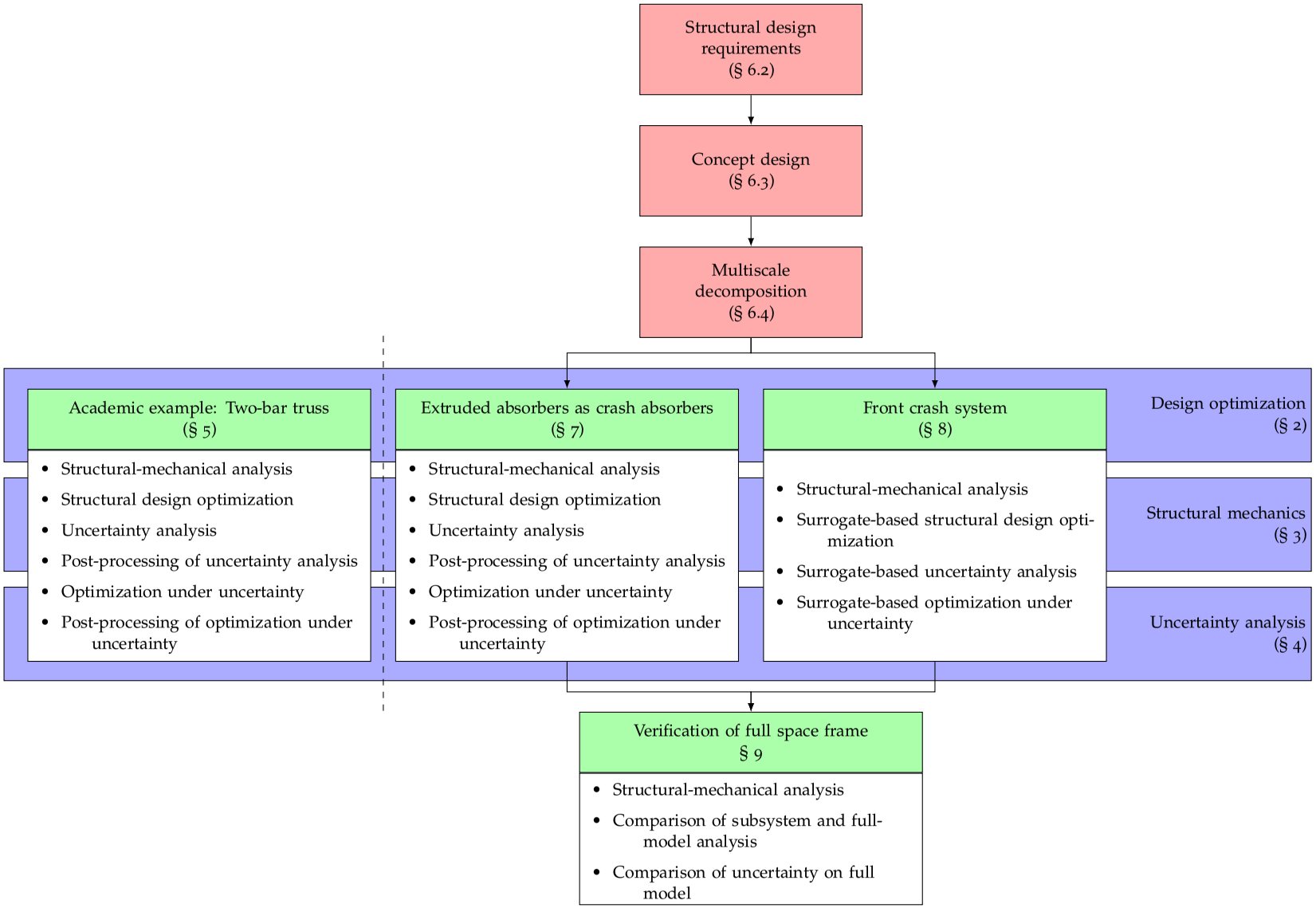

Figure 1.3: Organization of the dissertation within the decomposed design development philosophy

Part I

MODELS IN STRUCTURAL DESIGN OPTIMIZATION OF SPACE FRAMES

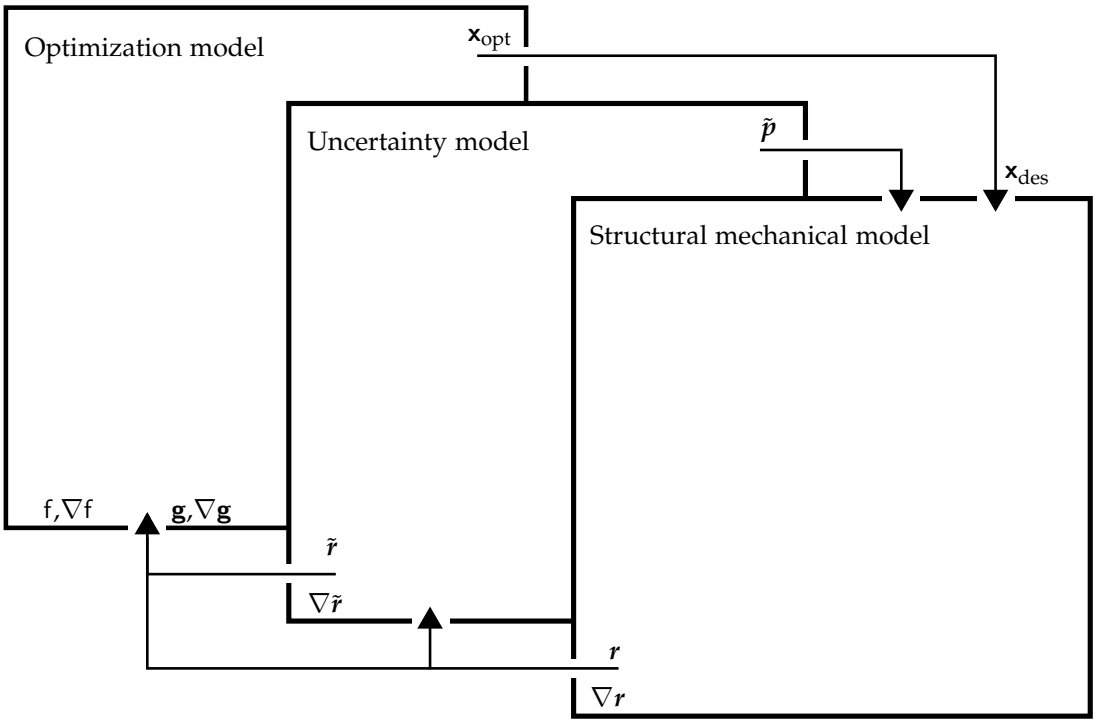

Flow of structural design optimization under uncertainty

2

FUNDAMENTALS OF STRUCTURAL DESIGN OPTIMIZATION

> *Cum enim Mundi universi fabrica sit perfectissima, atque a Creatore sapientissimo absoluta, nihil omnino in mundo contingit, in quo non maximi minimive ratio quæpiam eluceat.*[1]
>
> Leonhard Euler in *Methodus inveniendi lineas curvas maximi minimive proprietate gaudentes, sive solutio problematis isoperimetrici latissimo sensu accepti* (1744)

Structural design optimization replaces the time intensive trial and improvement cycles that are customary in engineering design: A design is built, either in scale or in full, and then tested. Improvements are made and it is then rebuilt and retested (fig. 2.1). These design cycles, which in the past took years, can now be simulated on a computer in hours, minutes or even seconds. The iterative improvements are controlled by means of mathematical optimization. These algorithms use mathematical methods to choose the design of the next iteration, thus enabling the consideration complexity not fathomable by an engineer. Structural design optimization, properly used, can put a design years ahead of its competition.

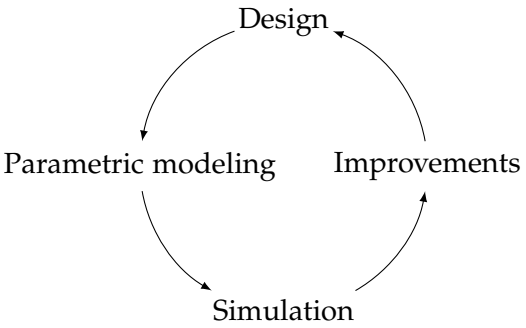

Figure 2.1: Design improvement cycle

2.1 MATHEMATICAL PRELIMINARIES

The goal of mathematical optimization is to find a vector of design variables $\mathbf{x}$ for which no lower objective value f can be found that satisfies the inequality constraints

1 As the fabric of the world is most perfect and from the omniscient Creator of the universe, nothing at all happens in the world in which no relationship of maximum or minimum emerges. I.e.: Nothing ever occurs without optimization playing a role.

g and equality constraints **h** while staying within the allowable design domain $\mathbf{X}^{\text{allow}}$, i.e. in $\mathbf{X}$ (between the lower bounds $\mathbf{x}^L$ and upper bounds $\mathbf{x}^U$). This is expressed mathematically as

$$\begin{aligned} \text{find} \quad & \mathbf{x}^* \\ \text{subject to} \quad & \mathsf{f}(\mathbf{x}^*) \leq \mathsf{f}(\mathbf{x}) \ \forall \mathbf{x} \in \mathbf{X} \subseteq \mathbb{R}^n \\ \text{where} \quad & \mathbf{X}^{\text{allow}} = \left\{ \mathbf{x} \in \mathbb{R}^n \mid \mathsf{g}_j(\mathbf{x}) \leq 0,\ \mathsf{h}_k(\mathbf{x}) = 0,\ \mathsf{x}_i^L \leq \mathsf{x}_i \leq \mathsf{x}_i^U \right\}. \end{aligned} \tag{2.1}$$

In the optimization problems in this work, a notation and nomenclature found in the following will be used:

$$\begin{array}{rlll} \text{minimize} & \mathsf{f}(\mathbf{x}) & & \text{objective function} \\ \text{so that} & \mathsf{g}_j(\mathbf{x}) \leq 0 & j \in \mathbb{N}[1,\, p] & \text{inequality constraints} \\ \text{and} & \mathsf{h}_k(\mathbf{x}) = 0 & k \in \mathbb{N}[1,\, q] & \text{equality constraints} \\ \text{as well as} & {\mathsf{x}^L}_i \leq \mathsf{x}_i \leq {\mathsf{x}^U}_i & i \in \mathbb{N}[1,\, n] & \text{bounds} \\ \text{where} & \mathbf{x} = \begin{bmatrix} \mathsf{x}_1 & \mathsf{x}_2 & \dots & \mathsf{x}_n \end{bmatrix}^T & \mathbf{x} \in \mathbb{R}^n & \text{vector of design variables} \end{array} \tag{2.2}$$

and compacter

$$\min_{\mathbf{x} \in \mathbf{X}} \left\{ \mathsf{f}(\mathbf{x}) \,|\, \mathbf{g}(\mathbf{x}) \leq \mathbf{0},\ \mathbf{h}(\mathbf{x}) = \mathbf{0} \right\}. \tag{2.3}$$

As equality constraints h are not used here, they will be not considered or written below.

2.2 TYPES OF STRUCTURAL DESIGN OPTIMIZATION

The optimization problems discussed here use structural mechanics as their system equation and is, thus, defined as structural design optimization. Depending on the type of design variables, there are four different structural optimization categories: material, topology, shape and size (fig. 2.2). The concentration in this work is on shape and sizing optimization.

Material optimization

In material optimization (fig. 2.2a), the material or material properties are varied to find the optimal application of material. This is understood in structural design optimization as algorithm-supported material selection, which is an inherently discrete problem. Therefore, the design variables must be continualized or the problem must be handled as an integer programming problem. Continualization of the problem is possible as shown by Schatz et al. (2014) to avoid the computational effort involved with using a genetic algorithm (Huber et al. 2010) or nonlinear mixed-integer algorithm (Exler and Schittkowski 2007 as well as Zhang and Baier 2011).

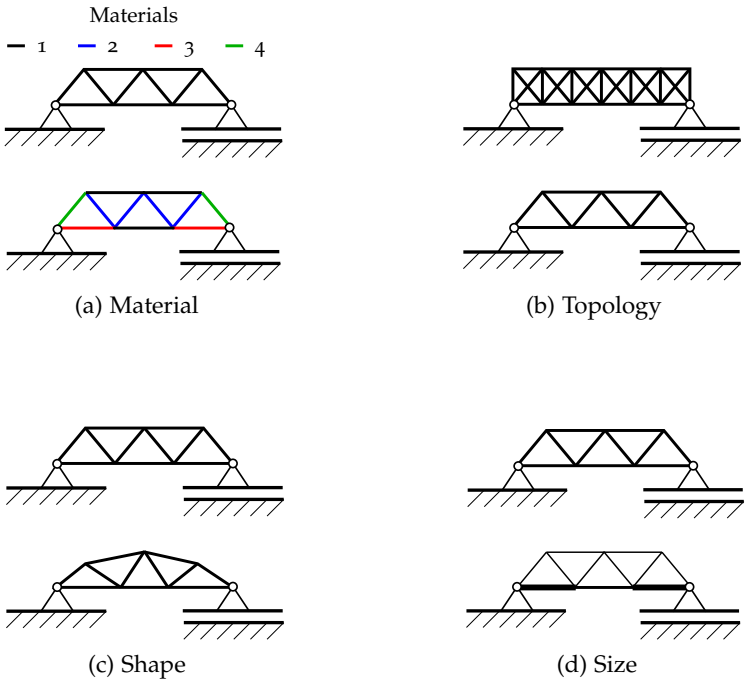

(a) Material (b) Topology

(c) Shape (d) Size

Figure 2.2: Comparison of structural design optimization types; top: start design, bottom: optimal design

Topology optimization

In topology optimization (fig. 2.2b) the optimal placement of material or positioning of members is found. This results in discrete optimization (i.e. present or not present and this or that), which has restrictively high computational effort, i.e. number of evaluations. Therefore, methods have been developed to continualize this discrete space, e.g. solid isotropic material with penalization (Bendsøe and Sigmund 2003). The proper topology is critical to further stages of design. Further optimization of a structure with suboptimal topology results cannot be alleviated through shape or sizing optimization. This method can be especially helpful in initial design phases to identify the optimal load paths through a design space (Wehrle et al. 2012 and Sauerer et al. 2014).

Shape optimization

The outer shape of a structure is to be designed in shape optimization (fig. 2.2c). This type also includes so-called topography optimization in which the tangent direction of the nodes is variable. Shape optimization is further divided into geometry and finite-element based categories. The former utilizes parametric geometry descriptors, often in a CAD model, as design variables and the latter the position of the node of the finite-element model. Each method has advantages and disadvantages depending

on their applications, though, the main compromise is between flexibility of the model and dimensionality. In this dissertation, the geometry-based approach will be used.

Sizing optimization

Sizing optimization (fig. 2.2d), also known as dimensioning, finds the optimal dimensions of a structure, e.g. the member thickness (with shell models) or cross-sectional areas (with truss and frame models). Generally in terms of the mechanical analysis model, the element descriptions are the design variables and not geometric nodal positions. This allows for a well-conditioned continuous problem, as the responses with respect to the design variables are continuous through the design space.

2.3 STRUCTURAL DESIGN OPTIMIZATION IN DESIGN DEVELOPMENT PHASES

Structural design optimization can be used in all phases of structural design development: from the conceptual phase to the finalized design. In this work, the design development phases of mechanical structures are defined as the following: concept design, preliminary design and finalized design as follows:

Conceptual design

In this phase of structural design, decisions of discrete nature are met including concept, material and topology. When using optimization, it is thus necessary to use methods capable of handling discrete design variables. In this phase important decisions are met that can only be changed with enormous effort and costs in later phases. Structural-mechanical investigations with complex finite-element analysis are avoided due to the high effort in modeling and simulation.

Preliminary design

In this phase size and shape optimization is carried out to give the dimensions of the structure being developed. Finite-element analysis is used here, albeit often with abstract models. Exact material models for specific alloys can be unavailable at this time. This uncertainty will be handled below.

Final design

At the end of the design development, the details of design are set. Such details include welds, radii and allowable tolerances, which are analyzed and set for manufacturing of the structure. High-resolution models necessitate increasing analysis effort, though many degrees of freedom are fixed reducing the dimensionality of the design problem.

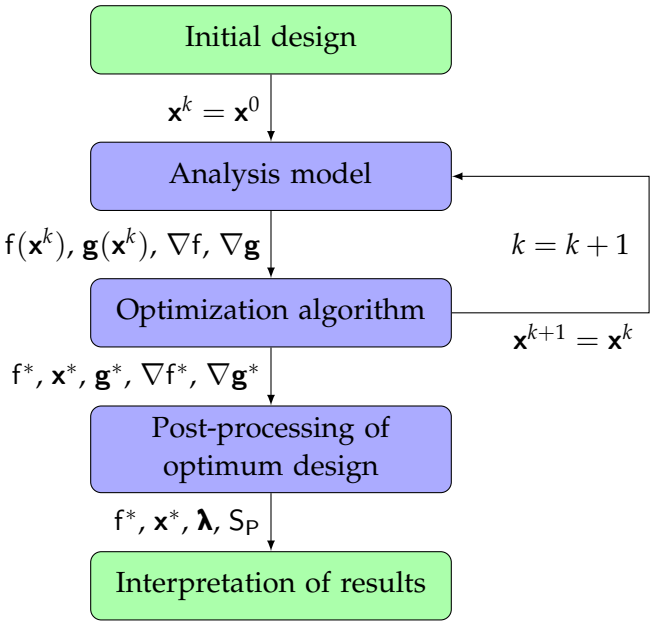

Figure 2.3: Flow chart of an optimization within the optimization model

2.4 OPTIMIZATION MODEL

The optimization model is comprised of the optimization algorithm, objective and constraint functions (and the system responses contained therein). In the following section the building blocks of the optimization will be defined and introduced (fig. 2.3 , where $\mathbf{x}$ is the design variable vector, $\mathbf{g}$ is the constrain vector, f is the objective function, $\boldsymbol{\lambda}$ is the vector of Lagrangian multipliers, S_P are the shadow prices, k the iteration and $\square^*$ denotes an optimal value).

2.4.1 *Optimization algorithms*

The optimization algorithm is the engine of the optimization process driving design improvement. It receives input of the iteration value for the objective function $f\left(\mathbf{x}^k\right)$ and the constraint function $\mathbf{g}\left(\mathbf{x}^k\right)$ (and in the cases of first- and higher-order algorithms partial derivatives $\nabla f\left(\mathbf{x}^k\right)$ and $\nabla \mathbf{g}\left(\mathbf{x}^k\right)$) and decides if the optimum has been reached or the design variables for the next iteration $\mathbf{x}^{k+1}$. Optimization algorithms are categorized in three families here based on their order: zeroth-, first-, and second-order. Further explanation and derivation of these algorithms (beyond that of their primary sources) including examples, are provided by Christensen and Klabring (2009).

Zeroth-order optimization algorithms

Zeroth-order optimization algorithms are those that do not base the calculation of the design variables for the following iteration on the first- or second-order design sensitivities. These include biology-inspired heuristic algorithms such as genetic algorithms, evolutionary strategies, particle swarm, bee hive, and ant hill. Yang (2010) provides an up-to-date summary and explanation of these and other algorithms.

First-order optimization algorithms

First-order optimization algorithms rely only on the value of the objective and constraint functions of the design and its design sensitivities. The simplest form is the method of steepest descent. Other methods include sequential linear programming (SLP), in which the functions are approximated with first-order Taylor approximations.

The method of moving asymptotes (MMA) is an efficient and advanced first-order algorithm used here. MMA, which was introduced by Svanberg (1987), improves on the successful algorithm of CONLIN (convex linearization) by Fleury and Braibant (1986). Both MMA and its predecessor are trimmed for structural optimization, especially when approximating the constraint functions, which are often reciprocal values, e.g. stress in a bar where the design variable is the cross-sectional area.

Second-order optimization algorithms

In this research, sequential quadratic programming (SQP), a second-order algorithm, is used due to its high efficiency for both structural optimization and uncertainty analysis (§ 4). Specifically NLPQLP (Schittkowski 2013) is used here. The original code was released as NLPQL by Schittkowski (1985), which has been expanded to its present form based on the work of Dai and Schittkowski (2008). This is a very robust algorithm, as the non-monotone line search accommodates computational errors of objective, constraint functions or their design sensitivities to ensure quick convergence.

2.4.2 *Analysis model*

The analysis model is comprised of the geometric model and its mechanical, manufacturing and uncertainty analysis, described in the following chapters. This includes the mapping of the optimization variables onto the design variables,

$$\mathbf{x}_{\text{opt}} \mapsto \mathbf{x}_{\text{des}}. \tag{2.4}$$

This mapping process is generally included in a normalization and denormalization such that that the optimizer only handles optimization variables between zero and unity. The analysis model must be calculated with the original design values. They will be referred to here as simply $\hat{\mathbf{x}}$ and $\mathbf{x}$ for the normalized and denormalized, respectively. Other normalization schemes are also possible.

The analysis of the system maps the design variables onto the system results,

$$\mathbf{x}_{\text{des}} \mapsto \boldsymbol{r}. \tag{2.5}$$

Further, the system responses of the analysis model r must be mapped on the objective and constraint values, f and $\mathbf{g}$ respectively,

$$\boldsymbol{r} \mapsto f \tag{2.6}$$

and

$$\boldsymbol{r} \mapsto \mathbf{g}. \tag{2.7}$$

Normalization is also critical for the conditioning of the optimization problem. An upper-bounded constraint is normalized here as

$$\mathsf{g} = \frac{r}{c} - 1, \tag{2.8}$$

and a lower-bounded constraint as

$$\mathsf{g} = 1 - \frac{r}{c}. \tag{2.9}$$

The analysis model also should provide the gradients in case of use of gradient-based algorithms (first-order and second-order algorithms), which shall be either of numerical or analytical nature. Therefore, the complete mapping of the analysis model is

$$\mathbf{x}_{\text{opt}} \overset{\text{Analysis model}}{\mapsto} \mathsf{f}, \quad \mathbf{g}, \quad \nabla_{\mathbf{x}}\mathsf{f}, \quad \nabla_{\mathbf{x}}\mathbf{g} \ . \tag{2.10}$$

This will be further discussed in the next sections, when the specific analysis models used will be introduced. These include structural analysis and uncertainty analysis.

2.4.3 *Design sensitivity analysis*

Using first- and second-order algorithms requires the gradients of the objective and constraint functions with respect to the design variables, defined by $\nabla\mathsf{f}$ and $\nabla\mathbf{g}$, respectively. A comprehensive review has been afforded by Martins and Hwang (2013). The calculation of the gradients is referred to as design sensitivity analysis. In the following it is discussed how the sensitivities,

$$\nabla\mathsf{f} = \left[\frac{\partial\mathsf{f}}{\partial\mathsf{x}_1} \quad \frac{\partial\mathsf{f}}{\partial\mathsf{x}_2} \quad \dots \quad \frac{\partial\mathsf{f}}{\partial\mathsf{x}_n}\right]^T \tag{2.11}$$

$$\nabla\mathbf{g} = \left[\frac{\partial\mathbf{g}}{\partial\mathsf{x}_1} \quad \frac{\partial\mathbf{g}}{\partial\mathsf{x}_2} \quad \dots \quad \frac{\partial\mathbf{g}}{\partial\mathsf{x}_n}\right]^T, \tag{2.12}$$

are calculated in structural design optimization. Direct sensitivity analysis methods rely on directly taking the derivatives, while adjoint sensitivity analyses uses a further

term (adjoint term). The latter have shown to be especially efficient when the number of design variables n_x is higher than the number of constraint functions n_g as can be the case in structural design optimization. Though the implementation of adjoint methods is outside the scope of this work and sensitivities, when provided, are calculated via direct methods. Higher-order gradients, such as the Hessian matrix, are typically not calculated directly in structural design optimization due to computational and programming effort and, instead, are approximated when needed.

When provided, the sensitivities are given in the form of the partial derivative of the response with respect to the design variables $\frac{\partial r}{\partial x_i}$, i.e. for the upper-bounded constraints $g_j = \frac{r}{c} - 1$, this is

$$\frac{\partial g_j}{\partial x_i} = \frac{1}{c}\frac{\partial r}{\partial x_i}, \tag{2.13}$$

and for lower-bounded constraints $g_j = 1 - \frac{r}{c}$,

$$\frac{\partial g_j}{\partial x_i} = -\frac{1}{c}\frac{\partial r}{\partial x_i}. \tag{2.14}$$

Analytical sensitivity

In some cases the exact derivatives of the objective function $\frac{\partial f}{\partial x_i}$ and constraint functions $\frac{\partial \mathbf{g}}{\partial x}$ are available. These are often, though, in the form of response sensitivities and, thus, must be normalized (in agreement with the constraint functions themselves) by using eqs. 2.13–2.14.

Numerical sensitivity

Numerical gradients are generally calculated in structural design optimization problems using forward finite differencing. Backward or central differencing can also be used, albeit the later with significantly more computational effort.

Forward differencing for the sensitivity calculation of some response r with respect to some design variable x_i is defined as

$$\frac{\partial r}{\partial x_i} = \lim_{\Delta x_i \to 0} \frac{r(\mathbf{x} + \Delta x_i) - r(\mathbf{x})}{\Delta x_i}, \tag{2.15}$$

where Δx_i is the step size for the finite differencing. As Δx_i is defined with a finite numerical value, this is an approximation

$$\frac{\partial r}{\partial x_i} \approx \frac{r(\mathbf{x} + \Delta x_i) - r(\mathbf{x})}{\Delta x_i}. \tag{2.16}$$

Backward differencing and central differencing can be derived analogously. The step size is chosen in this dissertation between $\Delta x_i = 1 \times 10^{-6}$ and $\Delta x_i = 1 \times 10^{-2}$. A trade-off is performed between increase in the theoretical precision of the gradient by reducing Δx_i and the precision of the analysis model and possible noise in the function.

The sensitivities are found using the calculation of $n_x + 1$ evaluations for forward and backward differencing and $2n_x + 1$ for central differencing. These methods can, therefore, be restrictive for high number of design variables. This method, although exhibiting high computational effort, is generally robust and can be used with generally any analysis type or software, as long as the structural response is smooth with respect to the design variables.

Semi-analytical sensitivity

Semi-analytical sensitivities are a mix of the analytical and numerical methods described above. An example is when some implicit derivative is not available and is then approximated via numerical gradients,

$$\frac{\partial r\,(x, p)}{\partial x} \approx f\left(\frac{\Delta p}{\Delta x}\right). \tag{2.17}$$

This method can save drastically on the implementation time, as the sensitivity of all parts does not have to be coded.

2.4.4 *Approximation and surrogate model*

An approximation can be used instead of systems evaluations of high computational effort as are often found in structural-mechanical analysis, i.e. finite-element analysis. Approximation methods are used here for both design optimization as well as uncertainty analysis. Forrester et al. (2008) provide a review of methods of sampling and approximation, including those used here.

Approximation is a two-step process in which first the system is sampled with high computational effort using a design of experiments and then these sample points are used as support points for an approximating function. Further reduction in computational effort is possible with iterative adaptive sampling and approximation methods (Xu et al. 2012).

In this work, two methods for design of experiments are used: Latin hypercube and an extended Latin hypercube with the boundary points of the domain to be modeled. The latter has shown to function especially well with interpolations with Gaussian process inferences, which often show poor quality in the region of the boundary, therefore increasing the number of sampling points required.

Approximations are categorized in two families: interpolations in which the approximating function must go through the support points and regressions when this is not a condition. Gaussian process inference interpolations and second-order polynomial regressions are two methods used in this work and have found broad use in structural design optimization.

Polynomial regression

Polynomial regression is often referred to as response surface modeling in the context of structural design optimization. In this method the complex finite-element analyses are replaced by simple polynomials, providing the system equations for the optimization. This is posed generally as

$$\boldsymbol{r} = \boldsymbol{X}\boldsymbol{\beta}, \tag{2.18}$$

where $\boldsymbol{r}$ is the set of responses from a set of samples $\boldsymbol{X}$, composed of a vector $\boldsymbol{x}$ of each sample. Solving for the matrix $\boldsymbol{\beta}$ with least squares gives the model.

The simplest form is a linear approximation, which is defined for some response r as

$$r_i = \beta_0 + \sum_j \beta_j x_{ij}, \tag{2.19}$$

where x_{ij} are the sample points with i being the sample and j the term of sample.

The quadratic form is slightly more complex due to the mixed terms. This is formulated as follows:

$$r_i = \beta_0 + \sum_j \beta_j x_{ij} + \sum_j \sum_k \beta_{jk} x_{ij} x_{ik}. \tag{2.20}$$

Once the model $\boldsymbol{\beta}$ has been established, the approximated value of the response r^{approx} at a new design $\boldsymbol{x}^{\text{new}}$ can be found via

$$r^{\text{approx}} = \boldsymbol{x}^{\text{new}}\boldsymbol{\beta}. \tag{2.21}$$

Gaussian process inference

Gaussian process inference is an interpolation method (also known as Kriging) that brings together a regression model and a correlation model. Accordingly the approximation of a response is defined by

$$r^{\text{approx}} = \boldsymbol{x}^{\text{new}}\boldsymbol{\beta} + Z\left(\boldsymbol{x}^{\text{new}}\right), \tag{2.22}$$

where Z is a correlation function. The ability to interpolate complex functions with relatively small number of samples has resulted in use of Gaussian process interference in structural design optimization considering crashworthiness (Cadete et al. 2005, Forsberg and Nilsson 2005, Liao et al. 2008 and Xu et al. 2012). Further details and derivations of Gaussian process inference can be found in Lophaven et al. (2002b) and Forrester et al. (2008).

2.5 POST-PROCESSING OF STRUCTURAL DESIGN OPTIMIZATION

The use of first- and second-order optimization algorithms allow two important post-processing investigations without further computational effort: optimality and shadow prices. Both these are based on the Lagrangian function,

$$\mathsf{L} = \mathsf{f}\left(\mathbf{x}\right) + \boldsymbol{\lambda}^T \mathbf{g}\left(\mathbf{x}\right), \tag{2.23}$$

and its derivative with respect to the design variables,

$$\frac{\partial L}{\partial x_i} = \frac{\partial f}{\partial x_i} + \boldsymbol{\lambda}^T \frac{\partial \mathbf{g}}{\partial x_i}. \tag{2.24}$$

2.5.1 *Optimality*

When using first- and second-order algorithms, the optimality can be checked to confirm that indeed an optimum has been reached and not stopped due to i.a. algorithm errors. For unconstrained, unbounded minimization problems, the first-order optimality criteria is defined as

$$\frac{\partial f^*}{\partial \mathbf{x}} = \mathbf{0} \tag{2.25}$$

$$\frac{\partial^2 f^*}{\partial \mathbf{x}^2} \geq \mathbf{0}. \tag{2.26}$$

Optimality of a convex and constrained optimization problem can be proven by the optimality criteria after Karush (1939) and Kuhn and Tucker (1951), and are referred to as the Karush–Kuhn–Tucker criteria (KKT). This is necessary and sufficient for convex optimization problems and necessary for nonconvex problems. As such, this proves global optimality for the convex case and local optimality in the general case. This is defined as the following:

$$\begin{aligned} \text{Stationary:} \quad & \nabla L(\mathbf{x}, \boldsymbol{\lambda}) = \mathbf{0} \\ \text{Primal feasibility:} \quad & \mathbf{g} \leq \mathbf{0} \\ \text{Dual feasibility:} \quad & \lambda_i \geq \mathbf{0} \\ \text{Complementary slackness:} \quad & g_i \lambda_i = 0 \\ \text{Design feasibility:} \quad & \mathbf{x} \in \mathbf{X}, \end{aligned} \tag{2.27}$$

where

$$\nabla L(x_i, \boldsymbol{\lambda}) = \frac{\partial L}{\partial x_i} = \frac{\partial f(x_i)}{\partial x_i} + \boldsymbol{\lambda}^T \frac{\partial \mathbf{g}(x_i)}{\partial x_i} = 0, \tag{2.28}$$

assuming again local convexity (eq. 2.26).

For constrained and bounded problems this criteria must be expanded as introduced in Karush (1939) and Kuhn and Tucker (1951), where the derivative of the Lagrangian function with respect to the design variables must be equal to zero. Consideration of the bounds of the design variables as well as the inequality constraints in $\mathbf{g}$ is crucial, as in structural design optimization the bounds often respresent the limits of manufacturing and are often one of several active constraints.

2.5.2 *Shadow price*

The Lagrangian multipliers have a further meaning as shadow prices. These are referred to as such, as this is the detrimental price to the objective because of the shadows cast by the constraints. This linearization estimates the change in optimal objective value due to change in the limits of active constraints.

Assuming that the Lagrangian function is zero at the optimum (eq. 2.28) and rearranging this, this yields

$$\lambda_j = -\frac{\partial f^*}{\partial x_i}\frac{\partial x_i}{\partial g_j}. \tag{2.29}$$

Depending on the formulation of the constraint function, the Lagrangian multiplier is

$$\begin{aligned}
\text{upper bound, non-normalized } g_j = r - c: &\qquad \lambda_j = -\frac{\partial f^*}{\partial c_j} \\
\text{lower bound, non-normalized } g_j = c - r: &\qquad \lambda_j = \frac{\partial f^*}{\partial c_j} \\
\text{upper bound, normalized } g_j = \frac{r}{c} - 1: &\qquad \lambda_j = -\frac{\partial f^*}{\partial c_j} c_j \\
\text{lower bound, normalized } g_j = 1 - \frac{r}{c}: &\qquad \lambda_j = \frac{\partial f^*}{\partial c_j} c_j.
\end{aligned} \tag{2.30}$$

This meaning of the Lagrangian multipliers is known as shadow prices and thus defined

$$S_{Pj} = \frac{\partial f^*}{\partial c_j}. \tag{2.31}$$

As the optimization algorithm often returns the Lagrangian multiplier in domain of the normalized constraint function, this must be denormalized appropriately to give the shadow price S_{Pj}.

Using this linearization at the optimum, it is possible to estimate the value of the objective function by a loosening of the constraint bound c,

$$f^{*,\text{new}} = f^* - \Delta c_j S_{Pj}. \tag{2.32}$$

This can be an effective tool for accessing the reduction in the objective function, due to a reposing of the optimization (design) problem, without carrying out further optimization runs. As this is, though, a linearization (first derivative) and is only valid locally, i.e. the new objective function $f^{*,\text{new}}$ may not be able to be properly forecast if large changes in the constraint bound c are investigated.

2.6 IMPLEMENTATION OF A SOFTWARE TOOL FOR STRUCTURAL DESIGN OPTIMIZATION

The package DESOPTPY (Design Optimization in Python) was written by the author for use in structural design optimization for mechanical structures. The goal of this project was to design a general optimization toolbox for structural design optimization in which an optimization model can be set up easily, quickly, efficiently and effectively, allowing the modeling of the optimization problem without difficulty. It is also meant to be modular and easily expandable. The aspects discussed above have been integrated making it a relatively complete optimization toolbox.

DESOPTPY has a variety of optimization algorithms, which are available as this has a direct connection to PYOPT (Perez et al. 2012), which includes the algorithms introduced in § 2.4.1. Further, a surrogate-based optimization has been implemented. Here, the Gaussian process inference in SCIKIT-LEARN (Pedregosa et al. 2011) is utilized, which in turn is a Python implementation of the code DACE, presented by Lophaven et al. (2002a,b).

This code has been used by Wehrle et al. (2014a,b), yet not published as such. In addition to this, several theses advised by the author, including Rudolph (2013), Braun (2014), Richter (2014) and Wachter (2014), have utilized this code. In list. 2.1 an example of the straightforward and very readable syntax is given by pseudo code. This example can be easily used as a layout for programming future optimization problems.

Listing 2.1: Syntax of optimization problem with DESOPTPY

```
from DesOptPy import DesOpt

def SysEq(x, gc)
    # here: system equations
    f = ...
    g = ...
    return(f, g)

def SensEq(x, gc)  # optional
    # here: sensitivity equations
    dfdx = ...
    dgdx = ...
    return(dfdx, dgdx)

x0 = ...
xL = ...
xU = ...
gc = ...
xOpt, fOpt, SP = DesOpt(SysEq, x0, xU, xL, gc=gc, hc=[], Alg="MMA",
                        SensCalc="FD", DesVarNorm="xLxU", deltax=1e-3,
```

```
                        StatusReport=True, ResultReport=True,
                        OptVideo=False, DoE=False, SBDO=False,
                        Debug=False, PrintOut=True)
```

3

STRUCTURAL-MECHANICAL MODELING IN STRUCTURAL DESIGN OPTIMIZATION

The best material model of a cat is another, or preferably the same, cat.

Arturo Rosenblueth and Norbert Wiener in *The role of models in science* (1945)

In this chapter the structural-mechanical analysis and those models necessary to model, analyze and design a structure as shown in fig. 3.1 are introduced and discussed. First the preliminaries of structural mechanics will be introduced and this will be followed by the discretized geometric model, material model and load model. This will be limited to its use in the design and analysis of aluminum space frame structures. Along with the geometric model, structural-mechanical analysis is carried out with material modeling and load modeling (including boundary conditions).

Figure 3.1: A simulated automobile impact

3.1 PRELIMINARIES OF STRUCTURAL MECHANICS

The structural design optimization of structures is reliant on the structural-mechanical analysis. Below, the relevant aspects of structural mechanics will be introduced; further details and derivations can be found in i.a. Belytschko et al. (2000), Bonet and Wood (1997), de Borst et al. (2012) and Hughes (2000).

The mechanics of structures is defined by a system of second-order elliptic partial differential equations with boundary and initial conditions describing a continuum (in indicial notation),

$$\begin{aligned} \sigma_{ij,j} + \rho f_i &= \rho \ddot{u}_i \quad \text{in } \Omega \\ u_i &= \hat{u}_i \quad \text{on } \Gamma_D \\ \sigma_{ij} \cdot n &= t_i \quad \text{on } \Gamma_N \\ & u_o \quad \text{in } \Omega \\ & \dot{u}_0 \quad \text{in } \Omega, \end{aligned} \tag{3.1}$$

and the constitutive equation

$$\sigma_{ij} = C_{ijkl}\varepsilon_{kl} = C_{ijkl}u_{k,l}, \tag{3.2}$$

where σ is the stress, ρ the density, f_i the body forces, n the surface normal, u the displacement, $\dot{u}$ the velocity, $\ddot{u}$ the acceleration, C the constitutive relationship, ε the strain, Ω the spatial domain and Γ (also denoted as $\partial\Omega$) the boundary of domain, divided into Neumann boundary Γ_N and the Dirichlet boundary Γ_D. Prescribed terms due to boundary conditions are represented by $\hat{\square}$, while initial terms are denoted by $\square_0$.

The problem detailed in eq. 3.1, referred as the *strong formulation*, can be solved with i.a. the finite-element method using the *weak formulation* (or variational form). This is carried out through use of the *principle of virtual work*,

$$\delta\pi = \underbrace{\int_\Omega \rho\ddot{u}_i\delta u_i \,\mathrm{d}\Omega}_{\delta\pi_{\text{kin}}} + \underbrace{\int_\Omega \sigma_{ij}\delta u_{i,j} \,\mathrm{d}\Omega}_{\delta\pi_{\text{int}}} - \underbrace{\int_\Omega \rho f_i\delta u_i \,\mathrm{d}\Omega - \int_\Gamma t\delta u_i \,\mathrm{d}\Gamma}_{\delta\pi_{\text{ext}}} = 0, \tag{3.3}$$

where δu_i are virtual displacements, $\delta u_{i,j}$ are virtual strains and $\delta\pi$ is the virtual work, divided into kinetic, internal and external terms. The virtual work of eq. 3.3 is required to be stationary. The spatial (mesh) and temporal (discussed below) domains are then discretized. The resulting matrix representation is discussed in the next section (§ 3.2).

3.2 FINITE-ELEMENT ANALYSIS

The structural-mechanical analysis is carried out here via the finite-element method. The structure to be analyzed is discretized spatially in small elements of known shape and behavior. The geometric and material properties (eqs. 3.2–3.3) of the domain are mapped to their respective elements. These element matrices are then assembled to represent their structure counterparts. The governing equations discussed above (§ 3.1) is the base of the calculation of structural-mechanical analysis.

The governing equations have been further abstracted to be used on more computationally efficient elements to model structures. The first consideration is the dimensionality of the element. These are the following:

ONE-DIMENSIONAL: bar, beam, cable and spring

TWO-DIMENSIONAL: plate, membrane and shell elements

THREE-DIMENSIONAL: volume elements.

All of the above can be then mapped onto a three-dimensional manifold to represent a three-dimensional structure in space.

The procedure of discretizing, i.e. transforming the geometry model into a structural-mechanical analysis model, is known in finite-element analysis as meshing. Complex meshing software can also discretize higher-order geometry models into lower-order structural-mechanical analysis models, e.g. two-dimensional surface model into a one-dimensional beam model. The boundary conditions in eq. 3.1 are then applied and this problem is solved using efficient algorithms. The solving process is discussed in the following.

3.2.1 *Force equilibrium*

The discretization of the eq. 3.3 using the elements described above results in a system of equations in matrix form, which are the basis for the structural-mechanical analyses. The governing force equilibrium equation for mechanical behavior can be defined in two fashions. The first, *stiffness method* is formulated as

$$\boldsymbol{M}\left(\boldsymbol{u},t\right)\ddot{\boldsymbol{u}}\left(t\right)+\boldsymbol{D}\left(\boldsymbol{u},t\right)\dot{\boldsymbol{u}}\left(t\right)+\boldsymbol{K}\left(\boldsymbol{u},t\right)\boldsymbol{u}\left(t\right)=\boldsymbol{f}^{\text{ext}}\left(\boldsymbol{u},t\right), \tag{3.4}$$

where $\boldsymbol{M}$ is the mass matrix, $\boldsymbol{D}$ the damping matrix, $\boldsymbol{K}$ the stiffness matrix, $\ddot{\boldsymbol{u}}$ the nodal acceleration vector, $\dot{\boldsymbol{u}}$ the nodal velocity vector, $\boldsymbol{u}$ the nodal displacement vector and $\boldsymbol{f}^{\text{ext}}$ the external force vector. The second method, the *force method* is used often in cases of nonlinearities as it can be more efficient to avoid the assembly of the stiffness matrix. Here, the internal force $\boldsymbol{f}^{\text{int}}$ is used instead of the term of the stiffness matrix and displacements $\boldsymbol{Ku}$. The stiffness matrix $\boldsymbol{K}$ is in this case nonlinear with respect to geometry and material model as well as time. This formulation is

$$\boldsymbol{M}\left(\boldsymbol{u},t\right)\ddot{\boldsymbol{u}}\left(t\right)+\boldsymbol{D}\left(\boldsymbol{u},t\right)\dot{\boldsymbol{u}}\left(t\right)+\boldsymbol{f}^{\text{int}}\left(\boldsymbol{u},t\right)=\boldsymbol{f}^{\text{ext}}\left(\boldsymbol{u},t\right). \tag{3.5}$$

A compacter notation will be used here, which does not explicitly denote the dependence of time and displacement,

$$\boldsymbol{M}\ddot{\boldsymbol{u}}+\boldsymbol{D}\dot{\boldsymbol{u}}+\boldsymbol{K}\boldsymbol{u}=\boldsymbol{f}^{\text{ext}}, \tag{3.6}$$

and

$$\boldsymbol{M}\ddot{\boldsymbol{u}}+\boldsymbol{D}\dot{\boldsymbol{u}}=\boldsymbol{f}^{\text{ext}}-\boldsymbol{f}^{\text{int}}. \tag{3.7}$$

The damping can often be neglected, resulting in

$$\boldsymbol{M}\ddot{\boldsymbol{u}} + \boldsymbol{K}\boldsymbol{u} = \boldsymbol{f}^{\text{ext}}, \tag{3.8}$$

and

$$\boldsymbol{M}\ddot{\boldsymbol{u}} = \boldsymbol{f}^{\text{ext}} - \boldsymbol{f}^{\text{int}}, \tag{3.9}$$

respectively. Eqs. 3.9–3.8 and the forms derived from them will be used throughout to demonstrate the structural-mechanical system equations.

3.2.2 *Linear analysis*

Mechanical structures are often designed for static loading conditions and resulting small deformations not exceeding their linear elastic limit. Therefore, in most cases of structural design, linear finite-element analysis is sufficient. For linear elastostatic analysis, the terms of velocity and acceleration are zero, hence eq. 3.7 reduces to the following:

$$\boldsymbol{f}^{\text{ext}} = \boldsymbol{K}\boldsymbol{u}. \tag{3.10}$$

The stress σ in a structure can then be found by

$$\boldsymbol{\sigma} = \boldsymbol{C}\boldsymbol{\varepsilon}, \tag{3.11}$$

which is the matrix equivalent of eq. 3.2, C the constitutive or material matrix and ε linearized engineering strain. Strain is defined by

$$\boldsymbol{\varepsilon} = \boldsymbol{B}\boldsymbol{u}, \tag{3.12}$$

where $\boldsymbol{B}$ is the composite of the strain-displacement operator and element transformation matrices (simplified notation, actually two separate matrices)

The onset of plastic behavior of the material is often considered a design violation (i.e. constraint) for elastostatic structural design. Therefore, this measure is a common constraint in structural design optimization. Plastic behavior of many metallic materials is commonly quantified using equivalent stress after Mises (1913), which is defined as

$$\sigma_e = \sqrt{\frac{1}{2}\left[(\sigma_{11}-\sigma_{22})^2 + (\sigma_{22}-\sigma_{33})^2 - (\sigma_{33}-\sigma_{11})^2 + 6\left(\sigma_{12}^2+\sigma_{23}^2+\sigma_{31}^2\right)\right]}. \tag{3.13}$$

In metallic material such as aluminum used here, the denotation of the onset of plastic deformation occurs when

$$\sigma_e > \sigma_y. \tag{3.14}$$

Some nonlinear effects are still of great consequence and this too can be analyzed. As the stability of the structure is of utmost importance, this can be shown dynamically (modal) and statically (buckling) through the following eigenvalue problems:

$$(\boldsymbol{K} - \lambda\boldsymbol{M})\,\boldsymbol{\Phi} = \boldsymbol{0} \tag{3.15}$$

and

$$(\boldsymbol{K} - \lambda \boldsymbol{K}^{\mathrm{geo}})\,\boldsymbol{\Phi} = \boldsymbol{0}, \tag{3.16}$$

respectively. Here $\boldsymbol{\lambda}$ is the vector eigenvalues and $\boldsymbol{\Phi}$ is the matrix of the corresponding eigenvectors. In the buckling case, $\boldsymbol{\lambda}$ is the load factor between the force applied f^{app} to calculate the geometric stiffness matrix and the force under which the structure loses stability,

$$f_{cr} = \lambda f_{\mathrm{app}}. \tag{3.17}$$

3.2.3 *Nonlinear analysis*

As linear structural mechanics is a special case, albeit a core of structural design optimization, it is not valid when analyzing crashworthiness and other transient nonlinear phenomenon. In structural-mechanical analysis there are three categories of nonlinearities:

1. Geometric nonlinearity
2. Constitutive nonlinearity
3. Boundary condition nonlinearity

These are introduced in the following.

Geometric nonlinearity

Geometric nonlinearities refer to large strains and large displacements that occur in a structure, that no longer allow the linearization of these terms. In linear analysis, a linearized engineering strain is used; in nonlinear cases, this is no longer valid. This is depicted in fig. 3.2, in which it is clear to see that there is a divergence of the after ca. 10% strain. Further, large displacements require a modification of the structural matrices (i.e. mass $\boldsymbol{M}$, damping $\boldsymbol{D}$ and stiffness $\boldsymbol{K}$). In nonlinear analyses, these are reassembled for every time step, demonstrating the geometric deformation of the prior steps.

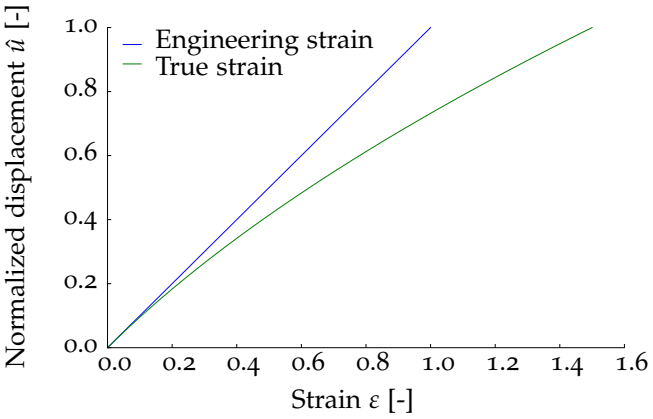

Figure 3.2: Comparison of linearized engineering strain with true strain

Constitutive nonlinearity

The behavior of a material can be nonlinear in several aspects including nonlinear elasticity, plasticity, strain rate dependency, damage as well as such time dependent aspects as creep and deterioration. Generally the constitutive relationship is dependent on the strain, strain rate and or time (as the case with creep),

$$C\left(\varepsilon, \dot{\varepsilon}, t\right). \tag{3.18}$$

In the following the concentration is placed on material behavior including plasticity, or the nonlinear stress–strain relationship (cf. fig. 3.3). The constitutive relationships used here will be discussed in § 3.4.

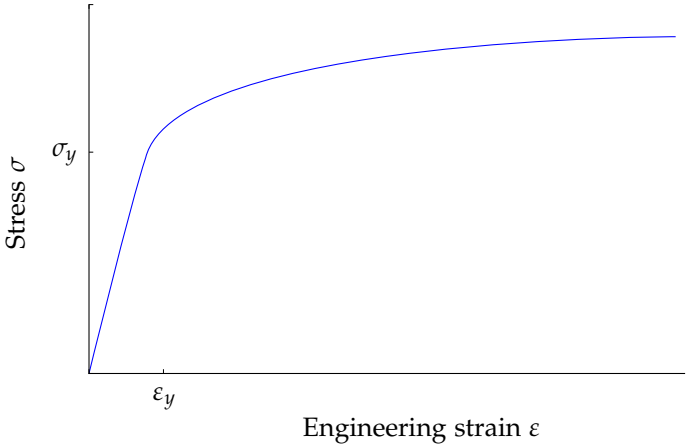

Figure 3.3: Exemplary stress–strain curve for a nonlinear constitutive relationship

Boundary condition nonlinearity

A further source of nonlinearities are in the boundary conditions of the problem. The Neumann and Dirichlet boundary conditions of eq. 3.1 can also be nonlinear. An example is Dirichlet boundary condition nonlinearity, commonly present in the analysis of impact loaded structures: This is found in the following in the form of contact:

$$u\left(\hat{u}\right). \tag{3.19}$$

In this case, the displacements u are dependent of previous displacements $\hat{u}$,

3.2.4 *Transient analysis*

For time-dependent processes, as the case is with impact, the force equilibrium equation must be integrated with respect to time. This requires temporal discretization schemes. There are two general methods for this: explicit and implicit time integration. These two methods will be introduced below, based on de Borst et al. (2012).

Transient nonlinear finite-element analysis with explicit time integration

The displacements are solved typically by using an iterative central differencing. After setting of the initial values for displacement $\boldsymbol{u}_0$ and velocity $\dot{\boldsymbol{u}}_0$, the following is calculated:

$$\dot{\boldsymbol{u}}_{\frac{1}{2}\Delta t} = \dot{\boldsymbol{u}}_0 + \frac{1}{2}\Delta t\ddot{\boldsymbol{u}}_0, \tag{3.20}$$

then for each time step (starting at $t = 0$),

$$\boldsymbol{u}_{t+\Delta t} = \boldsymbol{u}_t + \Delta t\dot{\boldsymbol{u}}_{t+\frac{1}{2}\Delta t}. \tag{3.21}$$

After updating $\boldsymbol{f}^{\text{ext}}$ and $\boldsymbol{f}^{\text{int}}$, the acceleration,

$$\ddot{\boldsymbol{u}}_{t+\Delta t} = \boldsymbol{M}^{-1}\left(\boldsymbol{f}^{\text{ext}}_{t+\Delta t} - \boldsymbol{f}^{\text{int}}{}_{t+\Delta t}\right), \tag{3.22}$$

is calculated. From this, once again the velocity,

$$\dot{\boldsymbol{u}}_{t+\frac{3}{2}\Delta t} = \dot{\boldsymbol{u}}_{t+\frac{1}{2}\Delta t} + \frac{1}{2}\Delta t\ddot{\boldsymbol{u}}_{t+\Delta t}, \tag{3.23}$$

and the displacement,

$$\boldsymbol{u}_{t+\frac{3}{2}\Delta t} = \boldsymbol{u}_{t+\frac{1}{2}\Delta t} + \Delta t\dot{\boldsymbol{u}}_{t+\Delta t}, \tag{3.24}$$

are calculated. This process is then continued to the end of the simulation time.

The maximum time step Δt is defined by the Courant–Friedrichs–Lewy condition (Courant et al. 1928), stating that it must be less than the time of a wave travels through the smallest finite element. This then dominates the computational effort needed for analysis and, therefore, necessitates well conditioned discretization of finite elements.

Transient nonlinear finite-element analysis with implicit time integration

In some cases it is more efficient to use an iterative method that allows for larger time steps. In implicit time integration after Newmark (1959), the residual R is set equal to o and a Newton–Raphson loop is used,

$$R = \boldsymbol{M}\ddot{\boldsymbol{u}}_{t+\Delta t} + \boldsymbol{D}\dot{\boldsymbol{u}}_{t+\Delta t} + \boldsymbol{f}_t^{\text{int}} - \boldsymbol{f}_{t+\Delta t}^{\text{ext}} = 0. \tag{3.25}$$

After setting $\boldsymbol{u}_0$ and $\dot{\boldsymbol{u}}_0$, the acceleration is calculated,

$$\ddot{\boldsymbol{u}}_0 = \boldsymbol{M}^{-1}\left(\boldsymbol{f}_0^{\text{ext}} - \boldsymbol{f}^{\text{int}}{}_0\right). \tag{3.26}$$

Then for each time step the following is done:

$$\dot{\boldsymbol{u}}_{t+\Delta t} = \dot{\boldsymbol{u}}_t + \Delta t\left((1-\gamma)\,\ddot{\boldsymbol{u}}_t + \gamma\ddot{\boldsymbol{u}}_{t+\Delta t}\right) \tag{3.27}$$

and

$$\boldsymbol{u}_{t+\Delta t} = \boldsymbol{u}_t + \Delta t\dot{\boldsymbol{u}}_t + \frac{1}{2}\Delta t^2\left((1-2\beta)\,\ddot{\boldsymbol{u}}_t + 2\beta\ddot{\boldsymbol{u}}_{t+\Delta t}\right), \tag{3.28}$$

where $\beta \in [0, 1]$ and γ is suggested to be 0.5 (Newmark 1959). After updating $\boldsymbol{f}^{\text{ext}}$ and $\boldsymbol{f}^{\text{int}}$, calculating

$$\ddot{\boldsymbol{u}}_{t+\Delta t} = \boldsymbol{M}^{-1}\left(\boldsymbol{f}_{t+\Delta t}^{\text{ext}} - \boldsymbol{f}^{\text{int}}{}_{t+\Delta t}\right). \tag{3.29}$$

As above, this is continued until the end of the simulation time. This method, in contrast to the explicit time integration, has the advantage of being independent of the smallest time step.

3.3 SIMPLIFIED MODELING OF CRASH ABSORBERS WITH ANALYTICAL RELATIONSHIPS

As transient nonlinear finite-element analysis requires high computational effort, its use can be limited in structural design optimization. Efficient modeling of crash absorbers, thin-walled, axially loaded compression-columns (fig. 3.4), can be achieved using analytical methods (Abramowicz and Jones 1984a,b, 1986 and Abramowicz 2003), in which an empirical-theoretical approach reduces the progressive buckling into basic collapse elements (fig. 3.5). Through proper triggering, the collapse mode behaves robustly in this nature and this was verified as such in quasistatic experiments. In the following these fundamental analytical relationships will be introduced limited to sections of square cross-sectional geometry.

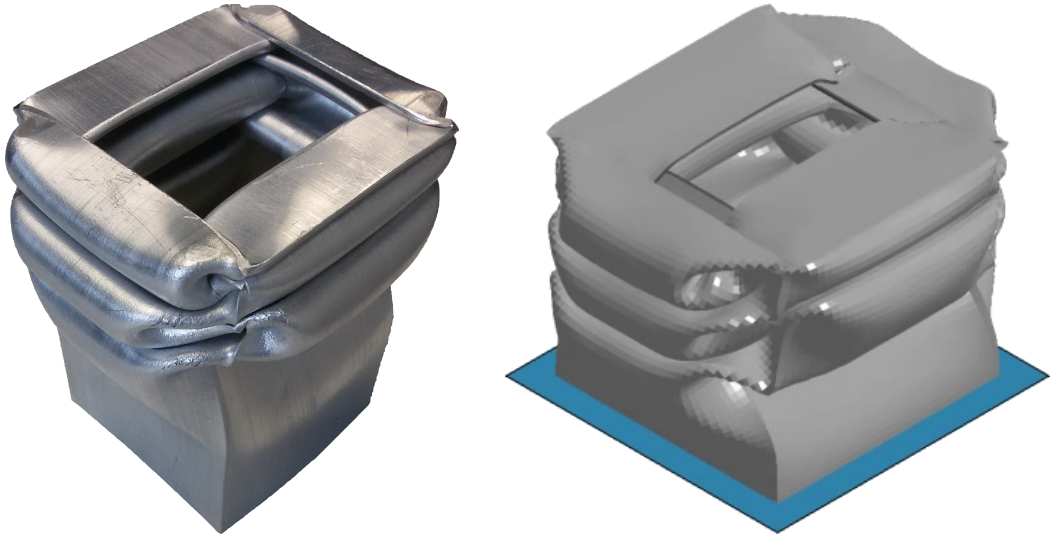

(a) Experiment (b) Simulation

Figure 3.4: Thin-walled, axially loaded, crash-absorbing section

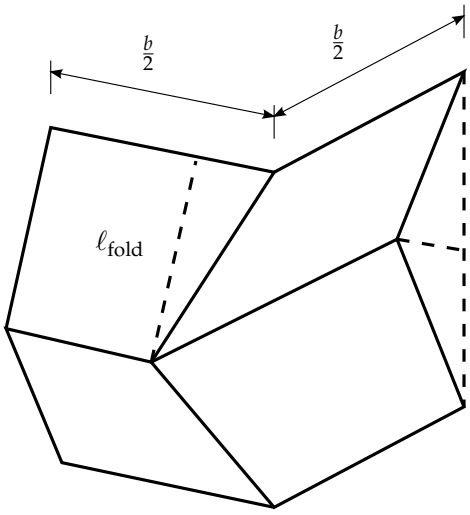

Figure 3.5: Basic collapse element for one corner (based on figure in Abramowicz and Jones 1984b)

The desired crushing mode of such crash absorbers can be broken down into a series of folds. The plastic moment M_o of each fold is defined for a single plastic hinge of a plot profile as (Abramowicz and Jones 1984b)

$$M_o = \sigma_y \frac{d^2}{4}, \tag{3.30}$$

where σ_y is the yield stress and d is the wall thickness. From the plastic moment, it is possible to calculate the mean force of the deformation or crushing process. This requires an empirical value found and is as follows (Abramowicz and Jones 1986):

$$f_{\text{mean}} = 38.12 M_0 \left(\frac{b}{d}\right)^{\frac{1}{3}}, \tag{3.31}$$

where b is the width of the fold. Further, from the mean force, the ideal energy absorption of the section $E_{\text{abs}}^{\text{ideal}}$ can be calculated using the effective length l_{eff},

$$E_{\text{abs}}^{\text{ideal}} = l_{\text{eff}} f_{\text{mean}}. \tag{3.32}$$

The deformation (crushing length) can be then calculated using the energy to be absorbed E_{abs} as follows:

$$u = \frac{E_{\text{abs}}}{f_{\text{mean}}}. \tag{3.33}$$

The maximum force is assumed to take place when the impact takes place causing the entire cross-section to deform plastically. This is an empirical value, though deviating from mechanical theory, has shown to work well to approximate the initial force. When this occurs, the folding of the section begins. Plastic deformation occurs, therefore, when

$$\begin{aligned} f_{\text{max}} &= a\sigma_y \\ &= \left((b+t)^2 - (b-d)^2\right)\sigma_y. \end{aligned} \tag{3.34}$$

As the crash absorbing sections in this study include trigger geometry to reduce this initial force, a knockdown factor is introduced as follows:

$$f_{\text{max,triggered}} = \frac{f_{\text{max}}}{c_{\text{kd}}}. \tag{3.35}$$

The trigger geometry further ensures an initial, proper folding mode. This was done by indenting two opposite sides (fig. 7.4) such that the progressive buckling would be initiated with a length of ℓ_{fold} (fig. 3.5). Typical numerical values for the knockdown factor vary from unity for no effect to two where the half of the cross section has been compromised. Values higher than two are physically possible but do not make sense

as the initial force would sink below that of the average, which is inefficient for the energy absorption.

As proper folding is to be promoted, a progressive local buckling is desired. The critical stress of elastostatic flat plate (i.e. one side of the square section) is used to ensure that the plate buckles and, therefore, folds (Timoshenko and Gere 1963),

$$\sigma_{cr} = \frac{4\pi^2 E}{12\left(1-\nu^2\right)}\left(\frac{d}{b}\right)^2, \tag{3.36}$$

where here E is the Young's modulus and ν is the Poisson's ratio.

To guarantee that the crash absorber does not simply buckle globally (i.e. kink and break away) when loaded, global buckling is also analyzed using the critical force,

$$f_{cr} = \frac{\pi^2 E I}{4\ell^2}, \tag{3.37}$$

where I is the second moment of area. Although eqs. 3.36–3.37 are a conservative simplification for the dynamic, elastoplastic nature of crushing, this method was utilized by the author and was shown to work well in both empirical and numerical studies (cf. Fellner 2013 and Xu 2014).

3.4 CONSTITUTIVE MODELS

The constitutive or material models used in this work will be discussed here. As the aluminum material used here has shown to be generally strain-rate independent for the range of strain rates seen here, this will not be considered. The material is also considered to be isotropic, i.e. uniform material properties in all directions. Other aspects such as those of thermomechanical nature have been neglected. The constitutive equation of material behavior is defined by the constitutive matrix $\boldsymbol{C}$, which connects element strains to element stresses (cf. eqs. 3.2–3.11).

In the linear cases here, it is sufficient to describe the material by its elasticity with the Young's modulus E, its transverse contraction via the Poisson's ratio ν and its density ρ (for dynamics and mass calculation). In the following, deterministic constitutive models for aluminum alloy AW EN-6060 T6 will be introduced; in the next chapter uncertain models will be discussed (§ 4).

3.4.1 *Linear elastostatic material models*

For structures that are designed using linear elastic analysis, linear constitutive models are used. This model is defined by

- Young's modulus
- Poisson's ratio

Table 3.1: Linear elastostatic model for aluminum alloy AW EN-6060 T6

Property	Symbol	Value	Unit
Young's modulus	E	70,000	MPa
Poisson's ratio	ν	0.3	–
Yield stress	σ_y	200	MPa
Density	ρ	2.693	$\times 10^{-9}\,\mathrm{t/mm^3}$

- yield strength
- density,

and the values of which are found in tab. 3.1.

3.4.2 *Nonlinear constitutive models*

Three nonlinear constitutive models have been developed for aluminum alloy AW EN-6060 T6 for use in nonlinear simulations. These three will be explained in the following. Material failure (i.e. tearing, ripping etc.) and strain-rate dependency are not considered here (cf. Morasch et al. 2014).

Bilinear

A bilinear model is the simplest constitutive model for the consideration of plasticity. A tangent modulus K_α is used to describe the strain hardening, i.e. the plastic zone after the yield stress has been reached. If the tangent modulus K_α is equal to zero, i.e. parallel to the x-axis, no strain hardening is present and the material behavior is referred to as ideal elastoplastic. In addition to the material properties found in the model for AW EN-6060 T6 in tab. 3.1, the tangent modulus is $K_\alpha = 1000\,\mathrm{MPa}$.

Ramberg and Osgood

A parametric constitutive model for material nonlinearity of problems that are static or of quasistatic nature with hardening is defined by Ramberg and Osgood (1943) as

$$\varepsilon = \frac{\sigma}{E} + \alpha \frac{\sigma_y}{E} \left(\frac{\sigma}{\sigma_y} \right)^n , \tag{3.38}$$

where α is the strain-hardening constant. Though showing good agreement for small plastic strains for many aluminum alloys, it is not appropriate for large strains as the case with crash simulations.

Table 3.2: Nonlinear model after Hockett and Sherby for aluminum alloy AW EN-6060 T6

Parameter	Symbol	Value	Unit
Saturation stress	σ_S	250	MPa
Plastic stress	σ_{pl}	50	MPa
Strain-hardening coefficient	c	10	–
Strain-hardening exponent	n	0.75	–

Hockett and Sherby

A further constitutive relationship was modeled after Hockett and Sherby (1975) to describe the nonlinear behavior of the aluminum alloy EN AW-6060 T6, which is described by the following:

$$\sigma = \sigma_y + \sigma_{pl} - \sigma_{pl} e^{-c\varepsilon_{pl}^n}, \tag{3.39}$$

where the stress state σ is dependent on the plastic strain state ε_{pl} , yield stress σ_y, the maximum plastic stress σ_{pl}, the strain-hardening constants c and n, as well as the exponential function e (≈ 2.7183). Plastic stress is used here to define the difference between saturation stress σ_S and yield stress σ_y,

$$\sigma_{pl} = \sigma_S - \sigma_y. \tag{3.40}$$

The properties for the model after Hockett and Sherby are found in tab. 3.2 (cf. tab. 3.1)

3.5 DESIGN OPTIMIZATION WITH STRUCTURAL-MECHANICAL ANALYSIS

Neglecting equality constraints h and expanding eq. 2.2 to account for the system equations of structural mechanics, the complete and general structural optimization problem is

$$
\begin{aligned}
\text{minimize} \quad & \mathsf{f}(\mathbf{x}) && \mathbf{x} \in \mathbb{R}^n \\
\text{so that} \quad & \mathsf{g}_j(\boldsymbol{r}(\mathbf{x})) \leq 0 && j \in \mathbb{N}[1, p] \\
& \mathsf{x}^L{}_i \leq \mathsf{x}_i \leq \mathsf{x}^U{}_i && i \in \mathbb{N}[1, n] \\
\text{where} \quad & \mathbf{x} = \begin{bmatrix} \mathsf{x}_1 & \mathsf{x}_2 & \dots & \mathsf{x}_n \end{bmatrix}^T \\
\text{governed by} \quad & \sigma_{ij,j} + \rho f_i = \rho \ddot{u}_i && \text{in } \Omega \\
& u_i = \hat{u}_i && \text{on } \Gamma_D \\
& \sigma_{ij} \cdot n = t_i && \text{on } \Gamma_N \\
& u_0 && \text{in } \Omega \\
& \dot{u}_0 && \text{in } \Omega \\
& \sigma_{ij} = C_{ijkl} u_{k,l}, &&
\end{aligned}
\tag{3.41}
$$

where the system responses $\boldsymbol{r}(\mathbf{x})$ and therefore the constraints $\mathbf{g}$ are derived from the system equations, i.e. u, $\dot{u}$, $\ddot{u}$, σ. In structural design optimization, the mass is typically the objective function, as it is here. This is a function of the density ρ and the volume of the body Ω.

The system equations are solved using the finite-element method, which has the advantage that the sensitivities of the response with respect to the design variables (or uncertain parameters) are often available. This will be explained in the following sections.

3.5.1 *Design sensitivities in linear elastostatic finite-element analysis*

Starting from the basic linear-elastostatic finite-element equations (repeated eqs. 3.10–3.12)

$$
\begin{aligned}
\boldsymbol{f}^{\text{ext}} &= \boldsymbol{K}\boldsymbol{u} \\
\boldsymbol{\varepsilon} &= \boldsymbol{B}\boldsymbol{u} \\
\boldsymbol{\sigma} &= \boldsymbol{C}\boldsymbol{\varepsilon},
\end{aligned}
$$

the derivatives with respect to the design variables x_i are

$$
\frac{\partial \boldsymbol{f}^{\text{ext}}}{\partial \mathsf{x}_i} = \frac{\partial \boldsymbol{K}}{\partial \mathsf{x}_i}\boldsymbol{u} + \boldsymbol{K}\frac{\partial \boldsymbol{u}}{\partial \mathsf{x}_i} \tag{3.42}
$$

and after reforming,

$$\frac{\partial \boldsymbol{u}}{\partial \mathrm{x}_i} = \boldsymbol{K}^{-1}\left(\frac{\partial \boldsymbol{f}^{\mathrm{ext}}}{\partial \mathrm{x}_i} - \frac{\partial \boldsymbol{K}}{\partial \mathrm{x}_i}\boldsymbol{u}\right). \tag{3.43}$$

As in most cases (except e.g. where self-weight plays a role) the sensitivity of the external force with respect to the design variables is zero, this further simplifies to

$$\frac{\partial \boldsymbol{u}}{\partial \mathrm{x}_i} = -\boldsymbol{K}^{-1}\frac{\partial \boldsymbol{K}}{\partial \mathrm{x}_i}\boldsymbol{u}. \tag{3.44}$$

As will be seen in the next chapter, the uncertainty analyses here use optimization algorithms and if the uncertain parameter is the external force, the sensitivity with respect to the uncertain parameter is then

$$\frac{\partial \boldsymbol{u}}{\partial \boldsymbol{f}^{\mathrm{ext}}} = \boldsymbol{K}^{-1}. \tag{3.45}$$

For the stress sensitivities, we begin with the strain sensitivities

$$\frac{\partial \boldsymbol{\varepsilon}}{\partial \mathrm{x}_i} = \frac{\partial \boldsymbol{B}}{\partial \mathrm{x}_i}\boldsymbol{u} + \boldsymbol{B}\frac{\partial \boldsymbol{u}}{\partial \mathrm{x}_i}, \tag{3.46}$$

then using these to find

$$\frac{\partial \boldsymbol{\sigma}}{\partial \mathrm{x}_i} = \frac{\partial \boldsymbol{C}}{\partial \mathrm{x}_i}\boldsymbol{\varepsilon} + \boldsymbol{C}\frac{\partial \boldsymbol{\varepsilon}}{\partial \mathrm{x}_i}. \tag{3.47}$$

Generally this can be written as

$$\frac{\partial \boldsymbol{\sigma}}{\partial \mathrm{x}_i} = \underbrace{\frac{\partial \boldsymbol{C}}{\partial \mathrm{x}_i}\boldsymbol{B}\boldsymbol{u}}_{\text{material sensitivities}} + \underbrace{\boldsymbol{C}\frac{\partial \boldsymbol{B}}{\partial \mathrm{x}_i}\boldsymbol{u}}_{\text{shape sensitivities}} + \underbrace{\boldsymbol{C}\boldsymbol{B}\boldsymbol{K}^{-1}\left(\frac{\partial \boldsymbol{f}^{\mathrm{ext}}}{\partial \mathrm{x}_i} - \frac{\partial \boldsymbol{K}}{\partial \mathrm{x}_i}\boldsymbol{u}\right)}_{\text{sizing or general sensitivities}}, \tag{3.48}$$

showing which terms play a role in which type of optimization: material, shape and sizing or general. The last referred to as general because the sensitivity of the stiffness matrix with respect to the design variables $\frac{\partial \boldsymbol{K}}{\partial \mathrm{x}_i}$ plays a role in material, shape and sizing sensitivities.

3.5.2 *Design sensitivities in transient nonlinear structural-mechanical analysis*

Beginning with the equilibrium of the force method (repeating eq. 3.9):

$$\boldsymbol{M}\ddot{\boldsymbol{u}} = \boldsymbol{f}^{\mathrm{ext}} - \boldsymbol{f}^{\mathrm{int}}, \tag{3.49}$$

the derivative with respect to the design variables x_i is

$$\frac{\partial}{\partial \mathrm{x}_i}\left(\boldsymbol{M}\ddot{\boldsymbol{u}}\right) = \frac{\partial}{\partial \mathrm{x}_i}\left(\boldsymbol{f}^{\mathrm{ext}} - \boldsymbol{f}^{\mathrm{int}}\right) \tag{3.50}$$

and, therefore,

$$\frac{\partial \boldsymbol{M}}{\partial \mathrm{x}_i}\ddot{\boldsymbol{u}} + \boldsymbol{M}\frac{\partial \ddot{\boldsymbol{u}}}{\partial \mathrm{x}_i} = \frac{\partial \boldsymbol{f}^{\mathrm{ext}}}{\partial \mathrm{x}_i} - \frac{\partial \boldsymbol{f}^{\mathrm{int}}}{\partial \mathrm{x}_i}. \tag{3.51}$$

Rearranging eq. 3.51 to solve for $\frac{\partial \ddot{\boldsymbol{u}}}{\partial \mathrm{x}_i}$ results in

$$\frac{\partial \ddot{\boldsymbol{u}}}{\partial \mathrm{x}_i} = \boldsymbol{M}^{-1}\left(\frac{\partial \boldsymbol{f}^{\mathrm{ext}}}{\partial \mathrm{x}_i} - \frac{\partial \boldsymbol{f}^{\mathrm{int}}}{\partial \mathrm{x}_i} - \frac{\partial \boldsymbol{M}}{\partial \mathrm{x}_i}\ddot{\boldsymbol{u}}\right). \tag{3.52}$$

from which $\frac{\partial \boldsymbol{u}}{\partial \mathrm{x}_i}$ and $\frac{\partial \dot{\boldsymbol{u}}}{\partial \mathrm{x}_i}$ can be calculated in the following sections, depending on the time integration scheme chosen.

3.5.2.1 *Sensitivities using the force method with explicit time integration*

The derivatives are then found analogously to § 3.2.4. This method was implemented and verified by Schroll (2013). First, the initialization is performed $\frac{\partial \boldsymbol{u}_0}{\partial \mathrm{x}_i} = \frac{\partial \dot{\boldsymbol{u}}_0}{\partial \mathrm{x}_i} = \frac{\partial \ddot{\boldsymbol{u}}_0}{\partial \mathrm{x}_i} = 0$ and

$$\frac{\partial \dot{\boldsymbol{u}}_{\frac{1}{2}\Delta t}}{\partial \mathrm{x}_i} = \frac{\partial \dot{\boldsymbol{u}}_0}{\partial \mathrm{x}_i} + \frac{1}{2}\Delta t\frac{\partial \ddot{\boldsymbol{u}}_0}{\partial \mathrm{x}_i}. \tag{3.53}$$

For each time step

$$\frac{\partial \boldsymbol{u}_{t+\Delta t}}{\partial \mathrm{x}_i} = \frac{\partial \boldsymbol{u}_t}{\partial \mathrm{x}_i} + \Delta t\frac{\partial \dot{\boldsymbol{u}}_{t+\frac{1}{2}\Delta t}}{\partial \mathrm{x}_i} \tag{3.54}$$

and then after updating $\frac{\partial \boldsymbol{f}^{\mathrm{ext}}}{\partial \mathrm{x}_i}$ and $\frac{\partial \boldsymbol{f}^{\mathrm{int}}}{\partial \mathrm{x}_i}$, calculating

$$\frac{\partial \ddot{\boldsymbol{u}}_{t+\Delta t}}{\partial \mathrm{x}_i} = \boldsymbol{M}^{-1}\left(\frac{\partial \boldsymbol{f}^{\mathrm{ext}}_{t+\Delta t}}{\partial \mathrm{x}_i} - \frac{\partial \boldsymbol{f}^{\mathrm{int}}_{t+\Delta t}}{\partial \mathrm{x}_i} - \frac{\partial \boldsymbol{M}}{\partial \mathrm{x}_i}\ddot{\boldsymbol{u}}_{t+\Delta t}\right) \tag{3.55}$$

and

$$\frac{\partial \dot{\boldsymbol{u}}_{t+\frac{3}{2}\Delta t}}{\partial \mathrm{x}_i} = \frac{\partial \dot{\boldsymbol{u}}_{t+\frac{1}{2}\Delta t}}{\partial \mathrm{x}_i} + \frac{1}{2}\Delta t\frac{\partial \ddot{\boldsymbol{u}}_{t+\Delta t}}{\partial \mathrm{x}_i}. \tag{3.56}$$

3.5.2.2 *Sensitivities using the force method with implicit time integration*

For the sensitivities of the residual R with respect to some variable x is zero:

$$\frac{\partial R}{\partial \mathrm{x}_i} = \frac{\partial}{\partial \mathrm{x}_i}\left(\boldsymbol{M}\ddot{\boldsymbol{u}}_{t+\Delta t} + \boldsymbol{f}^{\mathrm{int}}_t - \boldsymbol{f}^{\mathrm{ext}}_{t+\Delta t}\right) = 0 \tag{3.57}$$

and, therefore,

$$\frac{\partial R}{\partial x_i} = \frac{\partial \boldsymbol{M}}{\partial x_i}\ddot{\boldsymbol{u}}_{t+\Delta t} + \boldsymbol{M}\frac{\partial \ddot{\boldsymbol{u}}_{t+\Delta t}}{\partial x_i} + \frac{\partial \boldsymbol{f}_t^{\text{int}}}{\partial x_i} - \frac{\partial \boldsymbol{f}_{t+\Delta t}^{\text{ext}}}{\partial x_i} = 0. \tag{3.58}$$

Now we can calculate

$$\frac{\partial \dot{\boldsymbol{u}}_{t+\Delta t}}{\partial x_i} = \frac{\partial \dot{\boldsymbol{u}}_t}{\partial x_i} + (1-\gamma)\,\Delta t\frac{\partial \ddot{\boldsymbol{u}}_t}{\partial x_i} + \gamma\Delta t\frac{\partial \ddot{\boldsymbol{u}}_{t+\Delta t}}{\partial x_i}, \tag{3.59}$$

$$\boldsymbol{u}_{t+\Delta t} = \boldsymbol{u}_t + \Delta t\dot{\boldsymbol{u}}_t + (1-2\beta)\,\frac{1}{2}\Delta t^2\frac{\partial \ddot{\boldsymbol{u}}_t}{\partial x_i} + 2\beta\frac{1}{2}\Delta t^2\frac{\partial \ddot{\boldsymbol{u}}_{t+\Delta t}}{\partial x_i}, \tag{3.60}$$

and

$$\frac{\partial \ddot{\boldsymbol{u}}_{t+\Delta t}}{\partial x_i} = -\boldsymbol{M}^{-1}\left(\frac{\partial \boldsymbol{M}}{\partial x_i}\ddot{\boldsymbol{u}}_{t+\Delta t} + \frac{\partial \boldsymbol{f}_t^{\text{int}}}{\partial x_i} - \frac{\partial \boldsymbol{f}_{t+\Delta t}^{\text{ext}}}{\partial x_i}\right). \tag{3.61}$$

3.5.3 *Summary of sensitivities in nonlinear analysis*

Different design optimization and sensitivity analyses have different independent parameters (here x_i). A summary of the sensitivity equations depending on these and the time integration scheme is provided in tab. 3.3.

The successful use of analytical design sensitivities is shown in § 5, albeit without the complexities of bifurcations and contact. This, along with the practical aspects computational effort and memory usage, would need to be investigated before any assertion to general validity is given.

Table 3.3: Sensitives of acceleration with respect to different categories of independent parameters

Independent parameter x_i	Nonlinear stiffness method	Nonlinear force method
General	$\frac{\partial \ddot{\boldsymbol{u}}}{\partial x_i} = \boldsymbol{M}^{-1}\left(\frac{d f^{\text{ext}}}{\partial x_i} - \frac{\partial \boldsymbol{M}}{\partial x_i}\ddot{\boldsymbol{u}} - \frac{\partial \boldsymbol{D}}{\partial x_i}\dot{\boldsymbol{u}} - \boldsymbol{D}\frac{\partial \dot{\boldsymbol{u}}}{\partial x_i} - \frac{\partial \boldsymbol{K}}{\partial x_i}\boldsymbol{u} - \boldsymbol{K}\frac{\partial \boldsymbol{u}}{\partial x_i}\right)$	$\frac{\partial \ddot{\boldsymbol{u}}}{\partial x_i} = \boldsymbol{M}^{-1}\left(\frac{\partial f^{\text{ext}}}{\partial x_i} - \frac{\partial f^{\text{int}}}{\partial x_i} - \frac{\partial \boldsymbol{M}}{\partial x_i}\ddot{\boldsymbol{u}}\right)$
Shape	$\frac{\partial \ddot{\boldsymbol{u}}}{\partial x_i} = -\boldsymbol{M}^{-1}\left(\frac{\partial \boldsymbol{M}}{\partial x_i}\ddot{\boldsymbol{u}} + \frac{\partial \boldsymbol{D}}{\partial x_i}\dot{\boldsymbol{u}} + \boldsymbol{D}\frac{\partial \dot{\boldsymbol{u}}}{\partial x_i} + \frac{\partial \boldsymbol{K}}{\partial x_i}\boldsymbol{u} + \boldsymbol{K}\frac{\partial \boldsymbol{u}}{\partial x_i}\right)$	$\frac{\partial \ddot{\boldsymbol{u}}}{\partial x_i} = -\boldsymbol{M}^{-1}\left(\frac{\partial f^{\text{int}}}{\partial x_i} + \frac{\partial \boldsymbol{M}}{\partial x_i}\ddot{\boldsymbol{u}}\right)$
Material	$\frac{\partial \ddot{\boldsymbol{u}}}{\partial x_i} = -\boldsymbol{M}^{-1}\left(\frac{\partial \boldsymbol{M}}{\partial x_i}\ddot{\boldsymbol{u}} + \frac{\partial \boldsymbol{D}}{\partial x_i}\dot{\boldsymbol{u}} + \boldsymbol{D}\frac{\partial \dot{\boldsymbol{u}}}{\partial x_i} + \frac{\partial \boldsymbol{K}}{\partial x_i}\boldsymbol{u} + \boldsymbol{K}\frac{\partial \boldsymbol{u}}{\partial x_i}\right)$	$\frac{\partial \ddot{\boldsymbol{u}}}{\partial x_i} = -\boldsymbol{M}^{-1}\left(\frac{\partial f^{\text{int}}}{\partial x_i} + \frac{\partial \boldsymbol{M}}{\partial x_i}\ddot{\boldsymbol{u}}\right)$
External force	$\frac{\partial \ddot{\boldsymbol{u}}}{\partial x_i} = \boldsymbol{M}^{-1}\left(\boldsymbol{1} - \boldsymbol{D}\frac{\partial \dot{\boldsymbol{u}}}{\partial x_i} - \boldsymbol{K}\frac{\partial \boldsymbol{u}}{\partial x_i}\right)$	$\frac{\partial \ddot{\boldsymbol{u}}}{\partial x_i} = \boldsymbol{M}^{-1}\left(\boldsymbol{1} - \frac{\partial f^{\text{int}}}{\partial x_i}\right)$

4

UNCERTAINTY MODELING IN STRUCTURAL DESIGN OPTIMIZATION

Le doute n'est pas une condition agréable, mais la certitude est absurde.[1]

Voltaire in a letter to Frederick II of Prussia (April 6, 1767)

4.1 UNCERTAINTY, ROBUSTNESS AND RELIABILITY

There is no actual physical phenomenon such as probability or, in this case, fuzziness; instead they are simply models to represent and understand the effects of lack of knowledge in decision and analysis.

The world is indeed deterministic: there is only one set of inputs and one set of outputs for any single event. Consideration of uncertainty allows the representation of incomplete knowledge. This is relevant for the input parameters, the initial conditions and even the model, which we use. None of these can be fully known and understood. It can be that the influence of our lack of knowledge is small, thus allowing us to forgo its inclusion. Even for well understood phenomena, there are certain levels of uncertainty in our models. A single structure has a deterministic geometry, load, material and structural response. Yet determining the exact system inputs for each structure (in this case geometry, load, and material model) is not always possible and, therefore, not is the system responses (e.g. stress, buckling force, displacement).

We are going to design a structure to the theoretical optimal geometry, but manufacturing errors, natural variation of loading characteristics and further simplified, abstract models are used neglecting certain aspects. These are all imperfections to the "perfect" model of the system and data that we are able to use. The exact degree of these imperfections is uncertain, though certain bounds can be derived through empirical engineering knowledge.

Further, the difference between robustness and reliability is defined here as the following: *Robustness* is the amount that the response varies with respect to the uncertainty of the input. *Reliability* is the ability of a design constraint to remain nonviolated considering variation, irrespective of the amount of variation in the input parameters. It is, therefore, possible that a structure is reliable, yet not robust and vice versa.

1 Doubt is not an agreeable condition, but certainty is an absurd one.

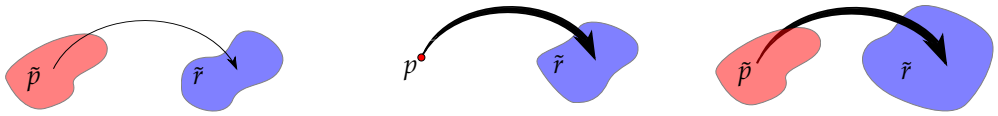

(a) Mapping of an uncertain parameter $\tilde{p}$ onto an uncertain response $\tilde{r}$

(b) Uncertain mapping of a parameter p onto an uncertain response $\tilde{r}$

(c) Uncertain mapping of an uncertain parameter p onto an uncertain response $\tilde{r}$

Figure 4.1: Mapping in uncertain domain

4.2 DEALING WITH UNCERTAINTY

Uncertainty analysis is defined by the mapping of uncertain input parameters $\tilde{p}$ onto uncertain response parameters $\tilde{r}$. The mapping operator $\mapsto$ can also itself be uncertain, designated as $\tilde{\mapsto}$. This results in three general mappings in uncertain domain (4.1):

$$\tilde{p} \mapsto \tilde{r} \tag{4.1}$$
$$p \tilde{\mapsto} \tilde{r} \tag{4.2}$$
$$\tilde{p} \tilde{\mapsto} \tilde{r}. \tag{4.3}$$

In this work, the concentration will be on a $\tilde{p} \mapsto \tilde{r}$ as a deterministic mapping (via finite-element analysis) is assumed.

4.2.1 *Safety factors*

Traditionally in engineering design, safety factors γ have been used to deal with such uncertainty (Elishakoff 2001, 2004 and Choi et al. 2006). Safety factors are empirically derived "smudge" factors and are defined by the relationship of some structural response r to its limit c,

$$\gamma = \frac{r}{c}. \tag{4.4}$$

A further development of this approach is the use of partial safety factors, which instead of one global safety factor, assign safety factors directly to the sources of uncertainty, e.g. to loading and material separately. This factor on the load is referred to as a partial safety factor and is defined by the ratio of the design load to the maximum expected load,

$$f_{\text{des}} = \gamma_f \cdot f, \tag{4.5}$$

and to the material,

$$\sigma_{\text{des}} = \frac{\sigma_y}{\gamma_M}. \tag{4.6}$$

Partial safety factors are typically determined via probabilistic methods.

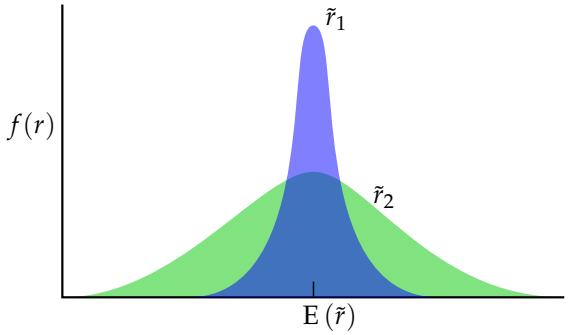

Figure 4.2: Probabilistic robustness comparing two uncertain responses with different variances yet the same mean

In this approach, robustness has no tangible meaning as the amount that the response varies is not ascertained. Reliability is maintained via the safety factor, which creates a gap between response and limit.

Safety factors are well established methods, understood by designers and easy to implement in the development process, including structural design process. Further, use of safety factors typically requires no further computational effort, which is not the case with the methods introduced below. Though, as they do not ascertain the actual effect of uncertain input parameters on the system responses, use of safety factors can lead to over- or underbuilt systems and structures.

4.2.2 *Probability theory*

Probability theory has become the standard method of dealing with uncertainty in structural design. In order to better clarify the possibilistic methods, the concentration of this work, probability will be briefly introduced; further details and explanation can be found in the literature used for this summary (Elishakoff 1999, Choi et al. 2006, Maymon 2008 and Lemaire 2014).

Robustness $\mathcal{R}$ is often understood in the probabilistic domain as the uncertain response's variance (or standard deviation). Fig. 4.2 demonstrates the comparison of two system responses with varying variance. Robustness is, thus, the ratio of the variance of the input parameters to variance of the system response. Other definitions of robustness can be found defined by Jurecka (2007).

Probability of failure $P_{\mathcal{F}}$ is

$$P_{\mathcal{F}} = P\left(\mathrm{g} < 0\right), \tag{4.7}$$

where g is defined as the constraint or state function, here set to be feasible where it has a value less then zero (cf. eq. 2.2). The probability of failure is then the probability that the uncertain response $\tilde{r}$ violates the uncertain state limit $\tilde{c}$,

$$P_{\mathcal{F}} = P\left(c < r\right), \tag{4.8}$$

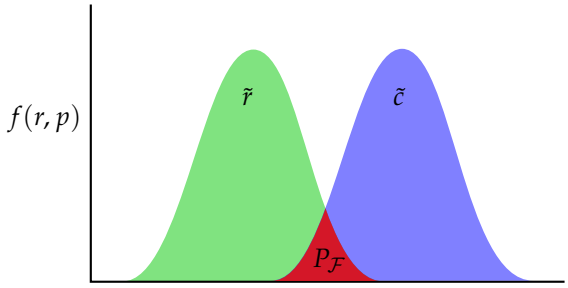

Figure 4.3: Probabilistic reliability considering exemplary distributions of an uncertain response and its state limit

e.g. stress and strength. The probability of failure is the area of this overlap (fig. 4.3) Reliability is then defined as $1 - P_{\mathcal{F}}$.

Here statistical information is needed for the modeling of the uncertain parameters (Gaussian, Weibull, etc.). After this is completed, probability of failure and robustness can be calculated by various methods. Typically those used are Monte Carlo simulations or first-order and second-order reliability methods (FORM and SORM, respectively). Further approximation methods can be used to reduce the computational effort. As these methods are outside the scope of this work, refer to Elishakoff (1999), Choi et al. (2006) and Bucher (2009).

4.2.3 *Interval theory*

Interval and anti-optimization methods (only worst-case side of interval) can be used in worst-case design of structures. Use of intervals can be attested at least to Archimedes of Syracuse (ca. 287–212 BC) with his accurate approximation of π, which he achieved via bounding of the solution.

Intervals are useful to model uncertainty, especially where only bounds of uncertain parameters are known. An interval parameter is defined by

$$\tilde{p} = \left[\begin{array}{cc} \underline{p} & \overline{p} \end{array} \right], \tag{4.9}$$

where $\underline{p}$ and $\overline{p}$ are the upper and lower bounds of the uncertain parameter, respectively. The analysis using intervals can be carried out via interval arithmetic or optimization and anti-optimization to find the minimum and maximum response values. The latter is utilized here.

Although interval arithmetic is efficient, it can greatly overestimate uncertainty because of *interval dependency problem*. This is exemplified via the simple example of $\tilde{p} - \tilde{p}$, which of course is zero. Standard interval arithmetic gives a solution of $[\underline{p} - \underline{p} \quad \overline{p} + \overline{p}]$, as the parameters are handled independently. In the system of linear equations of structural-mechanical analysis, this would then treat e.g. the Young's modu-

lus E of every component (every degree of freedom for every element) as independent, leading to greatly exaggerated uncertain bounds. Further, a finite-element code is needed that is able to calculate with interval arithmetic. To avoid both of these problems, methods based on optimization and anti-optimization can be used. These methods are not hampered by the interval dependency and can be easily interfaced to commercial structural-mechanical analysis software. Further details can be found in Moore et al. (2009), Zhang (2005), Ben-Haim (1994) and Elishakoff et al. (1994).

Variation is measured in intervals as the width of the interval and its normalized equivalent,

$$\overline{p} - \underline{p} \tag{4.10}$$

and

$$\frac{\overline{p} - \underline{p}}{\frac{1}{2}\left(\overline{p} + \underline{p}\right)}, \tag{4.11}$$

respectively. Interval robustness is then defined as the ratio of variation of the input parameters to the response. As there can be several uncertain input parameters, these are summed—revealing the definition of interval robustness as

$$\mathcal{R}_r = \frac{\sum\left(\overline{p} - \underline{p}\right)}{\overline{r} - \underline{r}} \tag{4.12}$$

and

$$\hat{\mathcal{R}}_r = \frac{\sum \frac{\overline{p} - \underline{p}}{\frac{1}{2}\left(\overline{p} + \underline{p}\right)}}{\frac{\overline{r} - \underline{r}}{\frac{1}{2}\left(\overline{r} + \underline{r}\right)}}. \tag{4.13}$$

Reliability is not possible within the context of interval theory. One can only take into consideration if the interval response violates a constraint, giving a digital zero or unity response, i.e. possible or not possible. This can also be of interest to the design engineer as the response is known for all uncertainty.

As intervals are treated here as a specific case of possibility theory, namely $\tilde{p} = \text{int}\,\langle a, b\rangle$, the methods of calculation and evaluation are discussed below in § 4.2.4.

4.2.4 *Possibility theory*

Possibility theory is an extension of interval theory (cf. § 4.2.3) and is a nontraditional approach to the imprecise and the uncertain (Dubois and Prade 1988). In the following section it will be explained the meaning of fuzzy models, or fuzzy numbers, and how to construct such models for uncertainty. Thereafter, their evaluation process will be shown.

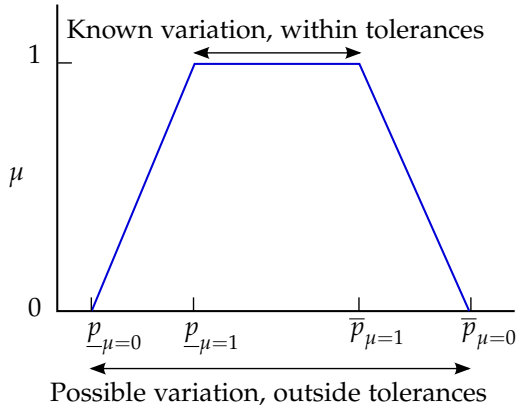

Figure 4.4: Meaning of fuzzy number explained

4.2.4.1 *Interpretation of fuzziness*

A fuzzy number is defined by a membership function using possibility μ varying from zero to unity, approaching impossible to fully possible. In this dissertation, the understanding of possibility has been developed in which known variance is represented by $\mu = 1$, e.g. through dimensioning tolerances, and worst-case possible variance is represented by $\mu = 0$. A known variance can be understood as variation in values within tolerance and possible tolerance as worst case variation, which is outside of permissible tolerances (fig. 4.4). Other understandings of fuzziness can be found in Dubois and Prade (1988), Möller and Beer (2004) and Hanss (2005).

The area $\mathcal{A}_p$ underneath the membership function,

$$\mathcal{A}_p = \int_0^1 p \, d\mu, \tag{4.14}$$

indicates the variation possible in a parameter, referred to here as *fuzzy uncertainty*. The robustness of a fuzzy system is defined by the ratio of the area $\mathcal{A}_p$ of the input parameters to that of the system response, i.e. fuzzy uncertainty of the input parameters to the fuzzy uncertainty of the responses, as follows:

$$\mathcal{R}_r = \frac{\mathcal{A}_p}{\mathcal{A}_r}. \tag{4.15}$$

Generally, systems of interest in structural mechanics have more than one uncertain input parameter and then the uncertainties (areas) are summed,

$$\mathcal{R}_r = \frac{\sum \mathcal{A}_p}{\mathcal{A}_r}. \tag{4.16}$$

In order to compare the robustness of different structures, the following system robustness will be used:

$$\mathcal{R}_{\text{sys}} = \frac{\sum_i \mathcal{R}_{p,i}}{\sum_i \mathcal{R}_{r,i}}. \tag{4.17}$$

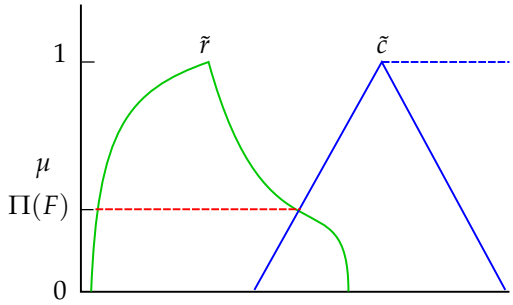

Figure 4.5: Possibility of failure with a fuzzy system response and a fuzzy state limit

As the fuzzy numbers can vary greatly in magnitude, a normalization of the fuzzy number is first carried out by dividing by the midpoint of $\mu = 1$,

$$\hat{\tilde{p}} = \frac{\tilde{p}}{\frac{1}{2}\left(\overline{p}_{\mu=1} + \underline{p}_{\mu=1}\right)}. \tag{4.18}$$

As robustness serves only of a comparison measure of different configurations of the same structure (the robustness measure as such with absolute meaning must be further studied), other measures of robustness are possible, including simply area $\mathcal{A}$ (less area is more robustness).

Failure can also be quantified in the fuzzy domain as possibility of failure $\Pi_{\mathcal{F}}$ (fig. 4.5), defined by the maximum possibility where the state limit is violated (i.e. $g < 0$),

$$\Pi_{\mathcal{F}} = \max \Pi \left(g < 0\right). \tag{4.19}$$

4.2.4.2 *Modeling uncertainty with fuzzy numbers*

Möller and Beer (2004) suggest defining fuzzy numbers by using linear, polygonal, Gaussian membership or quadratic functions as the possibilistic membership function. Further, empirically based statistical models can be supplemented with expert knowledge to also create fuzzy numbers. Fuzzy numbers are assumed here to be convex (fig. 4.6).

Fuzzy shapes can take on any number of forms. In the following some standard shapes and their nomenclature are introduced (cf. fig. 4.7).

Singleton membership functions

A precise (deterministic) parameter that has the value a is represented in fuzzy space by

$$\tilde{p} = \text{sing}\left\langle a \right\rangle. \tag{4.20}$$

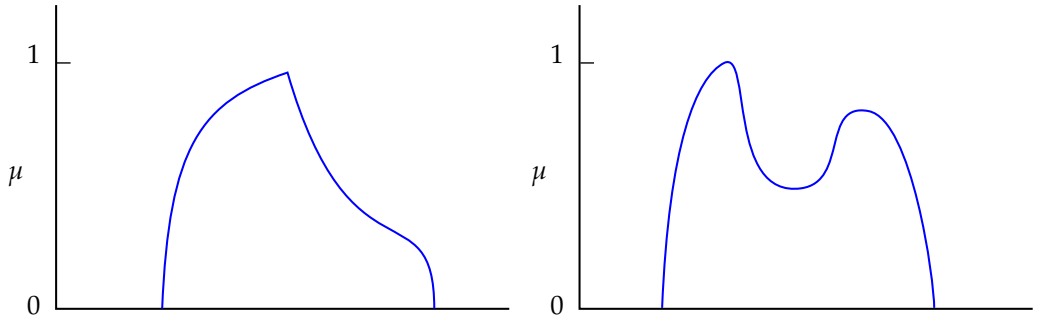

(a) Convex (b) Nonconvex

Figure 4.6: Example of convex and nonconvex fuzzy numbers

Interval membership functions

Interval values (cf. § 4.2.3) are a further special case of a fuzzy number and are represented in fuzzy space by

$$\tilde{p} = \text{int}\,\langle a,\, b\rangle\,, \tag{4.21}$$

where a is the minimum and b the maximum.

Triangular membership functions

Triangular fuzzy numbers are one of the most common form to be used in the literature. These are modeled by a fully possible value b and have an uncertain interval approaching impossible between the minimum value a and the maximum c, giving the following fuzzy membership function:

$$\tilde{p} = \text{tri}\,\langle a,\, b,\, c\rangle\,. \tag{4.22}$$

Trapezoidal membership functions

Trapezoidal fuzzy numbers are used in this work with the interpretation introduced in § 4.2.4.1. Having an upper interval between the minimum value b and the maximum c and the lower interval between a and c, this fuzzy number is defined as

$$\tilde{p} = \text{trap}\,\langle a,\, b,\, c,\, d\rangle\,. \tag{4.23}$$

Gaussian membership functions

Possibilistic membership functions can also be borrowed from the probability theory as in this case with a Gaussian form. Though in the possibilistic context, the membership functions must be cut-off at certain standard deviation to truncate the fuzzy number.

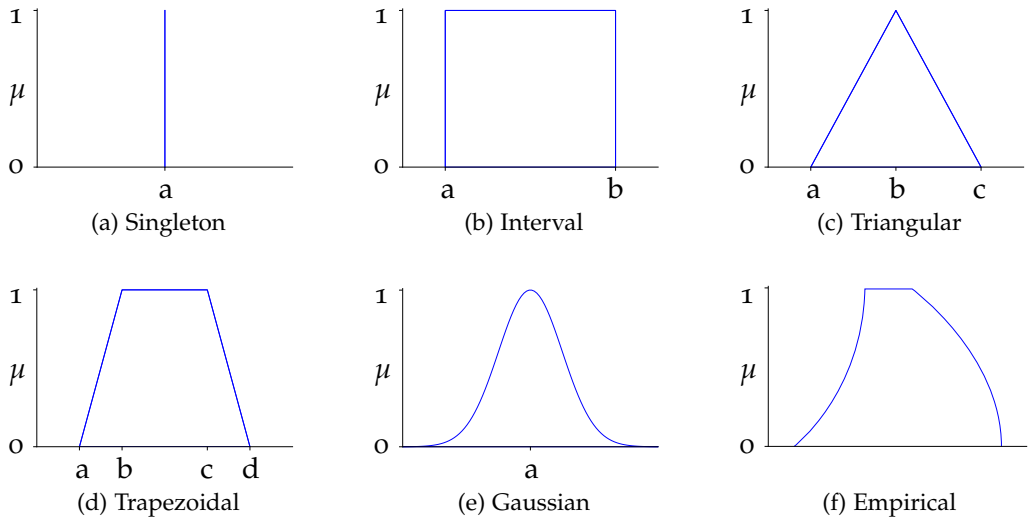

(a) Singleton (b) Interval (c) Triangular

(d) Trapezoidal (e) Gaussian (f) Empirical

Figure 4.7: Examples of shapes of fuzzy membership functions

This can be done for example at $\pm 3\sigma$ or $\pm 6\sigma$ to avoid having a fuzzy number that reaches a value of $\pm\infty$,

$$\tilde{p} = \text{gauss}\left\langle x_{\text{avg}},\ x_{\sigma_{\text{right}}},\ x_{\sigma_{\text{left}}},\ \sigma_{\text{cut-off}} \right\rangle . \tag{4.24}$$

Forms of other standard probabilistic membership functions, e.g. Weibull, can also be used.

Empirical membership functions

It is also possible to use general membership functions. These rely on experience, tests or are taken from previous uncertainty analyses.

4.3 FUZZY ARITHMETIC

The method of uncertainty analysis using fuzzy numbers based on possibility theory (Möller 1997 and Wehrle 2008) uses so-called α-level optimization. The first step is the discretization of the uncertain parameters at certain possibility values between zero and unity, known as α-levels α_k, where $k \in 1, 2, \ldots n_\alpha$ (fig. 4.8). The resulting $\left[\begin{array}{cc} \underline{p} & \overline{p} \end{array}\right]_{\alpha_k}$ gives the uncertain domain in which the maximum and minimum of each uncertain system response ($\underline{r}_{i,\alpha_k}$ and $\overline{r}_{i,\alpha_k}$ respectively) are found giving $\left[\begin{array}{cc} \underline{r}_i & \overline{r}_i \end{array}\right]_{\alpha_k}$,

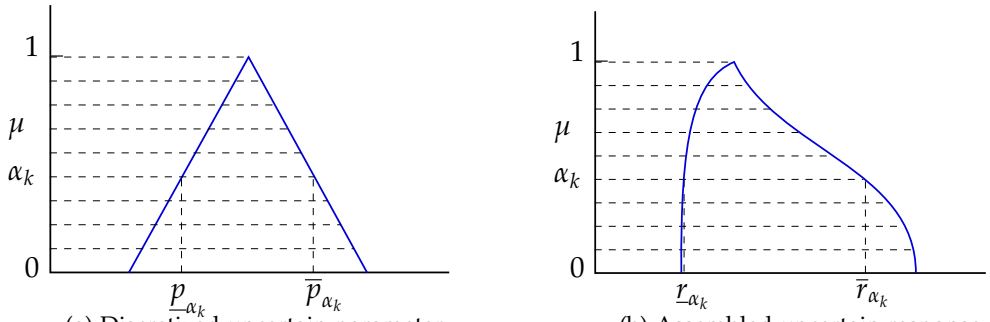

(a) Discretized uncertain parameter (b) Assembled uncertain response

Figure 4.8: Fuzzy arithmetic with α-level optimization

$$\underline{r}_{i,\alpha_k} \leftarrow \min_{p \in \left[\begin{array}{cc} \underline{p} & \overline{p} \end{array}\right]_{\alpha_k}} \{r_i(\boldsymbol{p})\} \tag{4.25}$$

$$\overline{r}_{i,\alpha_k} \leftarrow \max_{p \in \left[\begin{array}{cc} \underline{p} & \overline{p} \end{array}\right]_{\alpha_k}} \{r_i(\boldsymbol{p})\}. \tag{4.26}$$

The resulting intervals of the uncertain responses are then assembled ($\mathbf{A}_\alpha$) at said levels of possibility,

$$\tilde{r}_i = \underset{k}{\mathbf{A}_\alpha} \left[\begin{array}{cc} \underline{r}_i & \overline{r}_i \end{array}\right]_{\alpha_k}. \tag{4.27}$$

4.4 POST-PROCESSING OF UNCERTAINTY ANALYSIS

As uncertainty analysis with fuzzy and interval arithmetic uses gradient-based algorithms, it is possible to use the method of shadow prices discussed in § 2.5.2. This research extends these to introduce the term of *shadow uncertainty* $\mathsf{S_U}$ for uncertainty analysis and *shadow uncertainty price* $\mathsf{S_{UP}}$ for optimization under uncertainty.

4.4.1 *Shadow uncertainty*

As interval- and fuzzy-based uncertainty analysis is carried out using bounded optimization, the Lagrangian multipliers again play a role. Analogously to shadow prices (§ 2.5.2), this is the shadow cast by the uncertainty on the uncertain response, the function being minimized and maximized. Likewise, this linearization is used to estimate the change in the uncertain response due to the change of uncertain parameters.

The gradient Lagrangian function is defined in this case as

$$\nabla \mathsf{L} = \nabla \underline{r}(\boldsymbol{p}) + \boldsymbol{\lambda}^T \nabla \mathbf{g}(\boldsymbol{p}) \tag{4.28}$$
$$\nabla \mathsf{L} = -\nabla \overline{r}(\boldsymbol{p}) + \boldsymbol{\lambda}^T \nabla \mathbf{g}(\boldsymbol{p}) \tag{4.29}$$

for the minimization and maximization problem, respectively. As α-level optimization is bounded but has no nonlinear constraints, $\mathbf{g}$ contains only the boundaries of the uncertain domain $\tilde{p}$: $\underline{p}_j - p_j$ and $p_j - \overline{p}_j$. As these are typically non-normalized, the gradients $\frac{\partial \mathsf{g}_i}{\partial p_j}$ are negative unity and unity for the upper and lower bounds, respectively. The shadow uncertainties are, therefore:

$$\begin{aligned}
&\text{lower-bound response } \underline{r},\ \text{lower-bound parameter } \underline{p}_j: && \mathsf{S}_{\mathsf{U}ij} = \frac{\partial \underline{r}_i}{\partial \underline{p}_j} \\
&\text{lower-bound response } \underline{r},\ \text{upper-bound parameter } \overline{p}_j: && \mathsf{S}_{\mathsf{U}ij} = -\frac{\partial \underline{r}_i}{\partial \overline{p}_j} \\
&\text{upper-bound response } \overline{r},\ \text{lower-bound parameter } \overline{p}_j: && \mathsf{S}_{\mathsf{U}ij} = -\frac{\partial \overline{r}_i}{\partial \underline{p}_j} \\
&\text{upper-bound response } \overline{r},\ \text{upper-bound parameter } \overline{p}_j: && \mathsf{S}_{\mathsf{U}ij} = \frac{\partial \overline{r}_i}{\partial \overline{p}_j}.
\end{aligned} \tag{4.30}$$

Analogous to shadow prices, the shadow uncertainties are a linearization and the new lower-bound response is

$$\underline{r}_i^{\text{new}} = \underline{r}_i - \Delta \underline{p}_j \mathsf{S}_{\mathsf{U}ij} \tag{4.31}$$
$$\underline{r}_i^{\text{new}} = \underline{r}_i - \Delta \overline{p}_j \mathsf{S}_{\mathsf{U}ij}, \tag{4.32}$$

and the new upper-bound

$$\overline{r}_i^{\text{new}} = \overline{r}_i - \Delta \underline{p}_j \mathsf{S}_{\mathsf{U}ij} \tag{4.33}$$
$$\overline{r}_i^{\text{new}} = \overline{r}_i - \Delta \overline{p}_j \mathsf{S}_{\mathsf{U}ij}. \tag{4.34}$$

To simplify, p_i^{bound} is used to generalize the upper and lower bound, resulting in

$$r^{\text{new}} = r - \Delta p_i^{\text{bound}} \mathsf{S}_{\mathsf{U}ij}. \tag{4.35}$$

For fuzzy arithmetic this is performed at all α-levels. When assembled this gives then the gradient of robustness with respect to the bounds of the fuzzy system parameter.

4.4.2 *Shadow uncertainty price*

The shadow uncertainty price is used when carrying out optimization under uncertainty and is the sensitivity of the optimal value of the objective function with respect

to the uncertain parameters. As discussed in § 2.5.2, shadow prices are defined depending on the formulation of the constraint function (eq. 2.30). Now we can obtain the detrimental price of the objective at the optimum due to the shadows cast by the uncertainty of the system.

Assuming that the constraint function g is active and will stay after a perturbation in the limit of the optimization constraint c, the gradients of the system response and the limit with respect to the design variables are equal,

$$\frac{\partial r_j}{\partial x_i} = \frac{\partial c_j}{\partial x_i}, \tag{4.36}$$

resulting in

$$\begin{aligned}
\text{upper bounded, non-normalized } g_j = r_j - c_j: &\qquad S_{UP_j} = -\frac{\partial f^*}{\partial \tilde{p}_j} \\
\text{lower bounded, non-normalized } g_j = c_j - r_j: &\qquad S_{UP_j} = \frac{\partial f^*}{\partial \tilde{p}_j} \\
\text{upper bounded, normalized } g_j = \frac{r_j}{c_j} - 1: &\qquad S_{UP_j} = -\frac{\partial f^*}{\partial \tilde{p}_j} c_j \\
\text{lower bounded, normalized } g_j = 1 - \frac{r_j}{c_j}: &\qquad S_{UP_j} = \frac{\partial f^*}{\partial \tilde{p}_j} c_j.
\end{aligned} \tag{4.37}$$

Using the definition of shadow uncertainty (eq. 4.30), shadow uncertainty prices are then defined as

$$S_{UP_i} = \sum S_{P_i} S_{U_{ij}}. \tag{4.38}$$

Again, these can be used in post-processing the result of optimization under uncertainty, to estimate a new objective function for a change in the uncertain parameters

$$f^{*,\text{new}} = f^* - \Delta p_i^{\text{bound}} \sum S_{P_i} S_{U_{ij}}. \tag{4.39}$$

4.5 OPTIMIZATION UNDER UNCERTAINTY

Consideration of uncertainty in structural design optimization supplements the general structural optimization (eq. 3.41) to account for parametrical variation with the following:

$$
\begin{aligned}
\text{minimize} \quad & f(\mathbf{x}) && \mathbf{x} \in \mathbb{R}^n \\
\text{so that} \quad & g_j(\tilde{\boldsymbol{r}}(\mathbf{x})) \leq 0 && j \in \mathbb{N}[1,\, p] \\
\text{as well as} \quad & {x^L}_i \leq x_i \leq {x^U}_i && i \in \mathbb{N}[1,\, n] \\
\text{where} \quad & \mathbf{x} = \begin{bmatrix} x_1 & x_2 & \dots & x_n \end{bmatrix}^T && \\
\text{governed by} \quad & \tilde{\sigma}_{ij,j} + \tilde{\rho}\tilde{b}_i = \tilde{\rho}\tilde{\ddot{u}}_i && \text{in } \Omega \\
& \tilde{u}_i = \tilde{\hat{u}}_i && \text{on } \Gamma_D \\
& \tilde{\sigma}_{ij} \cdot \tilde{n} = \tilde{t}_i && \text{on } \Gamma_N \\
& \tilde{u}_0 && \text{in } \Omega \\
& \tilde{\dot{u}}_o && \text{in } \Omega \\
& \tilde{\sigma}_{ij} = \tilde{C}_{ijkl}\tilde{u}_{k,l}. &&
\end{aligned}
\tag{4.40}
$$

Eq. 4.40 shows all parameters of the governing system equations, which is the general case. As computational effort grows with larger numbers of uncertain parameters to consider, this set will be reduced by the engineer. An initial parameter study can also show which uncertainties are critical. The introduced measures of shadow uncertainties and shadow uncertainty prices can assist in this decision.

The formulation of optimization problems under uncertainty can take varying forms using reliability, robustness or a multiobjective of e.g. mass and robustness. This is set up depending on the structure being designed and its different design requirements.

4.6 IMPLEMENTATION OF A SOFTWARE TOOL FOR FUZZY UNCERTAINTY ANALYSIS

The package FuzzAnPy (Fuzzy Analysis in Python) was written by the author to provide a package for α-level optimization using efficient algorithms. As with DesOptPy, a variety of optimization algorithms can be used via pyOpt (Perez et al. 2012), though NLPQLP (cf. § 2.4.1) was vastly the most efficient. FuzzAnPy can use local and global optimization techniques with the optional use of surrogate models to further increase efficiency to solve the minimization and maximization problems eqs. 4.25–4.26 (cf. fig. 4.9). Although specifically developed for use in structural mechanics and design optimization, FuzzAnPy is a general solver for fuzzy arithmetic.

Pseudo code is provided in list. 4.1 for an example of an uncertainty analysis using this code. List. 4.2 shows the integration of FuzzAnPy in DesOptPy for an optimization under uncertainty using possibility theory.

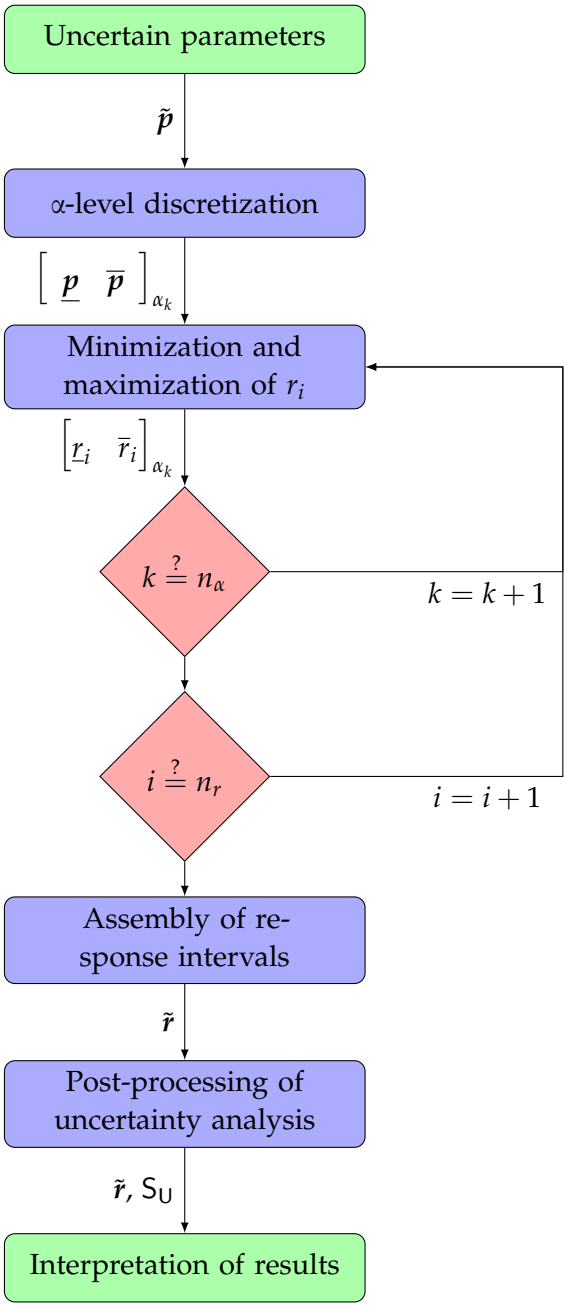

Figure 4.9: Flowchart for uncertainty analysis with fuzzy parameters using α-level optimization

Listing 4.1: Syntax of uncertainty analysis with FuzzAnPy

```
from FuzzAnPy import FuzzAn

def FuzzySysEq(p, x, ir):
    # here: system equations
    r = ...
    return(r)

def  FuzzySensEq(p, r, g, x, ir):  # optional
    # here: sensitivity equations
    drdp = ...
    return(drdp)

nAlpha = ...
nr = ...
pFuzz = ...
rFuzz, pOpt, nEval, SU, lambdaR = FuzzAn(FuzzyModel, pFuzz, nr=nr, Alg="NLPQLP",
                                         nAlpha=nAlpha, deltax=1e-3,
                                         paraNorm=True, para=[], SBFA=False,
                                         Surr="Kriging", epsStop=1.0e-4)
```

Listing 4.2: Syntax of optimization under uncertainty with DesOptPy and FuzzAnPy

```
from DesOptPy import DesOpt
from FuzzAnPy import FuzzAn

def FuzzySysEq(p, x, ir):
    # here: system equations
    r = ...
    return(r)

def SysEq(x, gc)
    nAlpha = ...
    nr = ...
    pFuzz = ...
    rFuzz, pOpt, nEval, SU, lambdaR = FuzzAn(FuzzyModel, pFuzz, nr=nr,
                                             Alg="NLPQLP", nAlpha=nAlpha,
                                             deltax=1e-3, paraNorm=True,
                                             para=x, SBFA=False,
                                             Surr="None", epsStop=1.0e-4)
    f = ...
    g = ...
    return(f, g)

x0 = ...
xL = ...
```

```
xU = ...
gc = ...
xOpt, fOpt, SP = DesOpt(SysEq, x0, xU, xL, gc=gc, hc=[], Alg="MMA",
                        SensCalc="FD", DesVarNorm="xLxU", deltax=1e-3,
                        StatusReport=True, ResultReport=True,
                        OptVideo=False, DoE=False, SBDO=False,
                        Debug=False, PrintOut=True)
```

Part II

STRUCTURAL-MECHANICAL INVESTIGATIONS AND OPTIMIZATION STUDIES

Wer gegen ein Minimum von Aluminium immun ist, besitzt eine Aluminium-minimumimmunität.

German tongue twister

5

OPTIMAL DESIGN OF A NONLINEAR TWO-BAR TRUSS UNDER UNCERTAINTY USING ANALYTICAL DESIGN SENSITVITIES—AN ACADEMIC EXAMPLE

The first structure to be optimized and analyzed for uncertainty is a two-bar truss structure (also known as a von Mises truss) having nonlinear material model under transient loading (fig. 5.1). The deterministic optimization will be carried out using analytical design sensitivities to show their effectiveness and efficiency. Although a simple structure, it exhibits the challenges of nonlinearity and stability (snap through) of larger problems for design optimization and uncertainty analysis.

5.1 DESIGN AND REQUIREMENTS

The two-bar truss is constructed out of extruded aluminum sections. The truss is 100 mm high and each member has a length ℓ of 500 mm. A bilinear, elastoplastic material model was used for the aluminum material AW EN-6060 T6 (fig. 5.2). The yield stress σ_y is assumed to be defined as 200 MPa, the Young's modulus E as 70000 MPa and the tangent modulus K_α as 1000 MPa. The force is applied to the top node via a linear ramping function from $f_{t=0} = 0$ kN to the end time of $f_{t=0.001} = 100$ kN.

The cross-sectional areas a_i of the truss are to be dimensioned for lowest possible mass, while limiting the vertical displacement u_y at 40 mm, which allows for some displacement but does not allow for a loss of stability (snap through, see below). Fur-

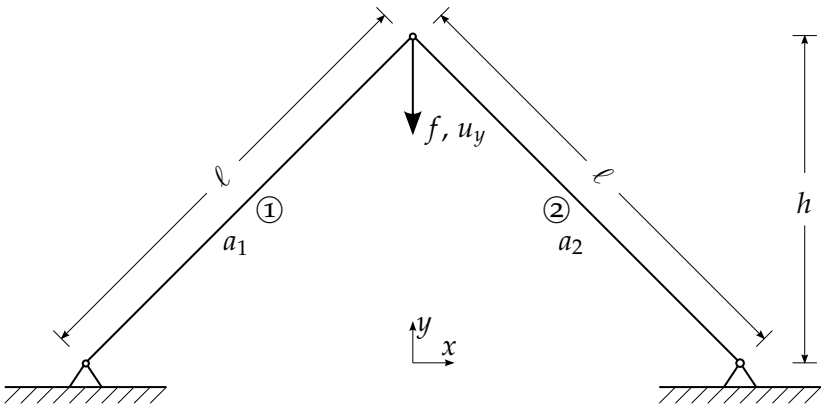

Figure 5.1: Two-bar truss

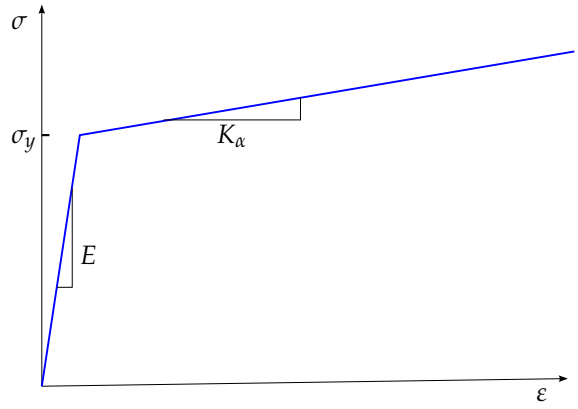

Figure 5.2: Bilinear material model for aluminum AW EN-6060 T6

ther, the design limits the horizontal displacement u_x at $\pm 2\,\mathrm{mm}$ to preserve a general symmetrical deformation of the structure.

5.2 STRUCTURAL-MECHANICAL ANALYSIS

The structural-mechanical analysis was carried out in MATLAB using explicit time integration. The simulation provides analytical design sensitivities, which were implemented via § 3.5.2. Analytical gradients of the system response displacement with respect to the cross-sectional area $\frac{\partial u}{\partial a_i}$ are calculated and given to the optimization algorithm. Sensitivities with respect to other parameters are also possible, i.e. the uncertain material parameters discussed below, but not implemented here. The verification of the analytical sensitivities can be seen in fig. 5.3. Even after the snap through where numerical instabilities are present, the sensitivities have nearly no deviation.

As the evaluations are very cheap, ca. 1.5 s for each transient nonlinear calculation[1], this served as an excellent benchmark example for the testing and development of the methods introduced here.

5.3 DIMENSIONING OF A TWO-BAR TRUSS

In the following, the design problem formulated above (§ 5.1) is transformed into an optimization problem and the optimal cross-sectional areas are found. The mass of the structure is to be minimized while constraining the vertical and horizontal displacements.

1 Dual-core computer with Intel Core i5-3320M at 2.60 GHz

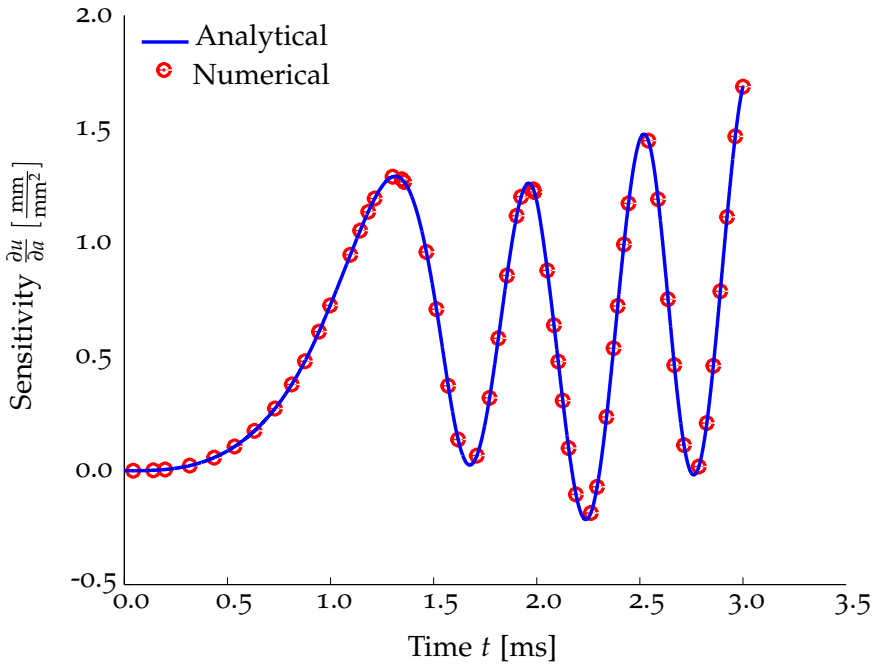

Figure 5.3: Verification of analytical sensitivities using numerical sensitivities for one design over the time of one snap through

5.3.1 *Optimization problem*

The mathematical formulation of the optimization problem for the design problem is described as follows:

$$\min_{\mathbf{x}\in\mathbf{X}} \left\{ \mathsf{f}\left(\mathbf{x}\right) | \mathbf{g}\left(\mathbf{x}\right) \leq \mathbf{0} \right\},$$

where

$$\begin{aligned} \mathsf{f}\left(\mathbf{x}\right) &= m \\ \mathsf{g}_1\left(\mathbf{x}\right) &= \frac{u_y}{u_{y,\max}} - 1 \\ \mathsf{g}_2\left(\mathbf{x}\right) &= \frac{u_x}{u_{x,\max}} - 1 \\ \mathsf{g}_3\left(\mathbf{x}\right) &= \frac{u_x}{-u_{x,\max}} - 1 \\ \mathbf{x} &= \begin{bmatrix} a_1 & a_2 \end{bmatrix}^T. \end{aligned}$$

In the following, this problem will be solved using different parameters.

5.3.2 *Optimization results*

The start value was chosen to challenge the algorithm and, therefore, a non-symmetrical, infeasible structural design was chosen in addition to a symmetrical starting design (cf. tab. 5.1). Using the first-order algorithm MMA with numerical sensitivities via forward finite differencing, a solution was found in 10 iterations and 30 system evaluations. Starting from a non-symmetrical design resulted in a slightly non-symmetrical design with a mass of 492.6886 kg. Starting from symmetrical designs resulted in the symmetrical design of 91.4782 mm² for each bar, resulting, albeit with a difference in objective function of only 0.0142 kg. The performance of the convergence was similar regardless of starting point needing between six and ten iterations. In both designs only the constraint g_1 for displacement in y-direction u_y is active, though there is some displacement in x-direction in the non-symmetrical designs and none in the symmetrical.

Table 5.1: Details of design variables for optimization with finite differencing

Design variable	Symbol	$\mathbf{x}^0$	$\mathbf{x}^L$	$\mathbf{x}^U$	$\mathbf{x}^*$	Unit
1	$\mathbf{x}_1$	10.0	10.0	500.0	97.4820	mm²
2	$\mathbf{x}_2$	500.0	10.0	500.0	85.4696	mm²

Utilizing the analytical sensitivities of transient nonlinear finite-element analysis with explicit time integration, the number of evaluations could be drastically reduced. Starting from a nonsymmetrical design, MMA needed a third of the number of evaluations, 10 evaluations and 10 iterations, coming to nearly the same design and a mass of 492.6735 kg. As with finite differencing, starting from symmetrical designs resulted in symmetrical designs of the same numerical value as above.

Table 5.2: Details of design variables for optimization with analytical sensitivity

Design variable	Symbol	$\mathbf{x}^0$	$\mathbf{x}^L$	$\mathbf{x}^U$	$\mathbf{x}^*$	Unit
1	$\mathbf{x}_1$	10.0	10.0	500.0	97.4983	mm²
2	$\mathbf{x}_2$	500.0	10.0	500.0	85.4477	mm²

The path of optimization is nearly identical, both showing good convergence behavior of objective, constraint and design variables (fig. 5.4). These results provide a reference to the analysis and optimization under uncertainty of the following sections.

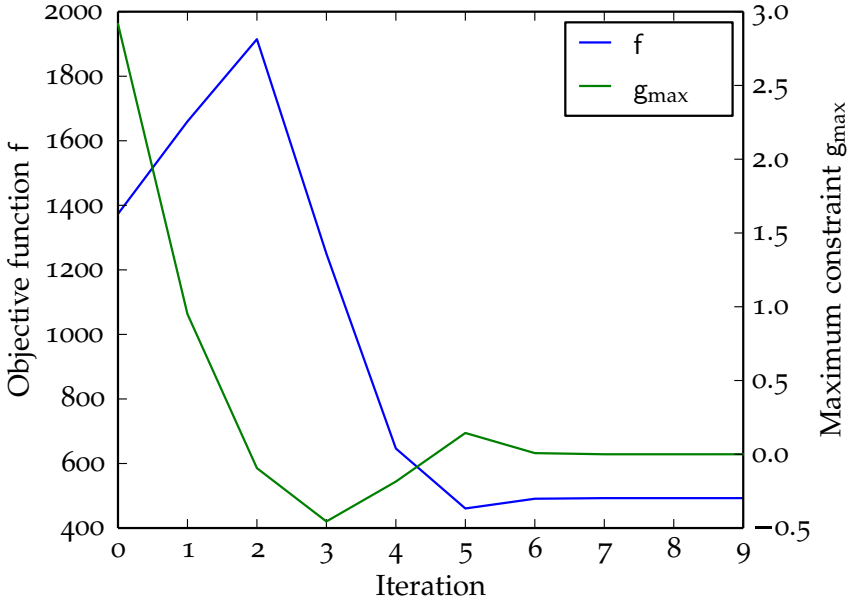

(a) Starting from non-symmetrical design

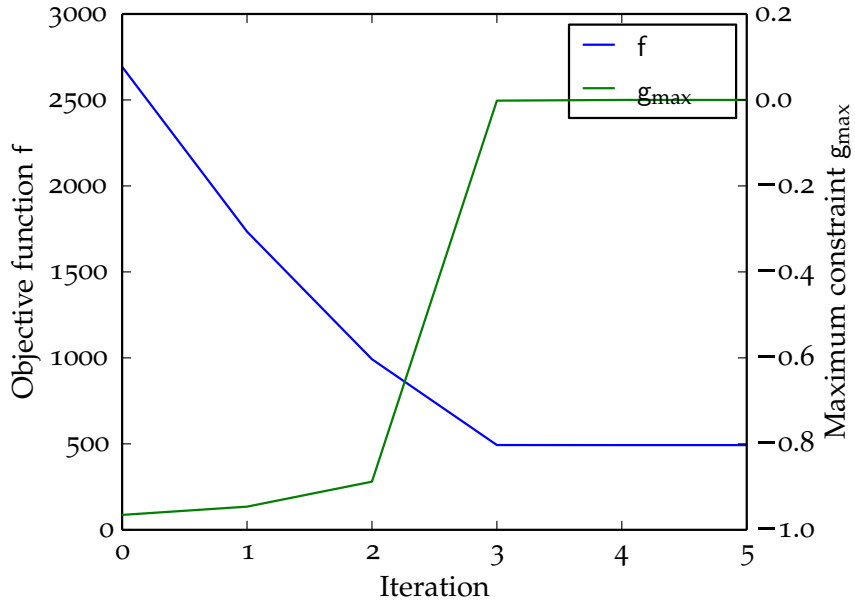

(b) Starting from symmetrical design

Figure 5.4: Convergence plots of the dimensioning of the two-bar truss

5.4 CONSIDERATION OF UNCERTAIN MATERIAL MODEL IN THE DESIGN OF THE TWO-BAR TRUSS

Assuming the problem above, yet now an uncertain bilinear elastoplastic material model is considered. In this model, the yield stress $\tilde{\sigma}_y$ as well as Young's modulus $\tilde{E}$ and the tangent modulus $\tilde{K}_\alpha$ are considered uncertain. The uncertain mapping is defined as

$$\begin{array}{ccc} \tilde{\boldsymbol{p}} & \mapsto & \tilde{\boldsymbol{r}} \\ \left\{ \begin{array}{c} \tilde{\sigma}_y \\ \tilde{E}_i \\ \tilde{K}_\alpha \end{array} \right\} & \mapsto & \left\{ \begin{array}{c} \tilde{u}_y \\ \tilde{u}_x \end{array} \right\}, \end{array}$$

where the uncertain material parameters are modeled with the following trapezoidal fuzzy numbers (fig. 5.5):

$$\begin{aligned} \tilde{\sigma}_y &= \text{trap}\,\langle 175,\, 190,\, 210,\, 225\rangle \text{ MPa} \\ \tilde{E} &= \text{trap}\,\langle 65000,\, 68000,\, 72000,\, 75000\rangle \text{ MPa} \\ \tilde{K}_\alpha &= \text{trap}\,\langle 500,\, 750,\, 1250,\, 1500\rangle \text{ MPa}. \end{aligned}$$

The uncertainty analysis here is performed with FUZZANPY using NLPQLP and this considers the material of each bar to be independent. This results in six independent uncertain parameters being mapped onto two uncertain structural responses. The *shadow uncertainties* S_U, sensitivities of the uncertain parameters to uncertain responses $\frac{\partial \tilde{r}_i}{\partial \tilde{p}_j}$, are calculated with FUZZANPY without further computational effort. These can be further used in concert with the shadow prices S_P of the optimization to give the *shadow uncertainty prices* S_UP, the sensitivity of the objective function due to uncertain parameters $\frac{\partial f}{\partial \tilde{p}_j}$, for possibility-based and robustness optimization.

5.4.1 *Uncertainty analysis of the optimal design*

An uncertainty analysis is performed with the uncertain material model described above for the symmetrical and non-symmetrical optimal designs of § 5.3. For the non-symmetrical optimal design, the uncertainty analysis for displacement results in the following trapezoidal fuzzy numbers (fig. 5.6):

$$\begin{aligned} \tilde{u}_y &= \text{trap}\,\langle 33.5823,\, 37.3237,\, 42.7807,\, 46.9190\rangle \\ \tilde{u}_x &= \text{trap}\,\langle -0.8385,\, 0.2800,\, 1.8203,\, 2.9317\rangle, \end{aligned}$$

and the symmetrical optimal design the following (fig. 5.7):

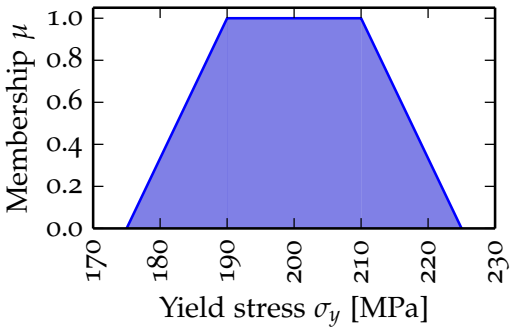

(a) Fuzzy yield stress

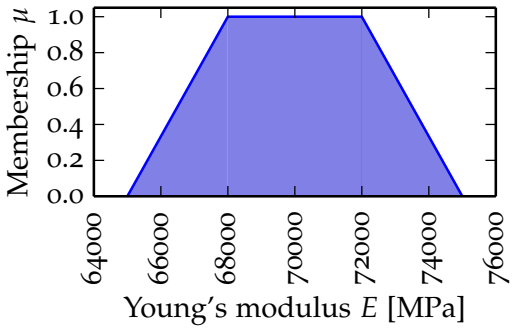

(b) Fuzzy Young's modulus

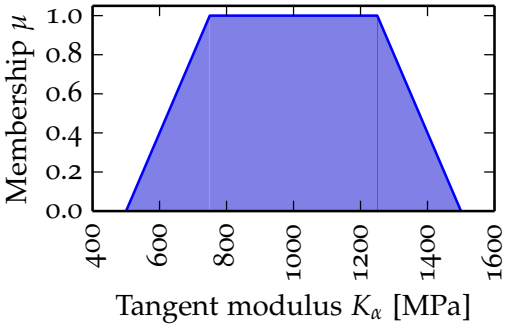

(c) Fuzzy tangent modulus

Figure 5.5: Uncertain material parameters for the two-bar truss

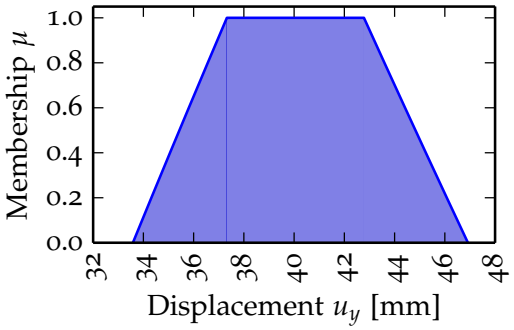

(a) Vertical displacement

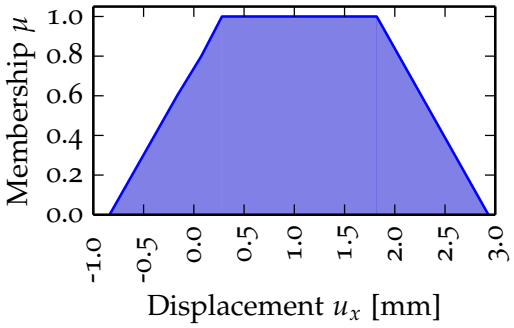

(b) Horizontal displacement

Figure 5.6: Uncertain structural response for the nonsymmetrical design

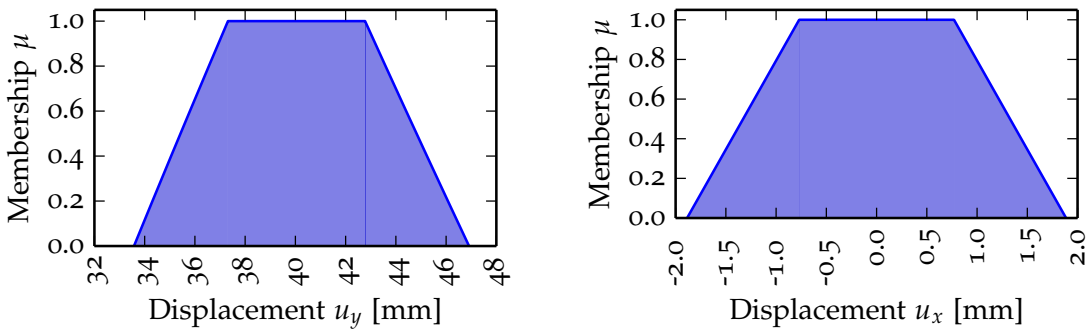

(a) Vertical displacement

(b) Horizontal displacement

Figure 5.7: Uncertain structural response for the symmetrical design

Table 5.3: Fuzzy uncertainty values of the optimized two-bar truss

Design	$\mathcal{A}_{\tilde{u}_y}$	$\mathcal{A}_{\tilde{u}_x}$	$\mathcal{A}_{\text{sys}}$
Nonsymmetrical	9.3960	2.6514	12.0474
Symmetrical	9.3970	2.6559	12.0529

$$\begin{aligned} \tilde{u}_y &= \text{trap}\,\langle 33.5746,\, 37.3166,\, 42.7740,\, 46.9127\rangle \\ \tilde{u}_x &= \text{trap}\,\langle -1.8858,\, -0.7705,\, 0.7705,\, 1.8858\rangle\,. \end{aligned}$$

It can be seen that the symmetrical design is a better design as it is only slightly outside the limit on horizontal displacement, while the nonsymmetrical design violates the limit by 50%, though, both have nearly the same vertical displacement.

Both designs have a possibility of failure $\Pi(\mathcal{F})$ of unity, meaning failure is fully possible. This is clear as the deterministic displacement is on the border to failure criteria. Any uncertainty to this design enables the structure to "fail", here defined by exceeding 40 mm of vertical displacement and 2 mm of horizontal displacement. In the next section, we will explore how to design such a structure under uncertainty.

The robustness is also calculated, here by using the nonnormalized area of the responses—fuzzy uncertainties. Again, robustness in a fuzzy domain is of abstract nature, yet the numerical value is useful for the comparison of the nonsymmetrical and symmetrical designs (tab. 5.3). The values of uncertainty quantify the results discussed above that the variation of the truss is nearly identical.

The algorithm FuzzAnPy required 70 evaluations for a worst-case design, 161 for two α-levels and 497 for six α-levels. Further, a surrogate-based approach has been implemented in which one sample is reused for all α-level optimizations for all uncertain responses. For reproducible and robust results for this example, this Gaussian

process approximation requires a sample size of approximately 100. Afterwards, a similar number of evaluations for the non-surrogate-based approach is needed on the computationally inexpensive approximation.

For these two designs the shadow uncertainties S_U were calculated. The shadow uncertainties of the non-symmetrical design are as follows, for vertical displacement u_y:

$$\begin{aligned}
\frac{\partial \tilde{u}_y}{\partial \tilde{\sigma}_{y,1}} &= \text{trap}\,\langle 1.0376, 1.0793, 1.1450, 1.1894\rangle \times 10^{-1} \\
\frac{\partial \tilde{u}_y}{\partial \tilde{\sigma}_{y,2}} &= \text{trap}\,\langle 5.0563, 5.9344, 7.2785, 8.3272\rangle \times 10^{-4} \\
\frac{\partial \tilde{u}_y}{\partial \tilde{E}_1} &= \text{trap}\,\langle 8.7823, 8.8878, 8.4101, 8.6318\rangle \times 10^{-5} \\
\frac{\partial \tilde{u}_y}{\partial \tilde{E}_2} &= \text{trap}\,\langle 0.9126, 0.9501, 1.0068, 1.0458\rangle \times 10^{-1} \\
\frac{\partial \tilde{u}_y}{\partial \tilde{K}_{\alpha,1}} &= \text{trap}\,\langle 4.5545, 5.3200, 6.4922, 7.4060\rangle \times 10^{-4} \\
\frac{\partial \tilde{u}_y}{\partial \tilde{K}_{\alpha,2}} &= \text{trap}\,\langle 7.6841, 7.7883, 7.3341, 7.5372\rangle \times 10^{-5},
\end{aligned}$$

and for horizontal displacement u_x:

$$\begin{aligned}
\frac{\partial \tilde{u}_x}{\partial \tilde{\sigma}_{y,1}} &= \text{trap}\,\langle 2.8366, 2.9194, 3.0595, 3.1624\rangle \times 10^{-2} \\
\frac{\partial \tilde{u}_x}{\partial \tilde{\sigma}_{y,2}} &= \text{trap}\,\langle 1.6437, 1.7050, 1.8130, 1.8952\rangle \times 10^{-4} \\
\frac{\partial \tilde{u}_x}{\partial \tilde{E}_1} &= \text{trap}\,\langle 3.2612, 3.2711, 3.1980, 3.2493\rangle \times 10^{-5} \\
\frac{\partial \tilde{u}_x}{\partial \tilde{E}_2} &= \text{trap}\,\langle 2.5080, 2.5733, 2.6971, 2.7794\rangle \times 10^{-2} \\
\frac{\partial \tilde{u}_x}{\partial \tilde{K}_{\alpha,1}} &= \text{trap}\,\langle 1.5076, 1.5384, 1.6014, 1.6491\rangle \times 10^{-4} \\
\frac{\partial \tilde{u}_x}{\partial \tilde{K}_{\alpha,2}} &= \text{trap}\,\langle 2.9877, 2.9932, 2.9448, 2.9730\rangle \times 10^{-5}.
\end{aligned}$$

As these numbers represent the sensitivity of the uncertain response at discrete levels of the fuzzy response, they are difficult to decipher in their entirety. These are also used to calculate shadow uncertainties of the fuzzy robustness, or here fuzzy uncertainty $\frac{\partial \mathcal{A}_{\tilde{r}}}{\partial \tilde{p}}$, which is more expediant for comparison (tab. 5.4).

Although both these methods are considered efficient for this number of uncertain parameters, further computational savings can be obtained via analytical design (or here uncertainty) sensitivities of displacement with respect to the yield strength $\frac{\partial u}{\partial \sigma_y}$,

Table 5.4: Shadow uncertainties of fuzzy uncertainty with respect to uncertain parameters of the optimized two-bar truss

Design	Nonsymmetric	Symmetric
$\frac{\partial \mathcal{A}_{\tilde{u}_y}}{\partial \tilde{\sigma}_{y,1}}$	2.225×10^{-1}	2.0916×10^{-1}
$\frac{\partial \mathcal{A}_{\tilde{u}_y}}{\partial \tilde{K}_{\alpha,1}}$	1.3295×10^{-3}	1.2597×10^{-3}
$\frac{\partial \mathcal{A}_{\tilde{u}_y}}{\partial \tilde{E}_1}$	1.7352×10^{-4}	1.6259×10^{-4}
$\frac{\partial \mathcal{A}_{\tilde{u}_y}}{\partial \tilde{\sigma}_{y,2}}$	1.9581×10^{-1}	2.0916×10^{-1}
$\frac{\partial \mathcal{A}_{\tilde{u}_y}}{\partial \tilde{K}_{\alpha,2}}$	1.1888×10^{-3}	1.2597×10^{-3}
$\frac{\partial \mathcal{A}_{\tilde{u}_y}}{\partial \tilde{E}_2}$	1.5175×10^{-4}	1.6259×10^{-4}
$\frac{\partial \mathcal{A}_{\tilde{u}_x}}{\partial \tilde{\sigma}_{y,1}}$	5.9877×10^{-2}	5.6305×10^{-2}
$\frac{\partial \mathcal{A}_{\tilde{u}_x}}{\partial \tilde{K}_{\alpha,1}}$	3.5276×10^{-4}	3.3395×10^{-4}
$\frac{\partial \mathcal{A}_{\tilde{u}_x}}{\partial \tilde{E}_1}$	6.4889×10^{-5}	6.2404×10^{-5}
$\frac{\partial \mathcal{A}_{\tilde{u}_x}}{\partial \tilde{\sigma}_{y,2}}$	5.2801×10^{-2}	5.6305×10^{-2}
$\frac{\partial \mathcal{A}_{\tilde{u}_x}}{\partial \tilde{K}_{\alpha,2}}$	3.1487×10^{-4}	3.3395×10^{-4}
$\frac{\partial \mathcal{A}_{\tilde{u}_x}}{\partial \tilde{E}_2}$	5.9501×10^{-5}	6.2404×10^{-5}

Young's modulus $\frac{\partial u}{\partial E}$ and tangent modulus $\frac{\partial u}{\partial K_\alpha}$. The shadow uncertainties are shown below in context of optimization in concert with shadow prices to give shadow uncertainty prices.

5.4.2 *Worst-case optimization problem under uncertain material properties*

The mathematical formulation of the optimization problem for the design problem in which the the constraint is now the worst-case displacement is described as follows:

$$\min_{\mathbf{x}\in\mathbf{X}} \left\{ \mathsf{f}\left(\mathbf{x}\right) | \mathbf{g}\left(\mathbf{x}\right) \leq \mathbf{0} \right\},$$

where

$$\begin{aligned} \mathsf{f}\left(\mathbf{x}\right) &= m \\ \mathsf{g}_1\left(\mathbf{x}\right) &= \frac{\max\left\{\tilde{u}_y\right\}}{u_{y,\max}} - 1 \\ \mathsf{g}_2\left(\mathbf{x}\right) &= \frac{\max\left\{\tilde{u}_x\right\}}{u_{x,\max}} - 1 \\ \mathsf{g}_3\left(\mathbf{x}\right) &= \frac{\min\left\{\tilde{u}_x\right\}}{-u_{x,\max}} - 1 \\ \mathbf{x} &= \begin{bmatrix} a_1 & a_2 \end{bmatrix}^T. \end{aligned}$$

Using MMA and starting from the same non-symmetrical start design as in the deterministic case, the optimization takes 10 optimization iterations and 30 uncertain evaluations for a total of system evaluations of 4158 (84 to 147 system evaluations per uncertain analysis) to reach the nearly symmetrical optimum design of 99.4048 mm^2 and 99.5889 mm^2 resulting in a mass of 535.8901 kg. From a symmetrical design it takes 10 iterations and 30 uncertain evaluations and a total of 3087 system evaluations.

Table 5.5: Details of design variables of worst-case optimization

Design variable	Symbol	$\mathbf{x}^0$	$\mathbf{x}^L$	$\mathbf{x}^U$	$\mathbf{x}^*$	Unit
1	$\mathbf{x}_1$	10.0	10.0	500.0	99.4048	mm^2
2	$\mathbf{x}_2$	500.0	10.0	500.0	99.5889	mm^2

The postprocessing of this design optimization shows a shadow price S_P for the sensitivity of the mass with respect to the limit of the active constraint, vertical displacement $\frac{\partial m}{\partial u_{y,\max}}$ to be -6.8712. The shadow uncertainty of the worst-case of this parameter with respect to the uncertainty is found in the first column of tab. 5.6.

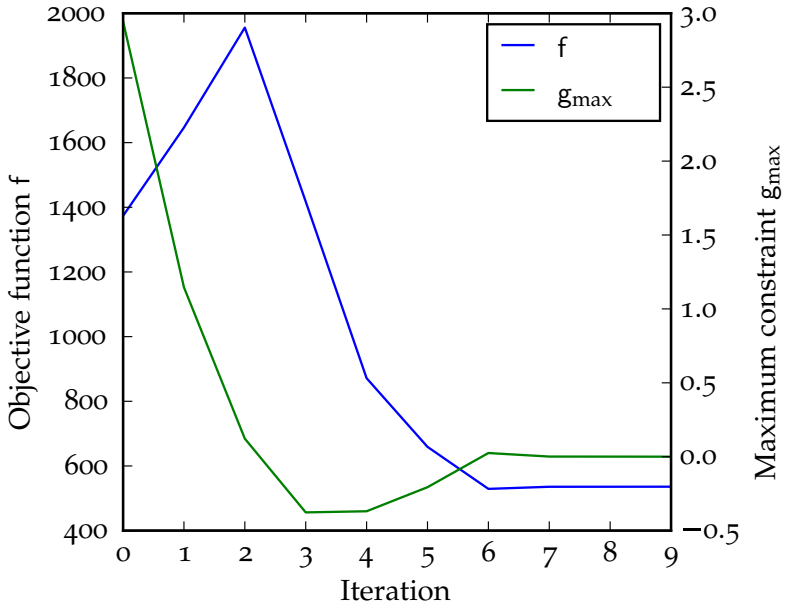

Figure 5.8: Convergence of the worst-case dimensioning of the two-bar truss

Table 5.6: Shadow uncertainties and shadow uncertainty prices of active constraint in worst-case design

	Shadow uncertainties $\frac{\partial \tilde{u}_y}{(\cdot)}$	Shadow uncertainty prices $\frac{\partial m_y}{(\cdot)}$
$\frac{(\cdot)}{\partial \tilde{\sigma}_{y,1}}$	-1.07261340e-01	7.37014119e-01
$\frac{(\cdot)}{\partial \tilde{K}_{\alpha,1}}$	-6.47816254e-04	4.45127504e-03
$\frac{(\cdot)}{\partial \tilde{E}_1}$	-7.92277118e-05	5.44389454e-04
$\frac{(\cdot)}{\partial \tilde{\sigma}_{y,2}}$	-1.07459727e-01	7.38377277e-01
$\frac{(\cdot)}{\partial \tilde{K}_{\alpha,2}}$	-6.48860493e-04	4.45845022e-03
$\frac{(\cdot)}{\partial \tilde{E}_2}$	-7.93667093e-05	5.45344533e-04

The quantification of the shadow uncertainties (tab. 5.7) shows that the reduction in the uncertainty of yield stress is the most critical for the objective function. If the yield stress of one bar would become 10% more uncertain, the mass would have to be increased by nearly 3.7 kg (0.7%).

Table 5.7: Reduction in mass resulting from 10% reduction in uncertainty for the worst-case design

	Reduction of mass	
10% reduction of uncertainty in	kg	%
Yield strength of bar 1	3.6851	0.6877
Tangent modulus of bar 1	0.4451	0.0831
Young's modulus of bar 1	0.5444	0.1016
Yield strength of bar 2	3.6919	0.6889
Tangent modulus of bar 2	0.4458	0.0832
Young's modulus of bar 2	0.5453	0.1018

5.4.3 *Possibility-based optimization problem under uncertain material properties*

In this case, a certain level of possibility of failure will be accepted, namely $\Pi(\mathcal{F}) = 0.2$. Failure $\mathcal{F}$ is defined by $u > u_{\max}$. This is formulated as follows:

$$\min_{\mathbf{x}\in\mathbf{X}} \left\{ \mathsf{f}(\mathbf{x}) \,|\mathbf{g}(\mathbf{x}) \leq \mathbf{0} \right\},$$

where

$$\begin{aligned} \mathsf{f}(\mathbf{x}) &= m \\ \mathsf{g}_1(\mathbf{x}) &= \frac{\Pi\left(\mathcal{F}\left(\tilde{u}_y\right)\right)}{0.2} - 1 \\ \mathsf{g}_2(\mathbf{x}) &= \frac{\Pi\left(\mathcal{F}\left(\tilde{u}_x\right)\right)}{0.2} - 1 \\ \mathsf{g}_3(\mathbf{x}) &= \frac{\Pi\left(\mathcal{F}\left(-\tilde{u}_x\right)\right)}{0.2} - 1 \\ \mathbf{x} &= \begin{bmatrix} a_1 & a_2 \end{bmatrix}^T. \end{aligned}$$

Starting from a nonsymmetrical design, the MMA algorithm needed 9 iterations and 27 uncertain analyses for a total of 3381 system evaluations reaching an optimal design of 99.5025 mm^2 for the cross-sectional area of each bar and a mass of 535.9205 kg.

Table 5.8: Details of design variables of possibility-based optimization

Design variable	Symbol	$\mathbf{x}^0$	$\mathbf{x}^L$	$\mathbf{x}^U$	$\mathbf{x}^*$	Unit
1	$\mathbf{x}_1$	10.0	10.0	500.0	99.5025	mm^2
2	$\mathbf{x}_2$	500.0	10.0	500.0	99.5025	mm^2

5.4.4 *Robustness optimization problem under uncertain material properties*

It is also of interest to maximize the robustness of a structure within the bounds of the design variables and the structural-mechanical constraints. Robustness is defined as the ratio of variation of the input parameters to the system response. As the area of the input parameters remains the same, maximizing the robustness is the equivalent of minimizing the uncertainty, i.e. summed areas of the responses. This is referred to here as system uncertainty $\mathcal{A}_{\text{sys}}$. The constraints are defined possibilistically as above. This problem is thus defined as

$$\min_{\mathbf{x}\in\mathbf{X}} \left\{ \mathsf{f}\left(\mathbf{x}\right) | \mathbf{g}\left(\mathbf{x}\right) \leq \mathbf{0} \right\},$$

where

$$\begin{aligned}
\mathsf{f}\left(\mathbf{x}\right) &= -\mathcal{A}_{\text{sys}} \\
\mathsf{g}_1\left(\mathbf{x}\right) &= \frac{\Pi\left(\mathcal{F}\left(\tilde{u}_y\right)\right)}{0.2} - 1 \\
\mathsf{g}_2\left(\mathbf{x}\right) &= \frac{\Pi\left(\mathcal{F}\left(\tilde{u}_x\right)\right)}{0.2} - 1 \\
\mathsf{g}_3\left(\mathbf{x}\right) &= \frac{\Pi\left(\mathcal{F}\left(-\tilde{u}_x\right)\right)}{0.2} - 1 \\
\mathbf{x} &= \begin{bmatrix} a_1 & a_2 \end{bmatrix}^T.
\end{aligned}$$

The MMA algorithm required 7 iterations, 21 uncertain evaluations and a total of 10395 system evaluations to come to the design of maximum robustness at 500.0 mm^2 for each bar, the upper bound (cf. tab. 5.9). For this optimization problem the robustness maximization is a trivial problem, but it is shown to be more interesting as a multiobjective problem or for other design problems below.

Table 5.9: Details of design variables of robustness optimization

Design variable	Symbol	$\mathbf{x}^0$	$\mathbf{x}^L$	$\mathbf{x}^U$	$\mathbf{x}^*$	Unit
1	$\mathbf{x}_1$	10.0	10.0	500.0	500.0	mm^2
2	$\mathbf{x}_2$	500.0	10.0	500.0	500.0	mm^2

5.4.5 *Multiobjective robustness optimization problem under uncertain material properties*

The objective of this optimization is to maximize the system robustness. As the sole maximization of the system robustness $\mathcal{R}$ has a trivial solution of $\mathbf{x}^U$, a composite objective function is formulated as the weighted addition of the system uncertainty via summed areas of the responses $\mathcal{A}_{\text{sys}}$ (robustness) and mass m. Again, the constraints are defined possiblistically as above. This is formulated as

$$\min_{\mathbf{x}\in\mathbf{X}} \left\{ \mathsf{f}\left(\mathbf{x}\right) | \mathbf{g}\left(\mathbf{x}\right) \leq \mathbf{0} \right\},$$

where

$$\begin{aligned}
\mathsf{f}\left(\mathbf{x}\right) &= \gamma_1 \mathcal{A}_{\text{sys}} + \gamma_2 m \\
\mathsf{g}_1\left(\mathbf{x}\right) &= \frac{\Pi\left(\mathcal{F}\left(\tilde{u}_y\right)\right)}{0.2} - 1 \\
\mathsf{g}_2\left(\mathbf{x}\right) &= \frac{\Pi\left(\mathcal{F}\left(\tilde{u}_x\right)\right)}{0.2} - 1 \\
\mathsf{g}_3\left(\mathbf{x}\right) &= \frac{\Pi\left(\mathcal{F}\left(-\tilde{u}_x\right)\right)}{0.2} - 1 \\
\mathbf{x} &= \begin{bmatrix} a_1 & a_2 \end{bmatrix}^T.
\end{aligned}$$

The weights γ_1 and γ_2 were chosen as 25 and 1 respectively, though other values are possible depending on the desired compromise between robustness and mass. The optimization required 10 iterations, 30 uncertain evaluations and 3630 system evaluations, coming to the slightly nonsymmetrical design 100.159 mm^2 and 98.7786 mm^2 (cf. tab. 5.10) for a mass of 535.89 kg.

Table 5.10: Details of design variables of multiobjective robustness optimization

Design variable	Symbol	$\mathbf{x}^0$	$\mathbf{x}^L$	$\mathbf{x}^U$	$\mathbf{x}^*$	Unit
1	$\mathbf{x}_1$	10.0	10.0	500.0	100.159	mm^2
2	$\mathbf{x}_2$	500.0	10.0	500.0	98.7786	mm^2

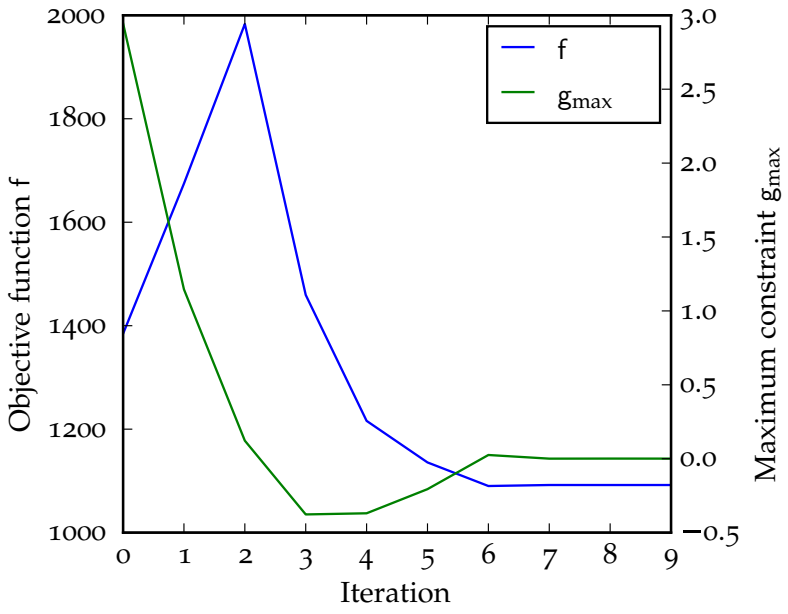

Figure 5.9: Convergence of the multiobjective robustness dimensioning of the two-bar truss

5.5 FINDINGS AND INTERPRETATION OF RESULTS

As this problem has two design variables, it is possible to plot the design domain to gain further insight on the design problem as well as the importance in considering uncertainty (fig. 5.10).

The possibility of analytical sensitivities by nonlinear finite-element analysis shows great speed-up. The generality of this must be investigated, especially concerning contact and bifurcations. As this is an academic example, the amount of data is small, which made the implementation in MATLAB feasible. The extent of use of memory for large examples should be monitored and more efficient implementations analyzed. Further, extension to the uncertain parameters would lead to drastically fewer system evaluations for optimization under uncertainty and is, thus, seen as the next step.

Efficient handling of uncertainties within the design optimization framework was proven. Although requiring more evaluations, this exact "dosage" against uncertainty is feasible.

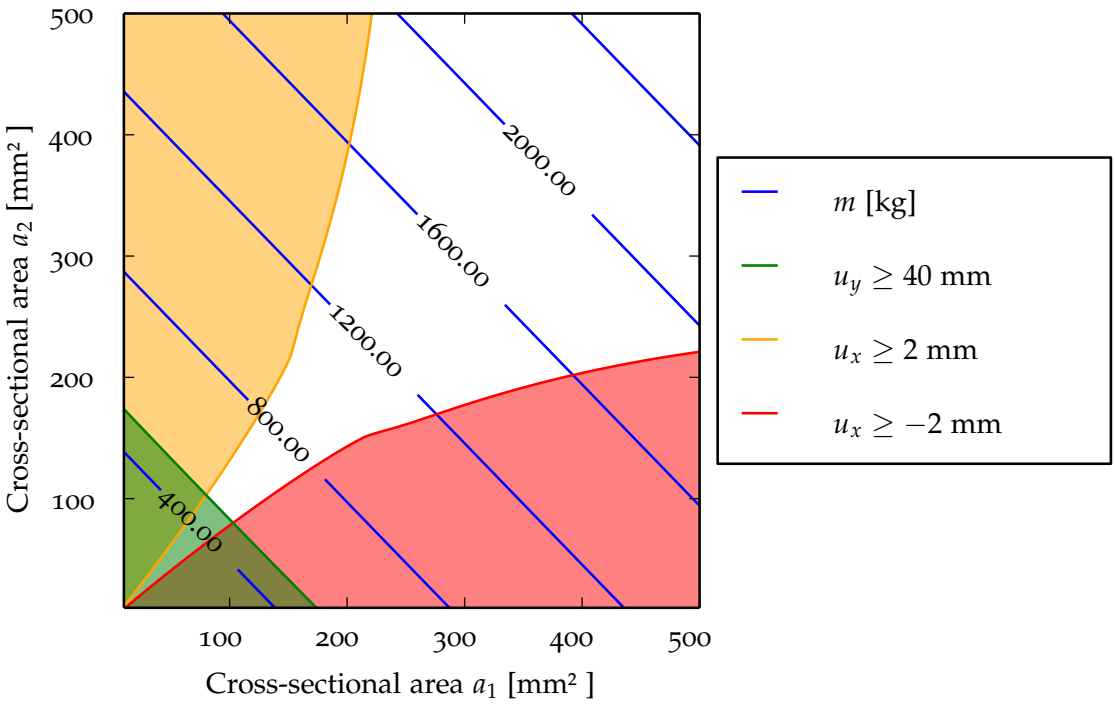

Figure 5.10: Design domain of the two-bar truss

Table 5.11: Comparison of results for the two-bar truss: I. Optimization with analytical sensitivities from a nonsymmetrical start design, II. Optimization with numerical sensitivities from a nonsymmetrical start design, III. Optimization with analytical sensitivities from a symmetrical start design, IV. Worst-case optimization, V. Possibility-based optimization, VI. Robustness optimization, VII. Multiobjective robustness and mass optimization

Property	Symbol	I	II	III	IV	V	VI	VII	Unit
Objective	f	492.6886	492.6735	492.7014	535.8901	530.2408	0.8786	1092.0366	–
Design variable 1	x_1	97.4820	97.49830	91.4782	99.4048	99.8207	500.0000	100.159	mm²
Design variable 2	x_2	85.4696	85.4477	91.4782	99.5889	97.0753	500.0000	98.7786	mm²
Mass	m	492.6886	492.6735	492.7014	535.8901	530.2408	2693.0	535.8900	kg
Vertical displacement	u_y	40.0072	40.0072	40.0003	33.4514	34.2383	1.3878	33.4722	mm
Horizontal displacement	u_x	1.0509	1.0509	0.0	-0.0143	0.2169	0.0	0.1076	mm
System uncertainty	$\mathcal{A}_{\text{sys}}$	12.0474	12.0474	12.0529	11.4018	11.4839	0.45028	11.4041	–
Possibility of failure	$\Pi(\mathcal{F})$	1.0	1.0	1.0	0.0	0.2	0.0	0.0067	–
Evaluations	n_{eval}	8	30	10	3087	3402	10395	3630	–

6

DEVELOPMENT OF A LIGHTWEIGHT EXTRUDED ALUMINUM FRAME FOR ELECTRIC VEHICLES—A DEMONSTRATOR FOR STRUCTURAL DESIGN OPTIMIZATION CONSIDERING CRASHWORTHINESS AND UNCERTAINTY

The numerical examples that follow are extracted from the Lightweight Extruded Aluminum Frame (LEAF) developed by the author as a demonstrator for structural design optimization using a multi-level design philosophy. This reduction of the large design problem with many design variables into a series of problems each of smaller dimensionality allowed the use of numerical design optimization and uncertainty analysis of the subproblems, which will be presented in subsequent chapters. In this chapter the concept LEAF (fig. 6.1) will be introduced.

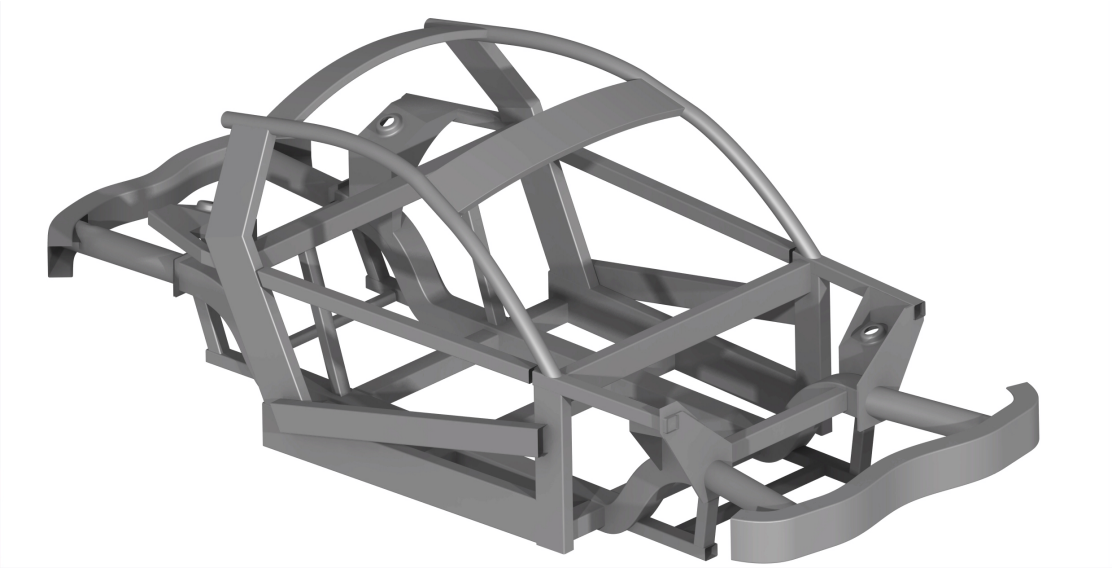

Figure 6.1: Lightweight Extruded Aluminum Frame

6.1 DESCRIPTION OF VEHICLE CONCEPT

This lightweight, innovative space frame was drafted to fit in the design envelope of MUTE (fig. 6.2, tab. 6.1), the electrical vehicle designed and built by the Technische Universität München. The design utilizes the aluminum-extrusion manufacturing technologies developed developed within the project Collaborative Research Center

Figure 6.2: Electric vehicle MUTE

SFB – Transregio 10 (Kleiner and Klaus 2003). In the following the conceptional design of this structure will be discussed.

Table 6.1: Specification data of the electric vehicle concept MUTE

Category	Specification
Registration class	L7e heavy quadricycle (minicar)
Maximum speed	$\geq 120\,\mathrm{km/h}$
Power at wheel	15 kW
Curb weight	≤ 400 kg excluding battery
Energy storage	Rechargeable battery and disposable electric range extender
Drive train	Rear-wheel-drive powered by a central electric motor with torque vectoring
Range	≥ 100 km
Cost	Total cost of ownership equal to contemporary subcompact

6.2 STRUCTURAL DESIGN REQUIREMENTS OF THE AUTOMOTIVE FRAME

The structural design requirements stem from the project MUTE and its European Community registration class, L7e (heavy quadricycles or microcars). This requires the vehicle to be lightweight (under 400 kg without the battery), yet has limited passive safety requirements, which were extended to cover requirements of front, side and rear impact as well as roll-over.

Foremost in the development of a passenger vehicle structure are the safety requirements in regards to vehicular impact: crashworthiness. Here this is further divided into front impact (100% and 40% overlap), side impact, rear impact and roof crush (fig. 6.3). Front impact is a case of the American New Car Assessment Program

(US NCAP) in which the vehicle is crashed against a rigid wall at 56 km/h. The second case involving front impact from the European New Car Assessment Program (Euro NCAP) sees the vehicle impacting a deformable barrier offset 40% at 64 km/h. The side impact case investigated here is performed with a deformable barrier crashing into the driver side of the vehicle at 50 km/h out of the Euro NCAP test catalog. The rear impact requirement is carried out using the standard FMVSS 301 and here a deformable barrier is impacted against a non-moving vehicle at 50 km/h. For these cases, deformation or intrusion of the structure and occupant acceleration are limited in order to ensure occupant survival of a road accident. The final crashworthiness requirement used for this concept is the roof crush test according to FMVSS 216. Here a roll-over of the vehicle is simulated by applying a load of 1.5 times the curb weight while limiting the displacement.

To guarantee driving comfort and proper handling, static and dynamic stiffness requirements are applied. Bending stiffness is investigated by applying simple supports to all four suspension-strut domes, while applying a downward force where both seats are located (fig. 6.4b). Torsional stiffness is measured by applying simple support to both rear suspension strut domes and applying an upward and a downward force on the left and right front suspension-strut domes, respectively (fig. 6.4a). Further, the first resonance frequency (dynamic stiffness) shall be high enough to ensure comfort for the vehicle occupants.

Further loads result from suspension of the vehicle and are accounted for by applying three cases to the four kinematic points of the chassis-frame interface: Ⓜ suspension-strut dome, Ⓕ longitudinal control arm and Ⓖ the transverse control arm (fig. 6.5). The following three cases are considered:

1. Brake and pot-hole bump
2. Curve and pot-hole
3. Brake, curve and pot-hole bump.

The structure was to be built a limited number of times and, therefore, complex tooling was not feasible. Further, the structure is to be cost-effective, to reduce both prototype costs as well as costs that would be incurred for a possible serial run and then passed on to consumers.

These structural requirements are to be upheld while the mass of the structure without doors was to be as light as possible, but not more than 120 kg.

6.3 CONCEPT OF THE SPACE-FRAME STRUCTURE

The structural design of LEAF culminates from the conceptual analysis of space frames (fig. 6.6), including topology optimization, the space frame of MUTE as well as the investigation of the DLR bulkhead space frame (Schöll et al. 2009 and Rudolph 2011).

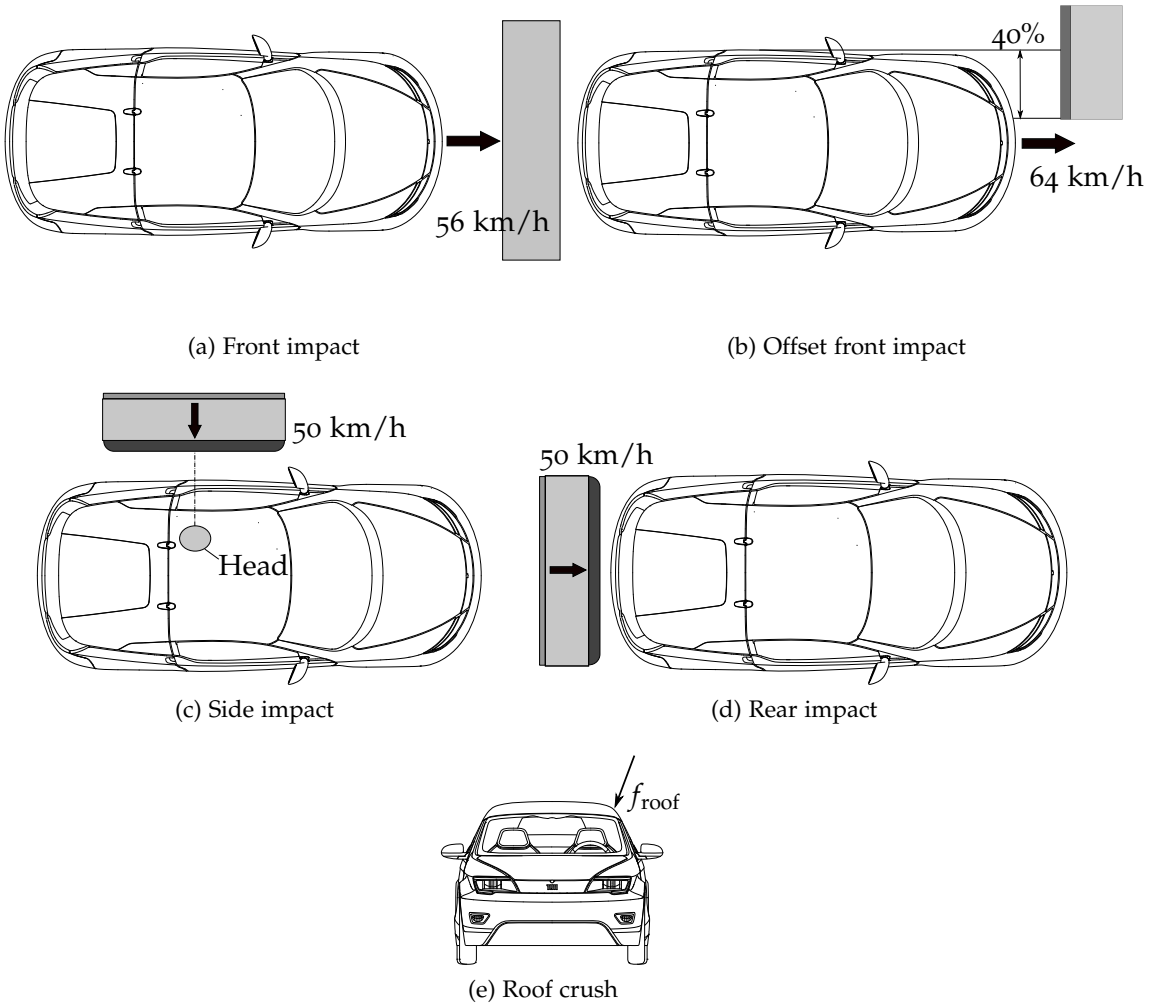

(a) Front impact

(b) Offset front impact

(c) Side impact

(d) Rear impact

(e) Roof crush

Figure 6.3: Crashworthiness cases considered for LEAF

Further inspiration was drawn from the AUDI SPACE FRAME (Paefgen and Leitermann 1994, Leitermann and Christlein 2000 and Christlein and Schüler 2000). As this vehicular frame is for very small production runs and must be cost-efficient, a lightweight space frame of aluminum extruded sections was selected, the majority of which are standard cross-sectional geometry. The combined extrusion-curving technology, developed in the research project Transregio 10, allows for the efficient manufacturing of the few non-straight elements.

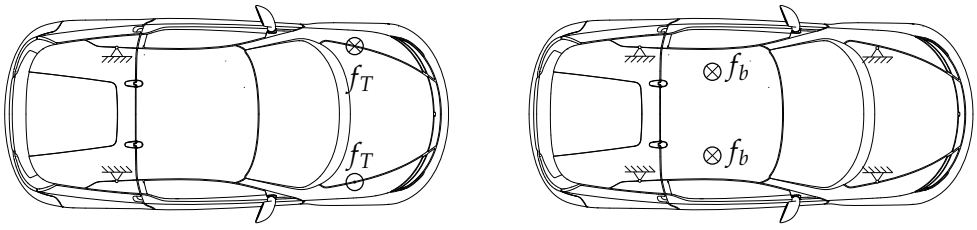

(a) Torsion stiffness (b) Bending stiffness

Figure 6.4: Stiffness cases considered for LEAF

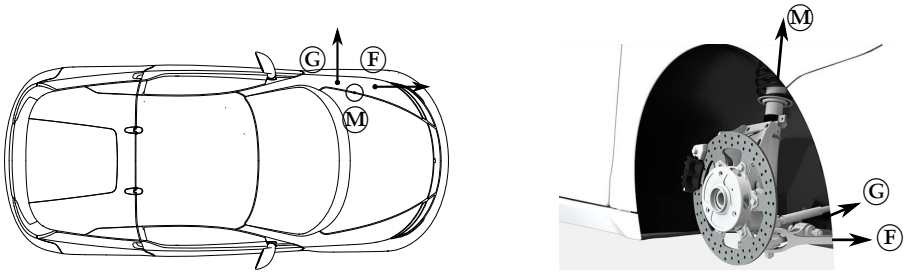

Figure 6.5: Chassis case considered for LEAF

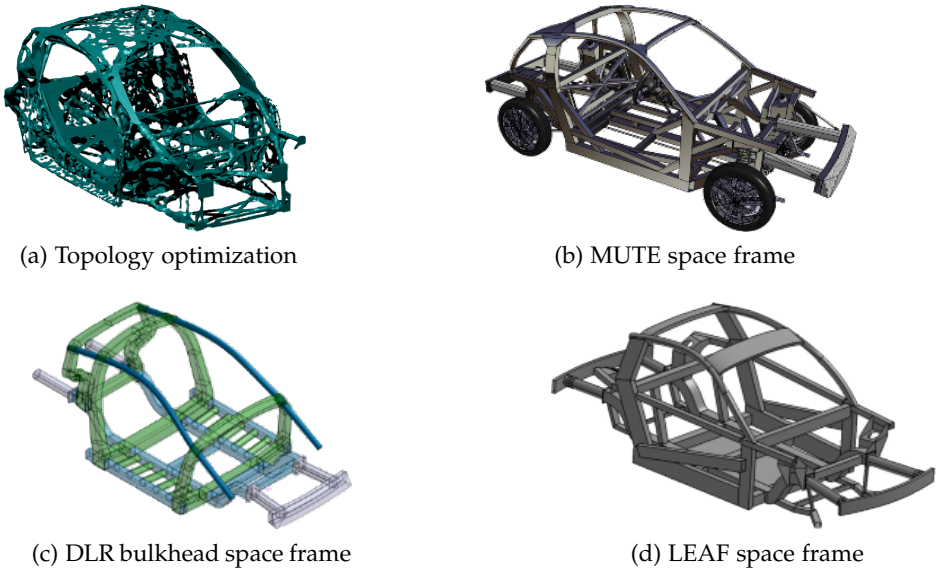

(a) Topology optimization (b) MUTE space frame

(c) DLR bulkhead space frame (d) LEAF space frame

Figure 6.6: Concepts considered in the development of LEAF

The structure of LEAF is divided into three performance-based zones: deformation, safety and chassis zones (fig. 6.7). The deformation zone allows for absorption of kinematic energy of a vehicular impact via plastic deformation in the front, rear and

sides of the structure. While allowing intrusion, and with it energy absorption, in the deformation structure (red), the structural integrity is sustained with the safety zone (blue). In this region of the structure, there shall be no plastic deformations present in the case of a vehicular impact. Thus, this zone guarantees the safety of the occupants in the inopportune event of a crash. The chassis structure is responsible for suspension loads as well torsional and bending stiffness (green).

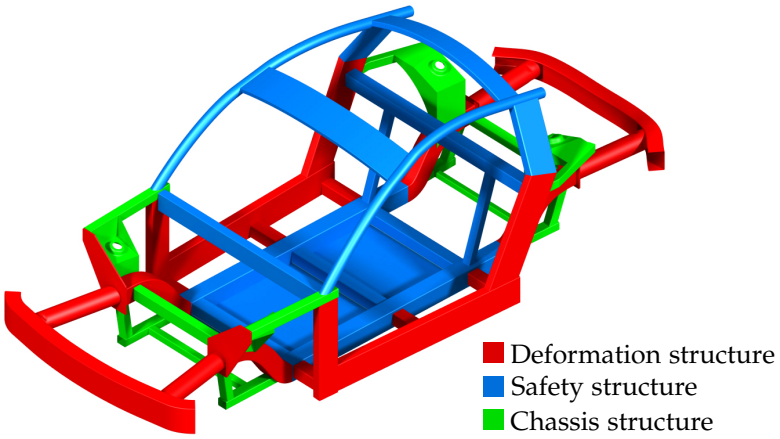

Figure 6.7: Functional concept of LEAF

The backbone of this concept are the two double-S-shaped sections that run from the front of the vehicle to the rear (fig. 6.8a). These are the main floor support and direct crash loads from both the front and the rear into the strong, stiff region beneath the feet of the occupants. The double-S-shaped sections are connected to each other with sheeting and transverse sections to ensure structural integrity also in the event of a side crash. This stiff floor component group further provides the concept with high bending and torsional stiffness.

Front and rear impacts are absorbed via crash systems made of a transverse member (bumper) and two longitudinal crash-absorbing sections (fig. 6.8b). These are attached to the frame at two thick plates at the end of the double-S-shaped sections.

Side impact is absorbed via crash boxes in the floor connecting the double-S-shaped section to the door-sill section (fig. 6.8c). Further, the lower B-pillar is able to displace at the bottom at extensive loading (i.e. impact) to allow deformation underneath the occupant.

The suspension is attached via a simple, yet mechanically efficient frame structure of sections and sheeting (fig. 6.8d). This structure creates the suspension-strut dome as well as the interfaces to the longitudinal and transverse control arms. This, in addition to the wide transverse sections in the roof, provides the frame with excellent torsional stiffness.

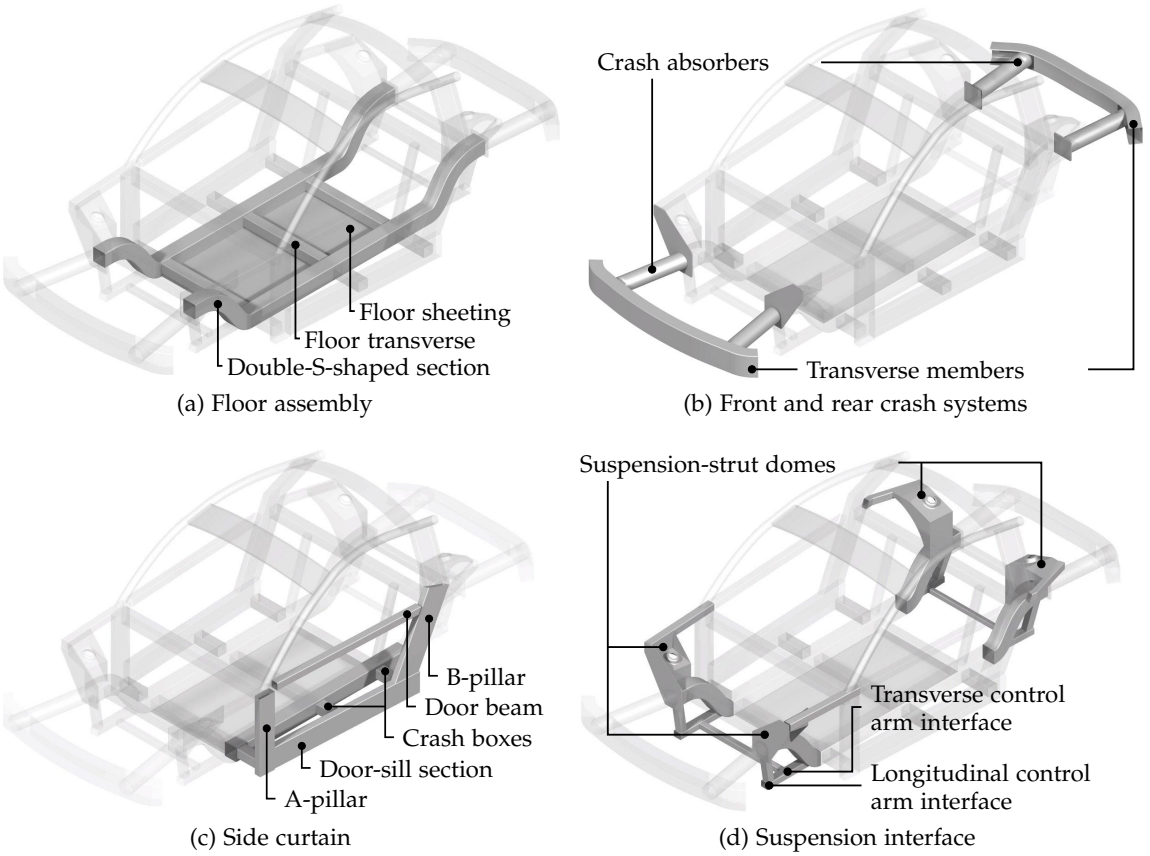

Figure 6.8: Functional assemblies of LEAF

To further ease manufacturing effort, the vast majority of connections are perpendicular. This reduces cutting and welding of complex joints and therefore, manufacturing costs and time.

Important to the conception was the structural flexibility for varying vehicle architectures and drive configurations. The architectural flexibility allows for using the same topology for one-seat, two-seat and four-seat configurations, albeit with adapted cross-sectional geometry of the space-frame sections (fig. 6.9).

(a) Single-seat city car (b) Two-seat coupé (c) Four-seat sedan

Figure 6.9: LEAF with different possible vehicle architectures

Beyond the size of the vehicle and the number of occupants, the structure enables the use of varying drive configurations (fig. 6.10). The development of this structure was carried out for a vehicular concept with a middle battery and rear-wheel drive, though it may be advantageous for dynamical and impact performace to have a floor battery. The LEAF concept is robust enough to allow for a front-mounted internal combustion engine with front-wheel drive. Further drive configurations such as hub motors would also be feasible.

(a) Electric with floor battery (b) Electric with middle battery (c) Internal combustion

Figure 6.10: LEAF with different possible drive configurations

6.4 DEVELOPMENT PROCESS AND INTEGRATION OF STRUCTURAL DESIGN OPTIMIZATION

After the conceptualization phase, the design of the cross-sectional geometry and wall thickness of each element is carried out. To develop and optimize the concept further, a multi-level design philosophy was chosen. In this philosophy, the space frame structure is divided into three component groups: crash absorbers, front crash system and

passenger cell (fig. 6.11). Starting with the crash absorbers, analytical relationships were found to design such impact-absorbing structures without the computational effort and time of crash simulations with nonlinear finite-element analysis using explicit time integration. Once these components and their behavior were designed, the component group of the front crash system was optimized. Separating the structure into regions of plastic and elastic deformation allows the passenger cell to be optimized using linear elastostatic analysis. Further, as this structure is safety relevant, uncertainty in models were analyzed and integrated in the optimization-supported design process. Uncertainty analysis and optimization will be shown in the following numerical examples, followed by a verification of the structure concept.

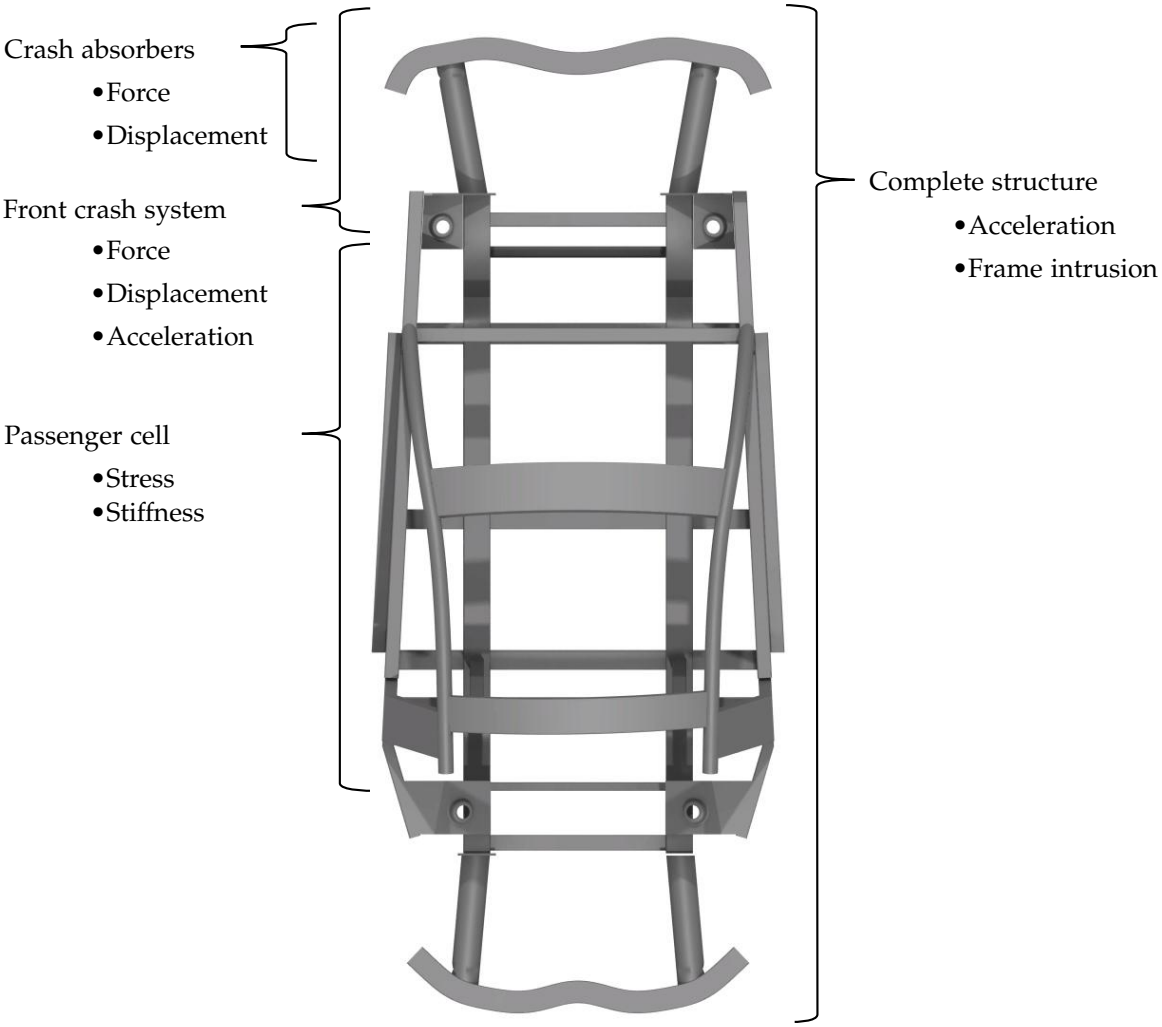

Figure 6.11: Multi-level design philosophy for LEAF (top view)

7

OPTIMAL DESIGN OF EXTRUDED SECTIONS FOR CRASH ABSORBERS WITH SIMPLIFIED MODELING UNDER UNCERTAINTY USING SIMPLIFIED MODELING

Extruded aluminum sections are used in the so-called crumple zone of automobiles for their ability to absorb the energy in a front impact (fig. 7.1). Thin-walled extruded profiles are lightweight and cost-effective structures. In this chapter, an efficient design method based on analytic relationships will be shown and used to dimension such structures, including material uncertainty. In this case, square cross-sectional geometries will be investigated.

Figure 7.1: Crash absorbers shown within the crumple zone of the Audi Space Frame

7.1 CROSS-SECTIONAL SHAPE

For the design of the crash absorbers, a square cross-section geometry has been chosen due to both structural-mechanical and availability. Varying cross-sectional shapes were studied including circular, square and hexagonal advised by the author and carried out by Urban (2012) and Fellner (2013) as well as a shape optimization advised by the author and carried out by Schulze Frenking (2013) resulting in hexagram (six-pointed star).

For the shape optimization (Schulze Frenking 2013), a quarter of the structure was parametrized with a cardinal spline with five control points. This symmetrical parametrization of the crash absorber resulted in eight design variables: seven for coordinates of the control points and one for a global tension parameter. This was shown to be flexible allowing for the limit cases of square to circular cross-section geometry. The objective function in this study was to maximize the mass-specific energy absorption. Geometrical constraints were used to guarantee the validity of the shape. As

this shape optimization may indeed be nonconvex, both a second-order algorithm and evolutionary strategy were used. These, though, resulted in the same general form (fig. 7.2). Although quite flexible, the use of a cardinal spline limits the possible cross-sectional shape. From the results, Schulze Frenking 2013 with the author postulated that the ideal shape has segments of equal length, though remaining thin enough to buckle locally. One such example is a hexagram (fig. 7.2).

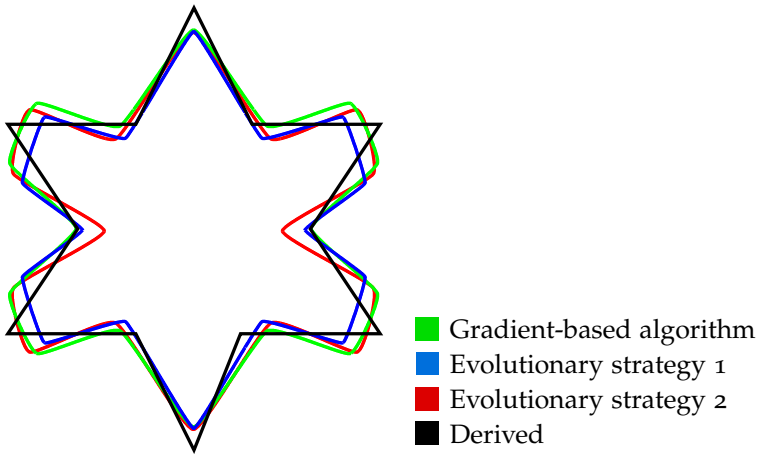

Figure 7.2: Results of shape optimization for cross-sectional geometry of a crash absorber

In a separate study, different cross-sectional shapes were investigated: After the optimization of circular and hexagonal cross-sectional geometry (wall thickness and cross-sectional size), a comparison of circular and hexagonal cross-sectional geometries considering uncertain material parameters was carried out by Urban 2012. The uncertainty of the resulting force due to a 10° crash of each cross-sectional shape can be seen in fig. 7.3, denoted by the area under the fuzzy number. In can be clearly seen that the hexagonal cross-sectional geometry is much robuster (less uncertainty) than the circular.

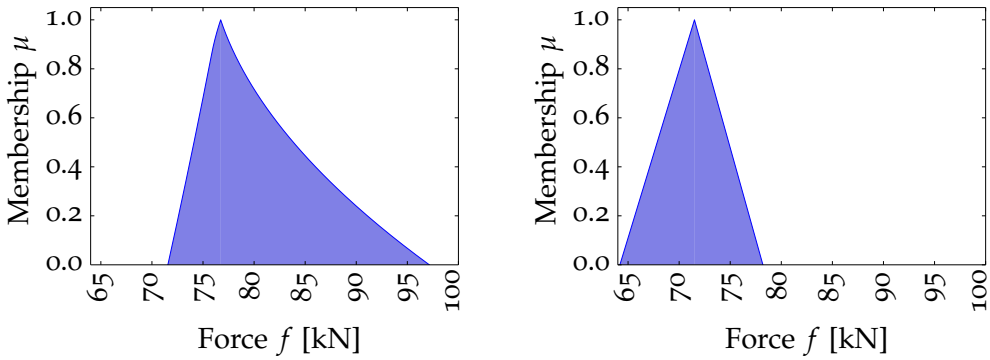

(a) Circular cross-sectional geometry

(b) Hexagonal cross-sectional geometry

Figure 7.3: Uncertain force response at optimum design

From these studies, it can, therefore, be deduced that the corners, thus forcing local buckling in the segments, along with the ratio of segment width to wall thickness play the vital role in the desired structural-mechanical behavior. From this finding also stems the use of the thinness criterion (eq. 3.36) to ensure proper and robust folding.

As it was decided to use standard cross-section geometry for the LEAF demonstrator, the hexagonal and hexgram shapes were not used. Instead a compromise between structural-mechanical behavior and availability was made. This resulted in square cross-sectional geometry, which is commonly procurable, which like the preferred shapes has segments of proper thinness and corners to contain the folding. These will be discussed below using simplified modeling.

7.2 DESIGN REQUIREMENTS

The length ℓ, wall thickness d and width b of a crash absorber of square cross-sectional geometry (fig. 7.4) are to be dimensioned to have a minimum mass and thereby to absorb a said amount of energy E. This shall be done while limiting a resulting force f_{res} so that its peak force f_{peak} does not cause unwanted plastic deformation in the rest of the structure (here: $f_{\text{allow}} = 150\,\text{kN}$).

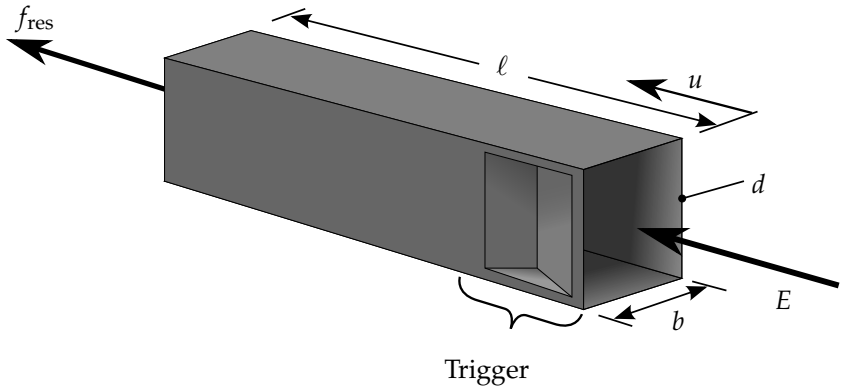

Figure 7.4: Schematic of crash-absorbing extruded section with trigger

These structures are to be impervious to global buckling, which would result in much less energy absorption. This force by which global buckling f_{cr} occurs is defined by the geometry and is assumed to not play a role as long as it is lower than the peak force f_{peak}.

As to warrent proper folding of the crash absorbers, a local criterion is used. This says that each side of the square tube shall buckle, reaching its critical stress σ_{cr}, before its yield stress σ_y is reached (here: $\sigma_y = 200\,\text{MPa}$). This static base, though a simplification, has shown good results in empirical tests and simulations conducted by the author.

In order to reduce the initial force, geometrical imperfections (or triggers) are used. These imperfections not only reduce the initial (and maximum) force f_{peak}, but instead also strongly influence the crushing pattern of such absorbers. This aspect is crucial for properly functioning crash absorbers.

Further, the crushing of the crash tube may not occur to the entire original length ℓ. The maximum allowed displacement u_{allow} here is limited to a leaving a minimum of 10% of the original length, $\frac{\ell}{10}$.

7.3 MECHANICAL BACKGROUND

In this section analytic models of axially loaded, extruded profiles will be introduced. This allows the designer to forgo computationally intense numerical methods with finite-element analysis. Using the relationships introduced in § 3.3, a system of equations was implemented for the initial design. This allowed for fast calculation and optimization including uncertainty of these structures.

The design domain of square crash absorbers can be also analyzed to better understand the problem. By setting one design variable (here: length ℓ) as constant, it is possible to visualize this design domain with all system equations (fig. 7.5). The feasible design space is limited to the center of the design domain (here: white).

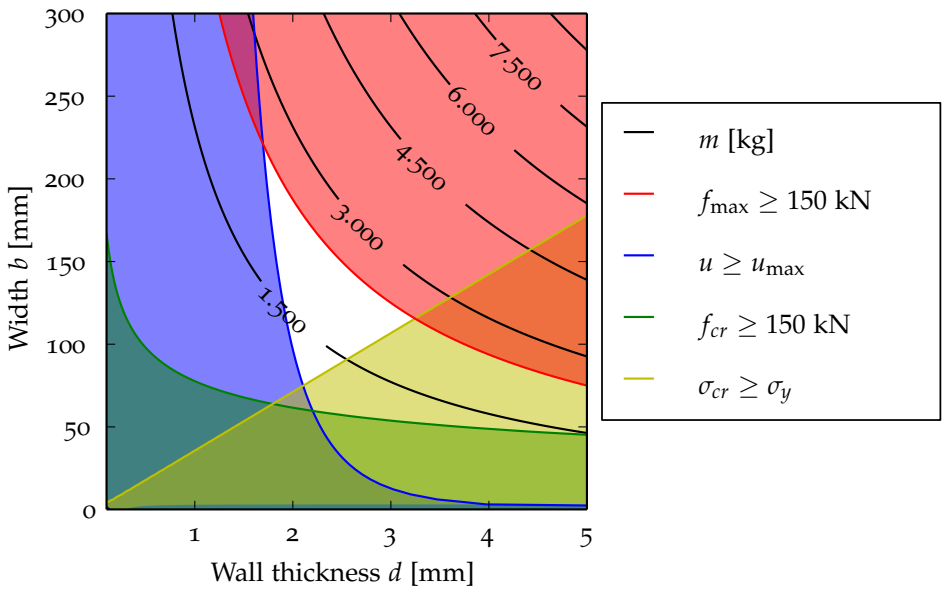

Figure 7.5: Design space for a crash-absorbing extruded section at $\ell = 600$ mm

7.4 DIMENSIONING OF CRASH ABSORBERS OF SQUARE CROSS-SECTIONAL GEOMETRY

The design problem of § 7.2 is here formulated as an optimization problem and the results are discussed.

7.4.1 *Optimization problem*

The mathematical formulation of the optimization problem for the design problem is described as follows:

$$\min_{\mathbf{x} \in \mathbf{X}} \{ f(\mathbf{x}) \, | \mathbf{g}(\mathbf{x}) \leq \mathbf{0} \},$$

where

$$\begin{aligned} \mathsf{f}(\mathbf{x}) &= m \\ \mathsf{g}_1(\mathbf{x}) &= \frac{f_{\text{peak}}}{f_{\text{allow}}} - 1 \\ \mathsf{g}_2(\mathbf{x}) &= \frac{u}{u_{\text{allow}}} - 1 \\ \mathsf{g}_3(\mathbf{x}) &= 1 - \frac{f_{cr}}{f_{\text{peak}}} \\ \mathsf{g}_4(\mathbf{x}) &= \frac{\sigma_{cr}}{\sigma_y} - 1 \\ \mathbf{x} &= \begin{bmatrix} d & b & \ell \end{bmatrix}^T. \end{aligned}$$

In the following this will problem will be solved and discussed.

7.4.2 *Optimization results*

The start value of the optimization was chosen with a thickness d of 3.0 mm, a width b of 100 mm and a length of 500 mm. The optimization of the crash absorbers converged quickly using the algorithm MMA to the general design in three iterations and 24 system evaluations to an optimum of 1.0214 kg. The convergence behavior can be seen in fig. 7.6, which needed a total of six iterations. The optimal design can be seen in tab. 7.1, which reduced all dimensions of the starting point slightly.

Table 7.1: Details of design variables for optimization of the crash absorber

Design variable	Symbol	$\mathbf{x}^0$	$\mathbf{x}^L$	$\mathbf{x}^U$	value $\mathbf{x}^*$
1	$\mathbf{x}_1$	3.0	1.0	5.0	2.4033
2	$\mathbf{x}_2$	100.0	25.0	150.0	85.4875
3	$\mathbf{x}_3$	500.0	300.0	600.0	460.3106

7.5 CONSIDERATION OF UNCERTAIN MATERIAL MODEL IN THE DESIGN OF CRASH ABSORBERS

The problem above was now considered with an uncertain material model. In this model, the yield stress $\tilde{\sigma}_y$ and Young's modulus $\tilde{E}$ are considered uncertain. The uncertain responses considered here are displacement $\tilde{u}$, peak force $\tilde{f}_{\text{peak}}$, critical global buckling force $\tilde{f}_{cr}$ and critical local buckling stress $\tilde{\sigma}_{cr}$.

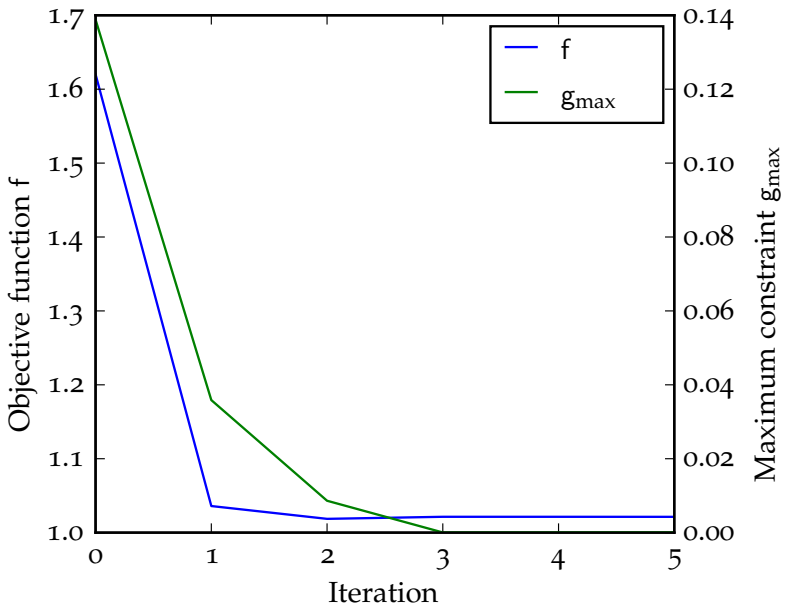

Figure 7.6: Convergence plots of the dimensioning of the crash absorber

The uncertain mapping is defined as

$$\begin{aligned} \tilde{\boldsymbol{p}} &\mapsto \tilde{\boldsymbol{r}} \\ \begin{Bmatrix} \tilde{\sigma}_y \\ \tilde{E} \end{Bmatrix} &\mapsto \begin{Bmatrix} \tilde{u} \\ \tilde{f}_{\text{peak}} \\ \tilde{f}_{cr} \\ \tilde{\sigma}_{cr} \end{Bmatrix}, \end{aligned}$$

where the uncertain material parameters are modeled with following trapezoidal fuzzy numbers (fig. 7.7):

$$\begin{aligned} \tilde{\sigma}_y &= \text{trap}\,\langle 175,\, 190,\, 210,\, 225\rangle \text{ MPa} \\ \tilde{E} &= \text{trap}\,\langle 65000,\, 68000,\, 72000,\, 75000\rangle \text{ MPa}. \end{aligned}$$

7.5.1 *Uncertainty analysis of the optimal design*

Considering the optimal design found above in § 7.4.2, an uncertain analysis was carried out. This resulted in the following uncertain response:

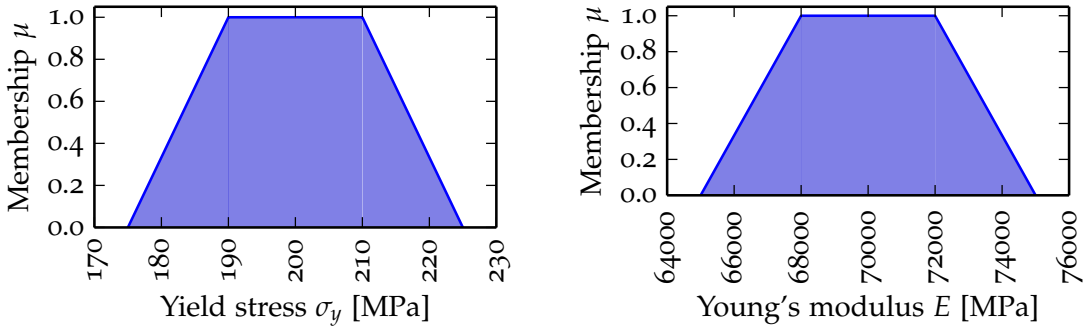

(a) Fuzzy yield stress

(b) Fuzzy Young's modulus

Figure 7.7: Uncertain material parameters for the crash absorber

$$
\begin{aligned}
\tilde{u} &= \text{trap}\,\langle 452.6412,\ 484.9727,\ 536.0225,\ 581.9672\rangle\ \text{mm} \\
\tilde{f}_{\text{peak}} &= \text{trap}\,\langle 71.9077,\ 78.0712,\ 86.2893,\ 92.4528\rangle\ \text{kN} \\
\tilde{f}_{cr} &= \text{trap}\,\langle 75.8256,\ 79.3253,\ 83.9915,\ 87.4911\rangle\ \text{kN} \\
\tilde{\sigma}_{cr} &= \text{trap}\,\langle 185.7183,\ 194.2899,\ 205.7187,\ 214.2903\rangle\ \text{MPa},
\end{aligned}
$$

which required 84 system evaluations for two α-levels and 228 system evaluations for six α-levels. Here it can be seen that with realistic and relatively small uncertainties in the material can result in an increase of uncertainty in the system responses, which would lead to a drastically suboptimal design.

7.5.2 *Worst-case optimization of analytical relationships under uncertain material*

In order to handle this uncertainty and still provide an optimal design, this must be integrated again in the design problem. This will be first done with a worst-case optimization, which is formulated as follows:

$$\min_{\mathbf{x}\in\mathbf{X}} \left\{ f(\mathbf{x}) \,|\mathbf{g}(\mathbf{x}) \leq \mathbf{0} \right\},$$

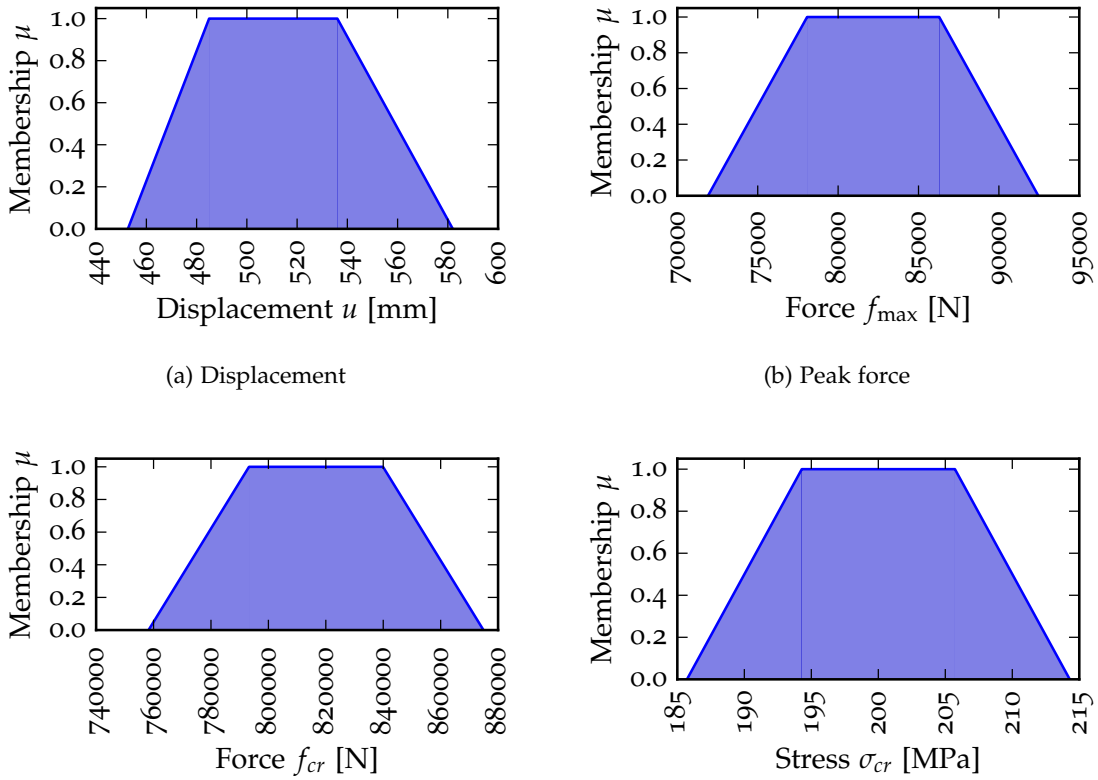

(a) Displacement

(b) Peak force

(c) Critical global buckling force

(d) Critical local buckling stress

Figure 7.8: Uncertain structural response for the optimal crash absorber

where

$$\begin{aligned} \mathsf{f}(\mathbf{x}) &= m \\ \mathsf{g}_1(\mathbf{x}) &= \frac{\max\{\tilde{f}_{\text{peak}}\}}{f_{\text{allow}}} - 1 \\ \mathsf{g}_2(\mathbf{x}) &= \frac{\max\{\tilde{u}\}}{u_{\text{allow}}} - 1 \\ \mathsf{g}_3(\mathbf{x}) &= 1 - \frac{\min\{\tilde{f}_{cr}\}}{\max\{\tilde{f}_{\text{peak}}\}} \\ \mathsf{g}_4(\mathbf{x}) &= \frac{\max\{\tilde{\sigma}_{cr}\}}{\min\{\tilde{\sigma}_y\}} - 1 \\ \mathbf{x} &= \begin{bmatrix} d & b & \ell \end{bmatrix}^T. \end{aligned}$$

From the identical starting design as above, the worst-case optimization converged again very quickly with the algorithm MMA to the general optimum in three iterations, finally arriving to a design of 1.4932 kg in four iterations (fig. 7.9). This design is nearly 50% heavier than the deterministic optimum design to accommodate the uncertainty, which has made the design thicker, wider and longer (tab. 7.2).

Table 7.2: Details of design variables for worst-case optimization

Design variable	Symbol	$\mathbf{x}^0$	$\mathbf{x}^L$	$\mathbf{x}^U$	value $\mathbf{x}^*$
1	$\mathbf{x}_1$	3.0	1.0	5.0	2.7562
2	$\mathbf{x}_2$	100.0	25.0	150.0	100.589
3	$\mathbf{x}_3$	500.0	300.0	600.0	487.4504

7.5.3 *Possibility-based optimization of analytical relationships under uncertain material*

As the worst-case design may be too conservative and, therefore, too heavy, in this case, a certain level of possibility of failure will be accepted, namely $\Pi(\mathcal{F}) = 0.2$. Failure $\mathcal{F}$ is defined by $r > c$. The possibility-based optimization problem is

$$\min_{\mathbf{x}\in\mathbf{X}} \{\mathsf{f}(\mathbf{x}) \,|\mathbf{g}(\mathbf{x}) \leq \mathbf{0}\},$$

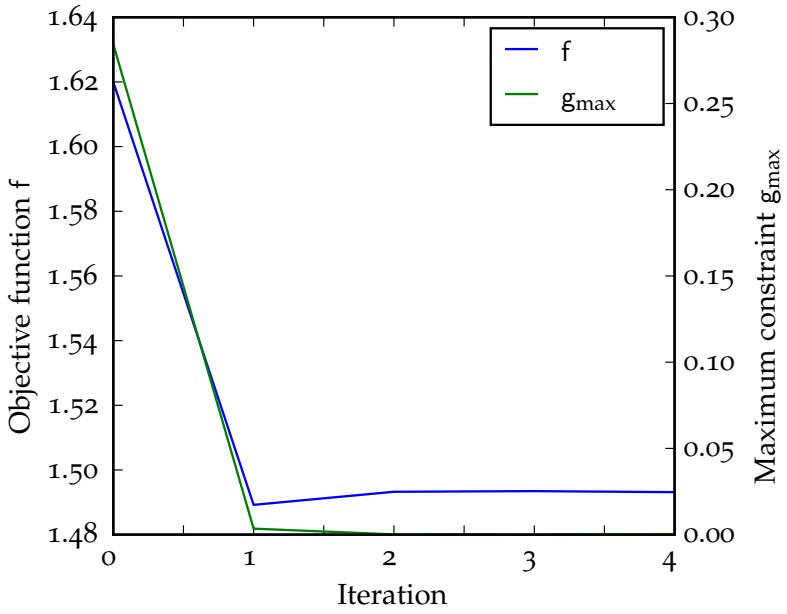

Figure 7.9: Convergence plots of the worst-case dimensioning of the crash absorber

where

$$
\begin{aligned}
\mathsf{f}(\mathbf{x}) &= m \\
\mathsf{g}_1(\mathbf{x}) &= \frac{\Pi\left(\mathcal{F}\left(\tilde{f}_{\text{peak}}\right)\right)}{0.2} - 1 \\
\mathsf{g}_2(\mathbf{x}) &= \frac{\Pi\left(\mathcal{F}\left(\tilde{u}\right)\right)}{0.2} - 1 \\
\mathsf{g}_3(\mathbf{x}) &= \frac{\Pi\left(\mathcal{F}\left(\tilde{f}_{cr}\right)\right)}{0.2} - 1 \\
\mathsf{g}_4(\mathbf{x}) &= \frac{\Pi\left(\mathcal{F}\left(\tilde{\sigma}_{cr}\right)\right)}{0.2} - 1 \\
\mathbf{x} &= \begin{bmatrix} d & b & \ell \end{bmatrix}^T.
\end{aligned}
$$

As above, using the algorithm MMA converged in four iterations to a lighter design of 1.3993 kg, or nearly 40% heavier than the deterministic design (fig. 7.10). The design was somewhat relaxed as seen by the design in tab. 7.3.

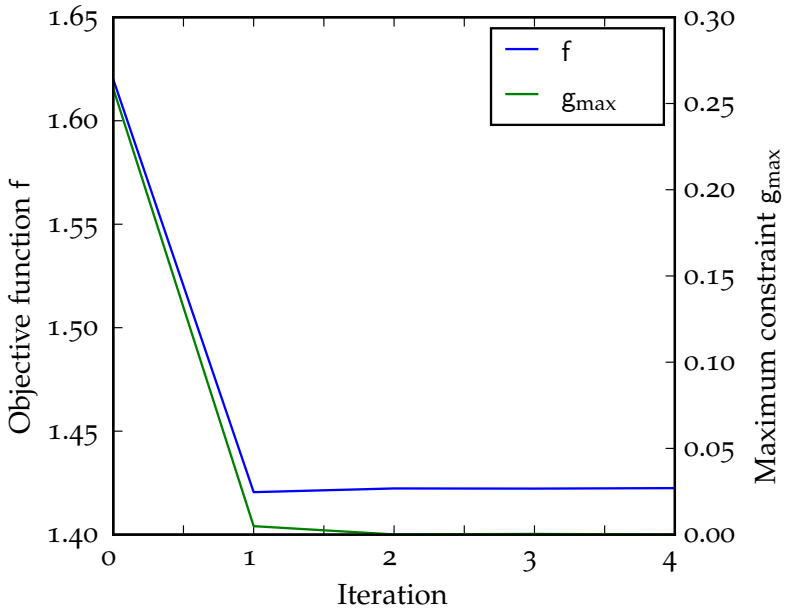

Figure 7.10: Convergence plots of the possibility-based dimensioning of the crash absorber

Table 7.3: Details of design variables for possibilistic optimization

Design variable	Symbol	$\mathbf{x}^0$	$\mathbf{x}^L$	$\mathbf{x}^U$	value $\mathbf{x}^*$
1	$\mathbf{x}_1$	3.0	1.0	5.0	2.7082
2	$\mathbf{x}_2$	100.0	25.0	150.0	98.852
3	$\mathbf{x}_3$	500.0	300.0	600.0	483.954

7.5.4 *Using shadow uncertainty prices for post processing*

After the optimization in § 7.5.2 results, the shadow prices S_P of the inequality and side constaints were calculated. As only the second and fourth inequality constraints are active, only these are displayed in tab. 7.4.

Table 7.4: Active shadow prices at optimal design of worst case optimization

Shadow price	Value	Unit
S_{P2}	-2.0929×10^{-3}	kg/mm
S_{P4}	-1.7023×10^{-3}	kg/MPa

The shadow uncertainties for the relevant structural responses, displacement u and σ_{cr} are

$$\begin{aligned}
\frac{\partial \tilde{u}}{\partial \tilde{\sigma}_y} &= \text{int}\,\langle -2.8209,\ -2.3092\rangle\ \text{mm/MPa} \\
\frac{\partial \tilde{u}}{\partial \tilde{E}} &= \text{int}\,\langle 0,\ 0\rangle\ \text{mm/MPa} \\
\frac{\partial \tilde{\sigma}_{cr}}{\partial \tilde{\sigma}_y} &= \text{int}\,\langle 0,\ 0\rangle\ \text{MPa/MPa} \\
\frac{\partial \tilde{\sigma}_{cr}}{\partial \tilde{E}} &= \text{int}\,\langle 2.8572 \times 10^{-3},\ 2.8572 \times 10^{-3}\rangle\ \text{MPa/MPa}.
\end{aligned}$$

Now using both shadow prices and shadow uncertainties to give shadow uncertainty prices, we get the following

$$\begin{aligned}
\frac{\partial m}{\partial \tilde{\sigma}_y} &= \text{int}\,\langle -5.7236 \times 10^{-3},\ -4.6854 \times 10^{-3}\rangle\ \text{kg/MPa} \\
\frac{\partial m}{\partial \tilde{E}} &= \text{int}\,\langle 4.8638 \times 10^{-6},\ 4.8638 \times 10^{-6}\rangle\ \text{kg/MPa}.
\end{aligned}$$

From these values, it is possible to forecase a reduction in the objective function. For a 10% reduction of the uncertain intervals

$$\begin{aligned}
\tilde{\sigma}_y &= \text{int}\,\langle 175,\ 225\rangle\ \text{MPa} \\
\tilde{E} &= \text{int}\,\langle 65000,\ 75000\rangle\ \text{MPa}
\end{aligned}$$

to

$$\begin{aligned}
\tilde{\sigma}_y &= \text{int}\,\langle 180,\ 220\rangle\ \text{MPa} \\
\tilde{E} &= \text{int}\,\langle 66000,\ 74000\rangle\ \text{MPa},
\end{aligned}$$

a reduction in mass is expected of 1.9171% (1.4642 kg) and 0.3258% (1.4879 kg) from the original 1.4928 kg, respectively for yield stress and Young's modulus. These values were then verified with optimization runs with the revised uncertainties to give a mass of 1.4519 kg and 1.4883 kg, respectively. As both state limit parameters are independent with respect to their critical uncertain parameters, the shadow uncertainty prices

Table 7.5: Comparison of results for the crash absorbers: I. Deterministic optimization, II. Worst-case optimization, III. Possibility-based optimization

Property	Symbol	I	II	III	Unit
Objective	f	1.0214	1.4932	1.3993	kg
Design variable 1	x_1	2.4033	2.7562	2.7082	mm
Design variable 2	x_2	85.4875	100.589	98.852	mm
Design variable 3	x_3	460.31.06	487.4504	483.954	mm
Possibility of failure	$\Pi(\mathcal{F})$	1.0	0.0	0.2	-

give a good forecast of 1.4593 kg when reducing the uncertainty in both. This was verified as being 1.4455 kg.

Via this method, one can then make judgment calls to carryout provisions to reduce the variability of the yield stress as this results in a greater reduction of mass. Further, cost of such provisions must be ascertained and weighted with the possible improvements.

7.5.5 *Findings*

Fast, analytical design methods for crash-absorbing extruded profiles were developed and validated. These were then used in the design of such crash absorbers, also under material uncertainty. Consideration of uncertainty in material parameters and interaction between these parameters has been shown to be critical in design and dimensioning.

Depending on the level of failure allowed, the design varied from just over 1 kg to nearly 1.5 kg (tab. 7.5). It is, therefore, important to analyze the uncertainty present in addition to the allowable uncertainty in a structure. Lastly the post-processing step of shadow uncertainty prices was carried out to assess this numerically, which showed the great influence of the uncertainty of yield stress on the cost of mass.

8

OPTIMAL DESIGN OF AN AUTOMOTIVE FRONT CRASH SYSTEM OF EXTRUDED SECTIONS UNDER UNCERTAINTY USING SURROGATE METHODS

Extending on the previous chapter, an assembly of extruded aluminum sections will be design and optimized. Here the use of surrogate modeling will be shown for optimization as well as optimization under uncertainty.

8.1 DESIGN REQUIREMENTS

As with the crash absorbers of the previous chapter, the front crash system is to be designed for minimal mass m. Here, the minimum mass is to be found while absorbing a said amount of energy E, respresenting the velocity and mass of a small electric vehicle in a front load case (Euro NCAP). This is to be done so that the peak force f_{peak} does not exceed a force that would cause unwanted plastic deformation in the rest of the structure f_{allow}. The energy shall be absorbed in an intrusion u less than u_{allow}. Lastly, the identical criteria to encourage local buckling is used as above (cf. 7.2).

The load case considered is based on the Euro NCAP front 40% offset (fig. 8.1, cf. § 6.2). Though, instead of a deformable barrier, which would only deform locally when being used with space-frame structures—as is the case here with the front crash system—a rigid barrier is used.

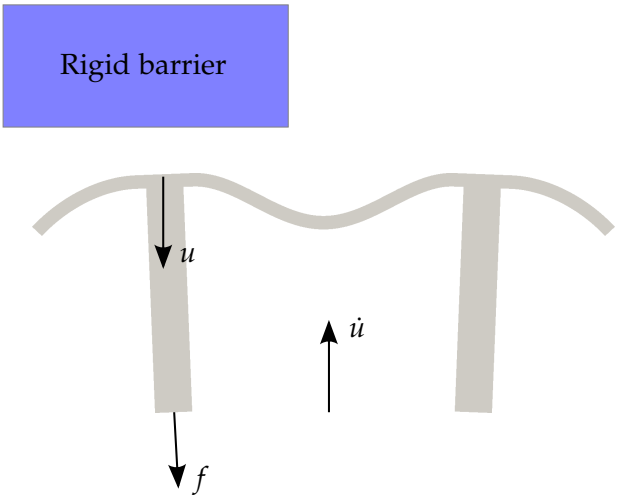

Figure 8.1: Modified Euro NCAP load case for the front crash system

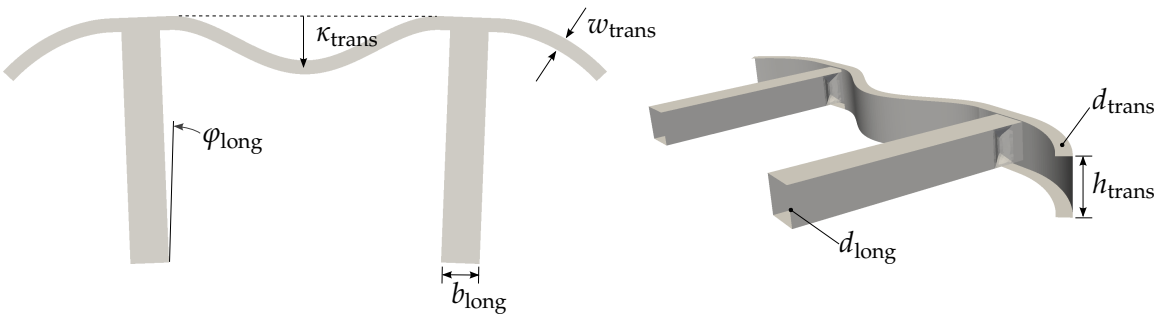

Figure 8.2: Design variables in top view (left) and back-right view (right)

The design variables are split into two domains (fig. 8.2): the transverse member (bumper) and the longitudinal members (crash absorbers). As above the width b_{long} and the wall thickness d_{long} are variable. In addition to these, the angular orientation of the crash absorbers φ_{long} is to be properly dimensioned. The transverse member allows for an m-shape via the design variable κ_{trans}. This was chosen to allow for the isolation of the crash tube of one side in the early phase of impact, thus discouraging global buckling. Further, the height h_{trans}, width w_{trans} and wall thickness d_{trans} of the bumper are to be found.

8.2 MECHANICAL BACKGROUND AND SYSTEM EQUATIONS

A rigid wall was used as a reduced barrier was used instead of a deformable barrier as it better accommodates a space-frame structure. A space-frame structure crashing into a deformable barrier would result in non-realistic local behavior of the barrier as the outer skin of the vehicle is not considered. The use of a rigid barrier also drastically reduces computational time. The finite-element model comprises of 13564 shell elements, 96 beam elements and one mass element to represent the mass of the complete vehicle (fig. 8.3). The Hockett–Sherby material model (§ 3.4.2) is used for aluminum, though, no material failure is used for purposes of simplicity. Optimal trigger geometry is mapped to the model based on the analytical modeling of crash absorbers (fig. 8.3b, cf. § 3.3). The crash simulation is calculated with the commercial software LS-DYNA.

A design of experiments is carried out for both the design variables as well as the uncertain parameters. The all-at-once sampling plan that includes 1010 internal points within the combined design and uncertain domain via Latin hypercube sampling (§ 2.4.4) and 512 additional points of all corner points of the combined design and uncertainty domain (2^9). The corner points are included as this has been shown to be problematic when approximating with fuzzy analysis, which often utilizes this part of the uncertain domain. The approximation models for each response are created via Gaussian process (Kriging). This uses a quadratic regression along with a

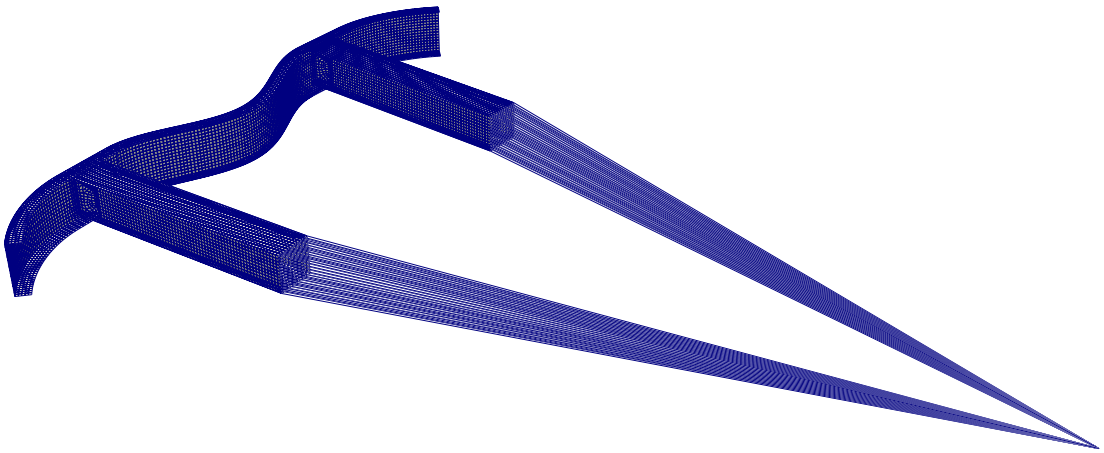

(a) Meshed front crash system

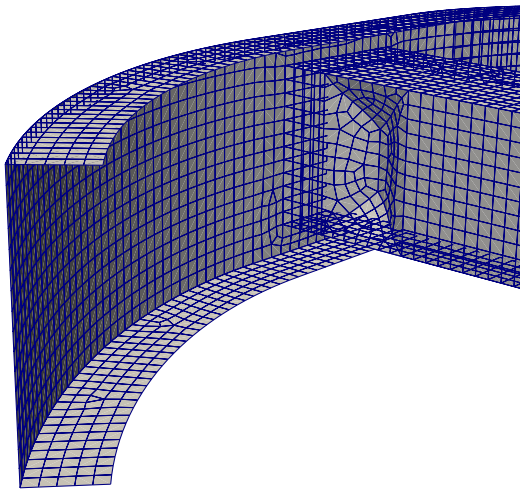

(b) Detail of trigger geometry and meshing

Figure 8.3: Finite-element model for the front crash system

squared-exponential correlation function. As single combined sampling was chosen to better compare the deterministic and fuzzy optimization results.

8.3 DIMENSIONING OF CRASH ABSORBERS OF ROUND AND SQUARE CROSS-SECTIONAL GEOMETRY

The following optimization results are based on a surrogate approach. Gaussian process was used for the system approximations based on a single design of experiments using samples chosen via Latin hypercube.

8.3.1 *Optimization*

The mathematical optimization problem for the design problem introduced above is

$$\min_{\mathbf{x}\in\mathbf{X}} \left\{ \mathsf{f}\left(\mathbf{x}\right) | \mathbf{g}\left(\mathbf{x}\right) \leq \mathbf{0} \right\},$$

where

$$\begin{aligned}
\mathsf{f}\left(\mathbf{x}\right) &= m \\
\mathsf{g}_1\left(\mathbf{x}\right) &= \frac{u}{u_{\text{allow}}} - 1 \\
\mathsf{g}_2\left(\mathbf{x}\right) &= \frac{f_{\text{peak}}}{f_{\text{allow}}} - 1 \\
\mathsf{g}_3\left(\mathbf{x}\right) &= \frac{\sigma_{cr}}{\sigma_y} - 1 \\
\mathbf{x} &= \begin{bmatrix} \varphi_{\text{long}} & b_{\text{long}} & d_{\text{long}} & \kappa_{\text{trans}} & h_{\text{trans}} & w_{\text{trans}} & d_{\text{trans}} \end{bmatrix}^T.
\end{aligned}$$

Below the optimal solution will be discussed.

8.3.2 *Optimization results*

For this problem a surrogate-based design optimization approach will be used in which the response surface is used instead of finite-element analysis. After starting at a slightly infeasible design, the algorithm MMA converged in 12 iterations to an optimal design of 5.1181 kg (fig. 8.4).

The optimal dimensions are found in tab. 8.1. The design shows good agreement the design optimization with analytical models being ca. 0.15 mm thicker and 4 mm wider. The design, further, demonstrates the ability to isolate the crash absorbers, thus forming the m-shaped bumper (fig. 8.5). Further, only a slight angle of ca. 2.25° was used to account for the nonsymmetry of the load case.

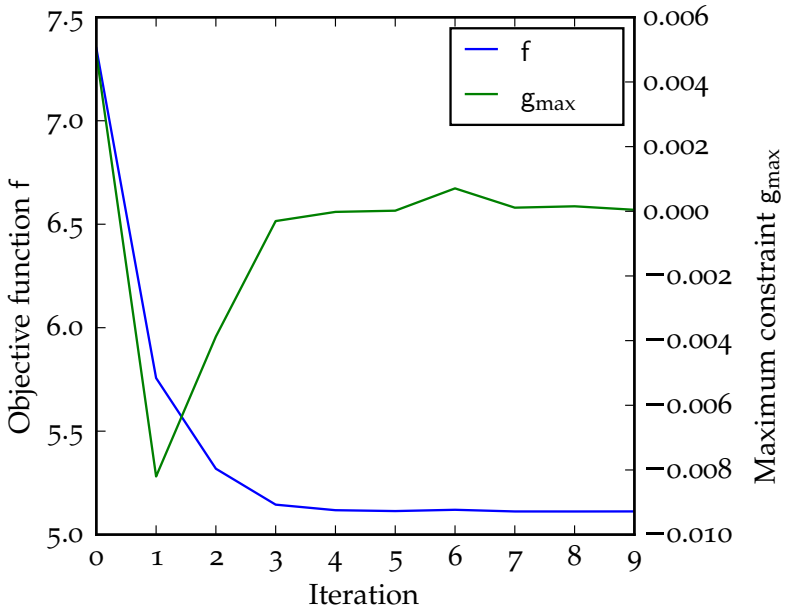

Figure 8.4: Convergence plots of the deterministic optimization of the front crash system

Table 8.1: Details of design variables for deterministic optimization of the front crash system

Design variable	Symbol	$\mathbf{x}^L$	$\mathbf{x}^U$	$\mathbf{x}^*$	Unit
1	$\mathbf{x}_1$	0	10	2.2616	deg
2	$\mathbf{x}_2$	70	150	89.4752	mm
3	$\mathbf{x}_3$	1	4	2.5156	mm
4	$\mathbf{x}_4$	-50	100	100.0	mm
5	$\mathbf{x}_5$	30	50	34.2913	mm
6	$\mathbf{x}_6$	30	75	32.3577	mm
7	$\mathbf{x}_7$	1	4	1.0	mm

8.4 CONSIDERATION OF UNCERTAIN MATERIAL MODEL IN THE DESIGN OF A FRONT CRASH SYSTEM

As above, the material model is now considered to be uncertain. In this model, based on the Hockett–Sherby model (§ 3.4.2), the yield stress $\tilde{\sigma}_y$, the plastic stress $\tilde{\sigma}_{pl}$ ($= \sigma_S - \sigma_Y$) and the strain-hardening constant $\tilde{c}$ are considered uncertain. The uncertain

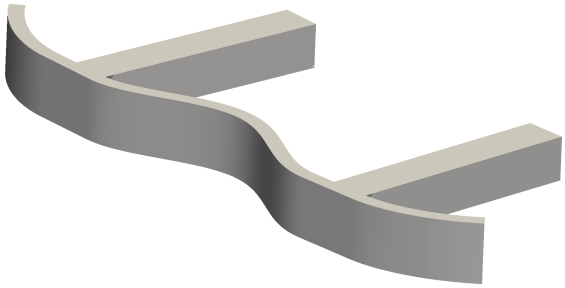

Figure 8.5: Optimal geometry for deterministic optimization of the front crash system

responses considered here are displacement $\tilde{u}$, peak force $\tilde{f}_{\text{peak}}$, critical global buckling force $\tilde{f}_{cr}$ and critical local buckling stress $\tilde{\sigma}_{cr}$.

The uncertain mapping for this model is defined as

$$\begin{array}{ccc} \tilde{\boldsymbol{p}} & \mapsto & \tilde{\boldsymbol{r}} \\ \left\{ \begin{array}{c} \tilde{\sigma}_y \\ \tilde{\sigma}_{pl} \\ \tilde{c} \end{array} \right\} & \mapsto & \left\{ \begin{array}{c} \tilde{u} \\ \tilde{f}_{\text{peak}} \end{array} \right\}, \end{array}$$

where the uncertain material parameters are modeled with following trapezoidal fuzzy numbers (fig. 8.6):

$$\begin{aligned} \tilde{\sigma}_y &= \text{trap}\,\langle 175, 190, 210, 225\rangle \text{ MPa} \\ \tilde{\sigma}_{pl} &= \text{trap}\,\langle 55, 60, 65, 70\rangle \text{ MPa} \\ \tilde{c} &= \text{trap}\,\langle 10, 11, 12, 13\rangle\,. \end{aligned}$$

8.4.1 *Uncertainty analysis of the optimal design*

The deterministic optimal design is now investigated using the uncertain material parameters above. This results in the following uncertain responses:

$$\begin{aligned} \tilde{u} &= \text{trap}\,\langle 457.3056, 471.1144, 492.7333, 524.3823\rangle \text{ mm} \\ \tilde{f}_{\text{peak}} &= \text{trap}\,\langle 140.5613, 142.0073, 150.7325, 170.6104\rangle \text{ kN}. \end{aligned}$$

This analysis was completed on the same complete surrogate model discussed above. The fuzzy numbers of the uncertain responses can be seen in fig. 8.7. Here, the clear nonlinearity and enhancement of the uncertainty towards the violated region is apparent.

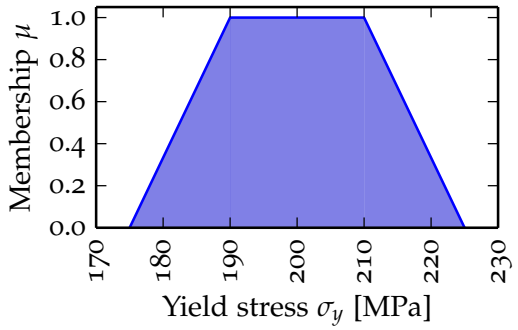

(a) Fuzzy yield stress

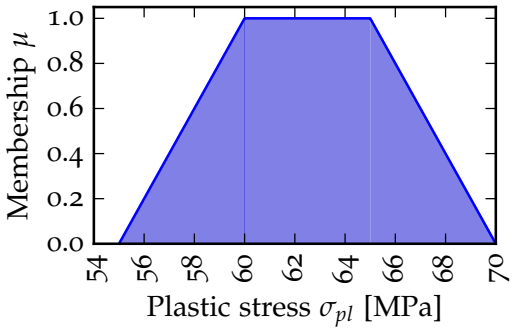

(b) Fuzzy plastic stress

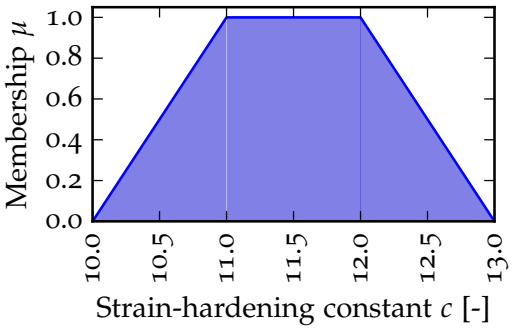

(c) Fuzzy strain-hardening constant

Figure 8.6: Uncertain material parameters for the front crash system

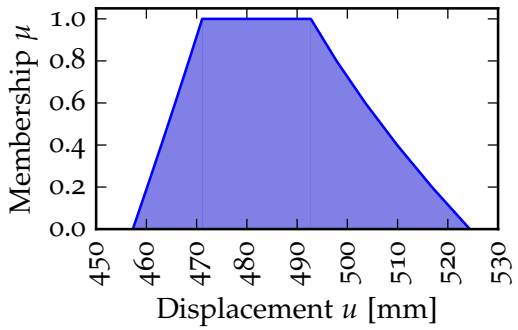

(a) Displacement

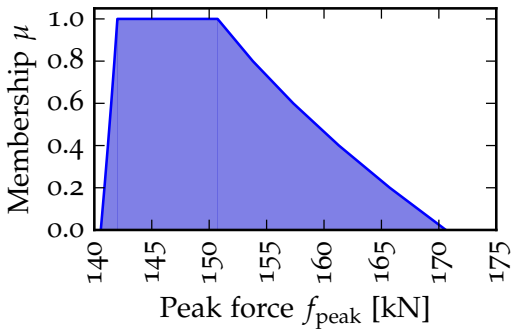

(b) Peak force

Figure 8.7: Uncertain structural response for the optimal front crash system

8.4.2 *Possibility-based design optimization*

To deal with the material uncertainty in the design optimization, a possibility-based design optimization was carried out. As above this was done using surrogate modeling with Gaussian process (Kriging). Again a certain level of possibility of failure will be accepted, namely $\Pi(\mathcal{F}) = 0.2$. Failure $\mathcal{F}$ is defined by $r > c$. The formulation of the possibility-based design optimization problem is then

$$\min_{\mathbf{x}\in\mathbf{X}} \{\mathsf{f}(\mathbf{x}) \,|\mathbf{g}(\mathbf{x}) \leq \mathbf{0}\},$$

where

$$\begin{aligned}
\mathsf{f}(\mathbf{x}) &= m \\
\mathsf{g}_1(\mathbf{x}) &= \frac{\Pi(\mathcal{F}(\tilde{u}))}{0.2} - 1 \\
\mathsf{g}_2(\mathbf{x}) &= \frac{\Pi\left(\mathcal{F}\left(\tilde{f}_{\text{peak}}\right)\right)}{0.2} - 1 \\
\mathsf{g}_3(\mathbf{x}) &= \frac{\Pi(\mathcal{F}(\tilde{\sigma}_{cr}))}{0.2} - 1 \\
\mathbf{x} &= \begin{bmatrix} \varphi_{\text{long}} & b_{\text{long}} & d_{\text{long}} & \kappa_{\text{trans}} & h_{\text{trans}} & w_{\text{trans}} & d_{\text{trans}} \end{bmatrix}^T.
\end{aligned}$$

The algorithm MMA converged to the optimum in 15 iterations and 120 evaluations to a design weighing 6.1038 kg. This is nearly 1 kg more or a 20% increase with respect to the deterministic optimal design.

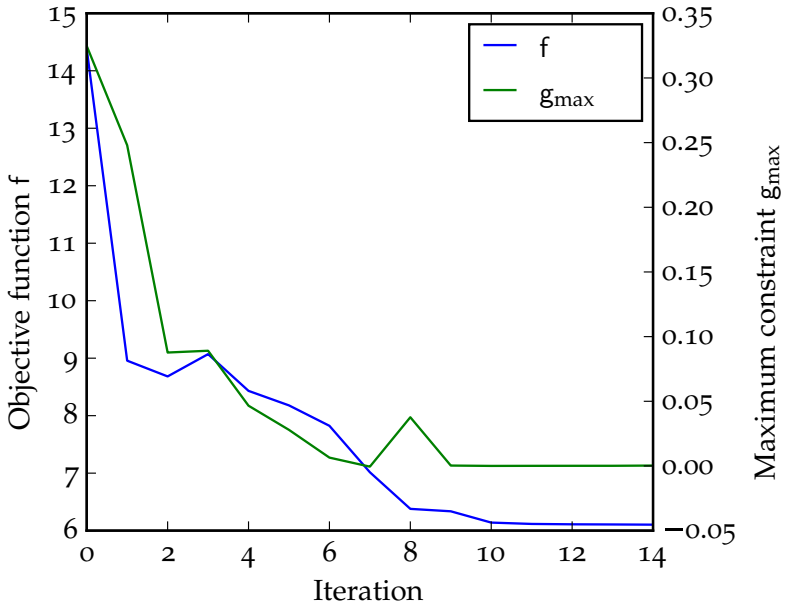

Figure 8.8: Convergence plots of the possibility-based optimization of the front crash system

The optimal dimensions are found in tab. 8.2. Once again, the design shows good agreement with the design optimization with analytical models being ca. 0.07 mm thicker and 0.5 mm narrower. The design, like in the deterministic case, uses the ability to isolate the crash absorbers, thus forming the m-shaped bumper (fig. 8.9). Again, only a slight angle of ca. 2.25° was used to account for the nonsymmetry of the load case.

Table 8.2: Details of design variables for possibility-based optimization of the front crash system

Design variable	Symbol	$\mathbf{x}^L$	$\mathbf{x}^U$	$\mathbf{x}^*$	Unit
1	$\mathbf{x}_1$	0	10	2.7740	deg
2	$\mathbf{x}_2$	70	150	98.3280	mm
3	$\mathbf{x}_3$	1	4	2.6072	mm
4	$\mathbf{x}_4$	-50	100	100.0	mm
5	$\mathbf{x}_5$	30	50	34.5227	mm
6	$\mathbf{x}_6$	30	75	43.5128	mm
7	$\mathbf{x}_7$	1	4	1.5165	mm

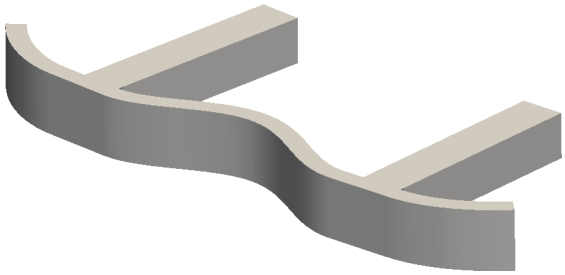

Figure 8.9: Optimal geometry for possibility-based optimization of the front crash system

8.5 FINDINGS

The designs show small differences with the uncertain model being generally dimensioned larger (fig. 8.10). Also, the angle of the longitudinal members are oriented 0.5° further outward to better avoid any global collapse problems. For this over dimensioning, the uncertain design is nearly 1 kg, 20% heavier.

Table 8.3: Comparison of results for the front crash system: I. Determinisitc optimization, II. Possibility-based optimization

Property	Symbol	I	II	Δ	Unit
Objective	f	5.1181	6.1038		kg
Design variable 1	x_1	2.2616	2.7740	0.5124	deg
Design variable 2	x_2	89.4752	98.3280	8.8528	mm
Design variable 3	x_3	2.5156	2.6072	0.0916	mm
Design variable 4	x_4	100.0	100.0	0.0	mm
Design variable 5	x_5	34.2913	34.5227	0. 2314	mm
Design variable 6	x_6	32.3577	43.5128	11.1551	mm
Design variable 7	x_7	1.0	1.5165	0.5165	mm
Possibility of failure	$\Pi(\mathcal{F})$	1.0	0.2	-0.8	-

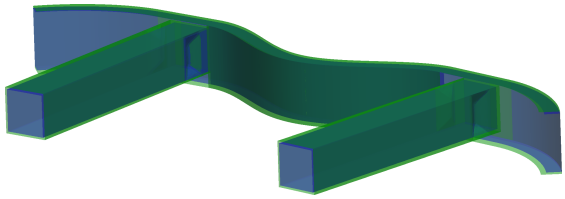

Figure 8.10: Comparison of deterministic and fuzzy designs: Deterministic design (blue), fuzzy design (green)

In this benchmark, the feasibility and value of the surrogate modeling was shown in using fuzzy methods for the optimization of structures. Although a design of experiments with a large number of samples was used, this can be further reduced in the future with e.g. adaptive surrogating.

9

COMPARISON OF RESULTS WITH THE FULL SPACE-FRAME STRUCTURE

In this chapter, the methods introduced in this dissertation will be validated using the LEAF space-frame structure in the Euro NCAP front-offset load case as a reference. First the decomposed design philosophy of the front crash system for the space frame will be investigated. This will be followed by an analysis of the consequence of the variation in the material model. The deterministic and fuzzy (possibilistic) optimal designs of the front crash system will be compared.

9.1 SPACE-FRAME STRUCTURE

In § 6, the decomposed design philosophy is discussed in which the passenger cell of the space frame LEAF was optimized. See Wehrle et al. (2011), Wehrle et al. (2012), Wehrle (2013) and Braun (2014) for the details on elastostatic design optimization of the passenger cell, which is outside the scope of the present document. In these works the optimal thickness of the passenger cell were found using static replacement loads for the crash load cases via inertia relief. This geometry (fig. 9.1) will be used in the verification of the optimal results of the front crash system within the decomposed design development philosophy of LEAF.

The finite-element model of LEAF, comprising of 225471 shell elements, 622 beam elements and 1667 solid elements (for details see Tischer 2012), is calculated with the commercial software LS-DYNA. The large components of the structure were modeled

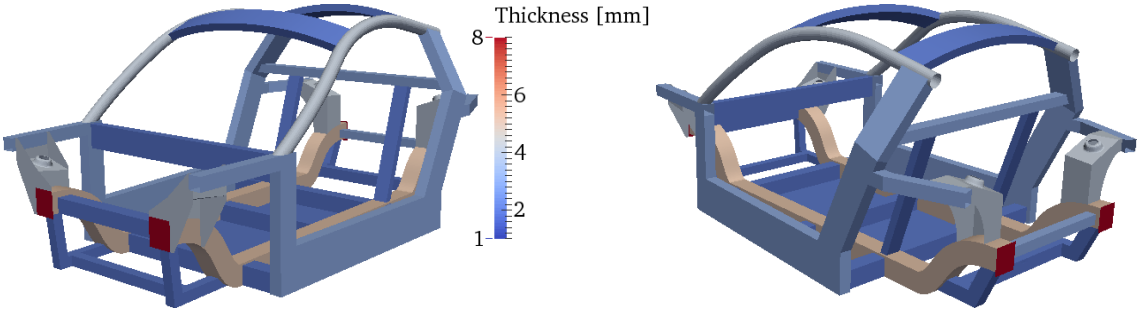

(a) Front-left view (b) Back-left view

Figure 9.1: Optimal wall thicknesses of passenger cell of LEAF

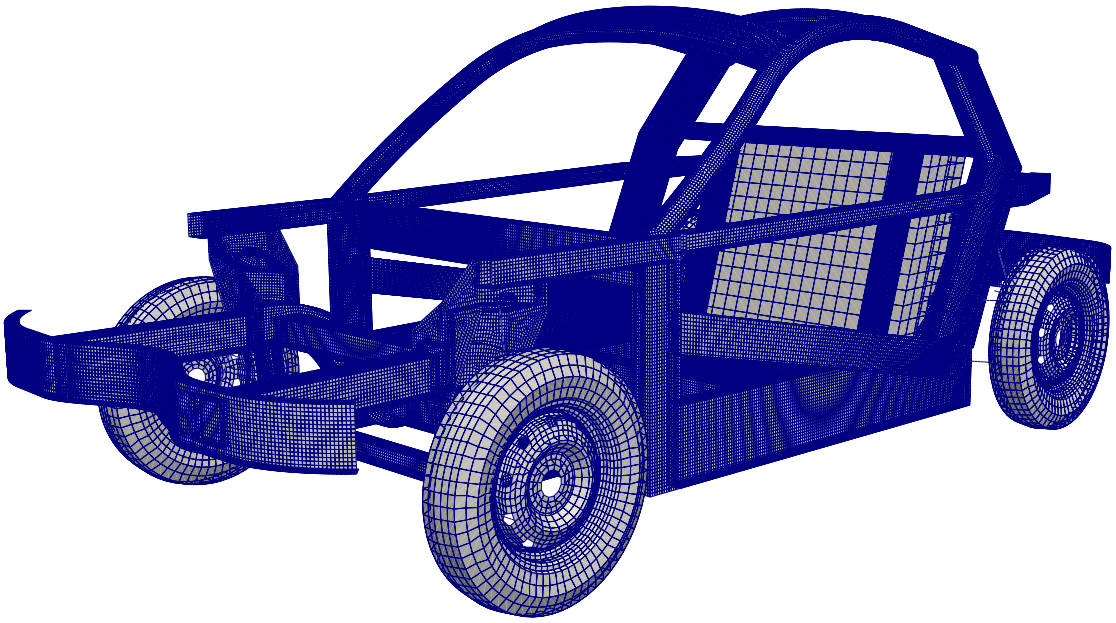

Figure 9.2: Finite-element model for LEAF

with solid elements with rigid constitutive models; these include the battery (behind the passenger cell) and the central electric motor (above rear axle).

9.2 VALIDATION OF DECOMPOSED DESIGN PHILOSOPHY

While having excellent agreement in the critical first phase of the crash—crushing of the energy absorbers—the force–time graph (fig. 9.4) shows a slightly delayed final force peak. The crushing shows nearly zero deviation (cf. fig. 9.3), which can by explained by proper design of trigger geometry and longitudinal member. The deviation of the end of the crash, on the other hand, stems from the s-rail of LEAF deforming plastically before the force peak occurs at when the tire makes contact with the A-pillar (cf. fig. 9.3, 0.04–0.06 s). Although the deformation fields of the two models deviate after 0.08 s, the force level is no longer critical in this region. The resulting plastic behavior of the forward section s-rail shows no degradation of the structural integrity of the safety cell in the front crash. A reduction in the allowable intrusion of the front crash system, however, would allow for a better conditioned decomposition of the design process, though at the price of a higher mass of both safety cell and front crash system.

As introduced in § 6 a decomposed design philosophy was used for the development of LEAF in which the space frame is not to deform plastically. Here the results of the front crash system (FCS) and the full space-frame LEAF will be compared.

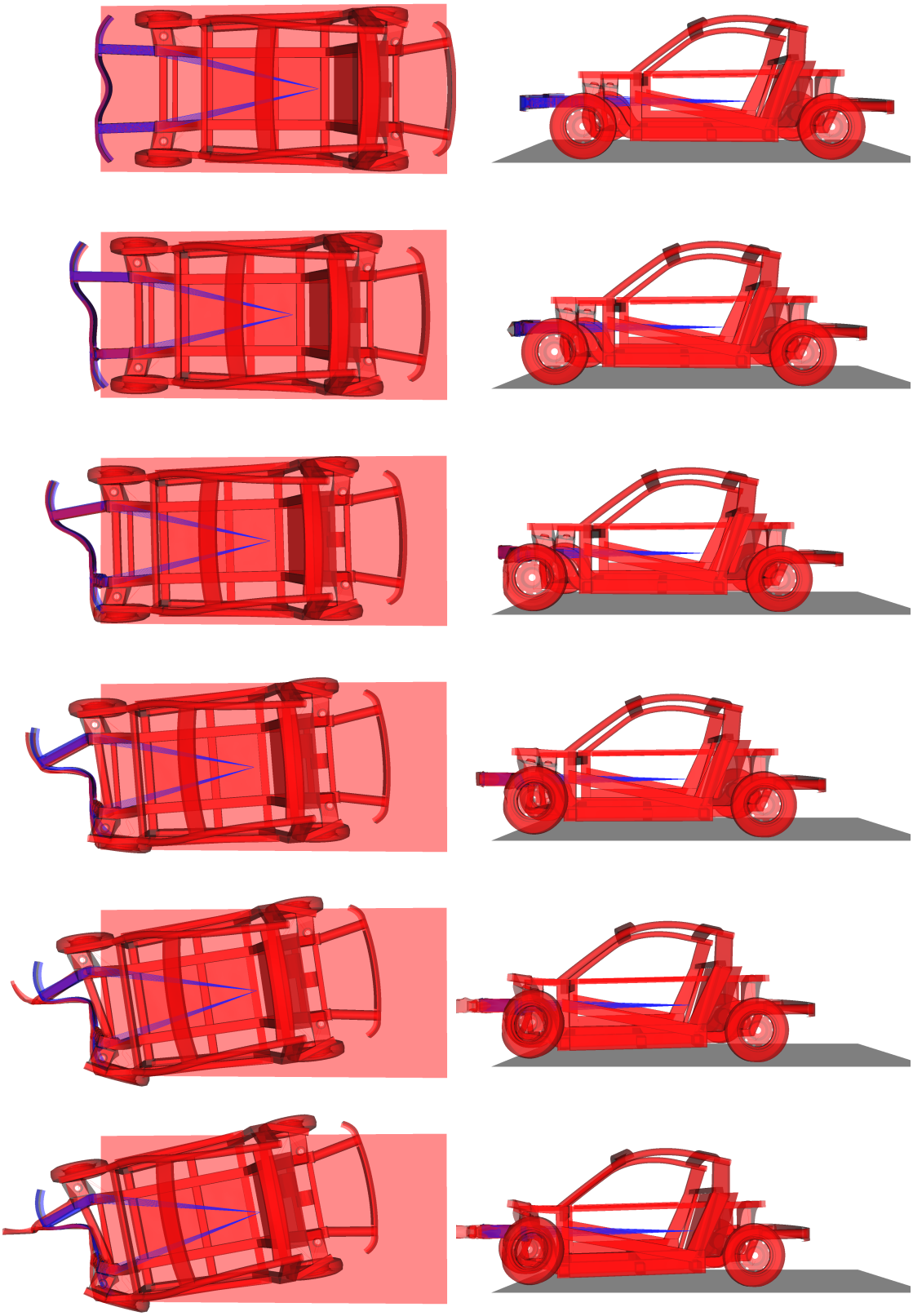

Figure 9.3: Comparison of between FCS (blue) and LEAF (red) for the deterministic optimal design at at t = 0.0, 0.02, 0.04, 0.06, 0.08, 0.1 s, top view (left) and left-side view (right)

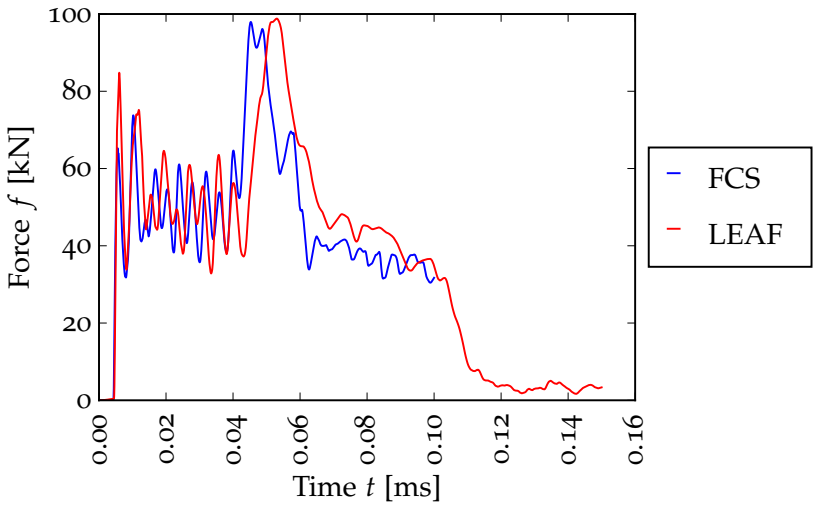

Figure 9.4: Force–time graph of the FCS and LEAF of the deterministic optimal design

9.3 COMPARISON OF BEHAVIOR CONSIDERING UNCERTAINTY CONSIDERATIONS

In fig. 9.5, it can be seen that large deformation (plastic behavior) occurs in the s-rail especially for material model with the lowest values (blue). One can also see that the upper longitudinal in the front of the vehicle buckles globally for the lowest level of material, though not in the case of the material model with middle (deterministic) and high values.

Although the deformation fields are similar between the deterministic and fuzzy design, in fig. 9.6 one sees drastically less deformation in the transverse member. This is due to the larger dimensioning resulting from the fuzzy design, which has reduced generally the deformation in the entire space-frame structure.

9.4 FINDINGS AND INTERPRETATION OF RESULTS

The proposed design philosophy, also considering optimization has proven itself to be an efficient and effective method in the development of a vehicle structure using structural design optimization. For this a step-wise approach was used that allowed a gradual increase of design variables and computational effort.

The reduction of the deformation is also apparent. Nonetheless, this example does not highlight the method as if a stability state limit was the active constraint. Here one would see a drastic change in the system responses from the consideration of uncertainty. This system remains well conditioned, also in consideration of uncertainty in the material parameters. This being the case, the integration of DesOptPy and

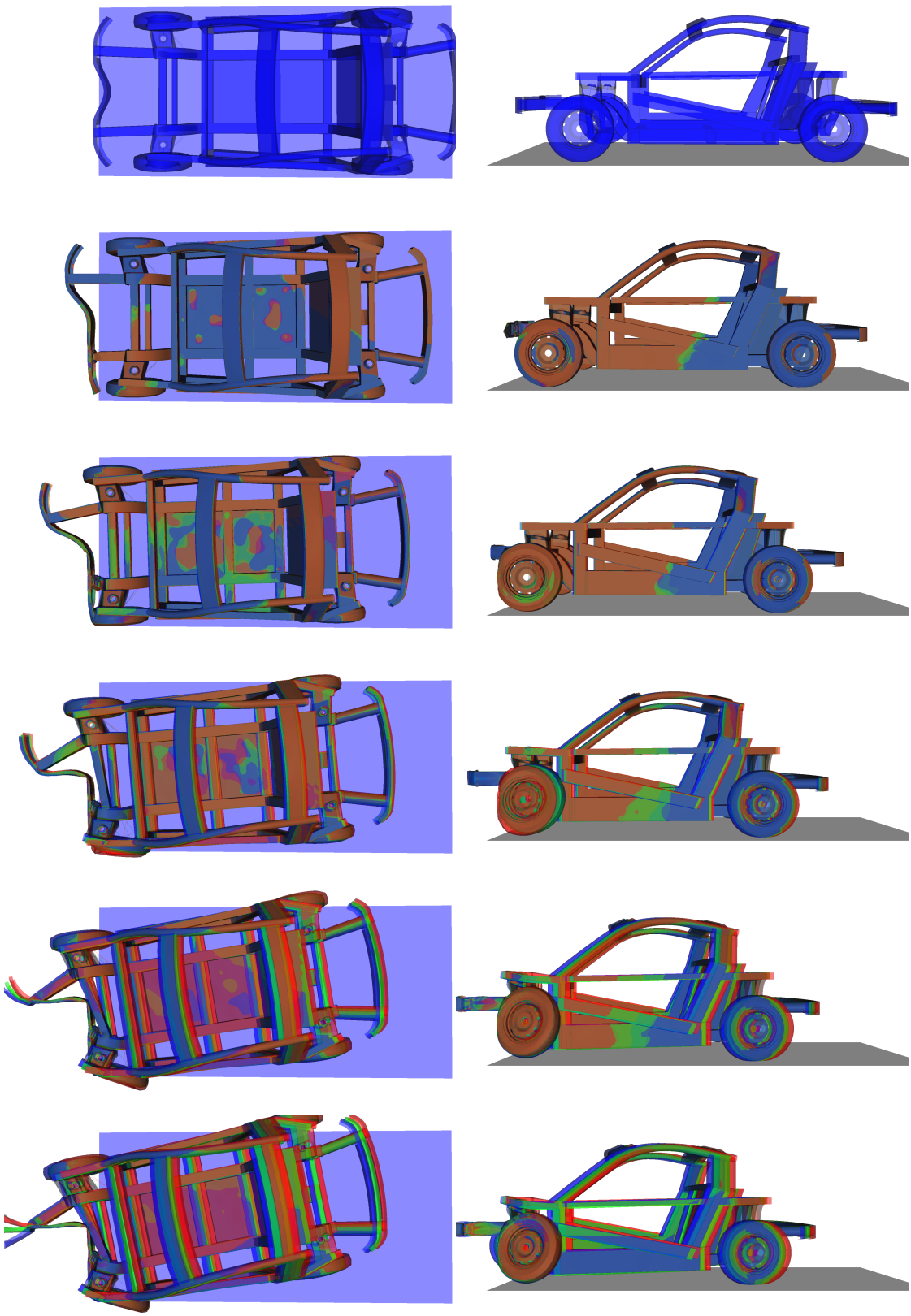

Figure 9.5: Comparison of the deterministic optimal design of the front crash system in LEAF different material properties: low (blue), middle (green) and high (red) at t = 0.0, 0.02, 0.04, 0.06, 0.08, 0.1 s, top view (left) and left-side view (right)

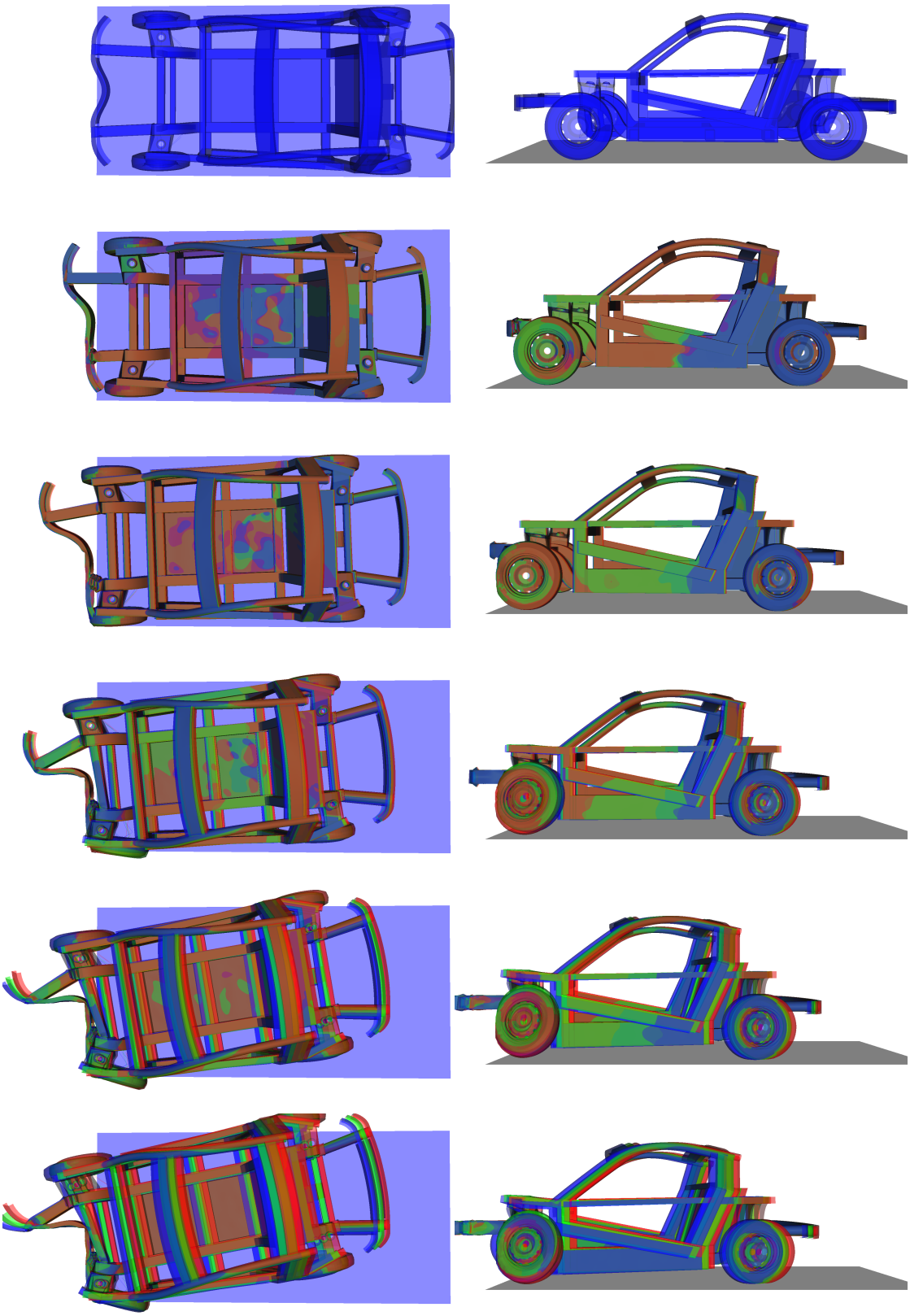

Figure 9.6: Comparison of the fuzzy optimal design of the FCS in LEAF different material properties low (blue), middle (green) and high (red) at t = 0.0, 0.02, 0.04, 0.06, 0.08, 0.1 s, top view (left) and left-side view (right)

FuzzAnPy, allowed for the exact dosing of material due to uncertainty. This would not have been possible with safety factor methods.

10 CONCLUSION

10.1 SUMMARY OF FINDINGS

In this dissertation, the understanding of structural design optimization under crashworthiness and uncertainty has been furthered in several respects. Although with this come several questions to be further answered and these aspects will be discussed in this summarizing section.

The dimensioning of crash absorbers with simplified analytical modeling works excellent for simple cross-sectional areas and the main axial load case. The addition of the thin-walled criteria for proper crushing—both in simplified analytical and finite-element modelling, constrained an unrealistic part of the design domain, where the designs behave nonrobust with respect to varying parameters due to the high wall thickness. This, thus, allowed for a better conditioned optimization problem. Of course, if the load case deviates far from the axial load considered, the analytical methods will fail. This, though, was not shown to be the case in these investigations.

Analytical design sensitivities were implemented for an academic problem, allowing for exact gradients and excellent convergence of the problem. On one hand, this alleviates the need for finite differencing and the problem in which it entails: computational effort and gradient problems for noisy responses. On the other hand, though, many questions must be answered in this regard to gradient calculation with e.g. contact or further the amount of memory such an approach would need for large models. Nonetheless, this has shown to have potential and can be used to increase efficiency of both design optimization as well as uncertainty analysis. The use of adjoint methods may further increase calculation efficiency.

Here, two software packages were developed and integrated for the application of design optimization under uncertainty with fuzzy methods. The main optimization toolbox DesOptPy uses efficient, mainly gradient-based algorithms. It, further, increases usability via easy set-up of optimization problems and gives graphical feedback to the user (e.g. via the convergence graphs found above). The development and implementation of uncertainty analysis with FuzzAnPy was carried out for fuzzy and interval analysis. Analysis with this toolbox is quite efficient due to use of numerical optimization methods and the introduction of surrogate modeling.

The concepts of *shadow uncertainty* and *shadow uncertainty price* were introduced for the post-processing for uncertainty analysis and optimization under uncertainty using the Lagrangian multipliers. These are therefore an extension of the idea of shadow price. These proved to be useful and efficient, especially when using optimization

algorithms for uncertainty analysis. These values allow the connection between uncertainty and their role in the uncertain system response or objective function to allow an assessment of a compromise between manufacturing tolerances and desired behavior. These may also be of use in the probabilistic realm, for instance when using gradient-based optimization algorithms FORM and SORM for reliability calculation.

Developed as a demonstrator for structural design optimization considering crashworthiness, LEAF is a structural-mechanically efficient space-frame body-in-white for small electric vehicles. Beyond the topics and load cases handled above, this simple, yet flexible and modular vehicular frame shows potential for application for small scale production runs.

10.2 DISCUSSION

10.2.1 *Use of* possibility *instead of* probability

Probability is a well-established methodology for handling uncertainty. Although this may be the case, possibilistically (i.e. intervals and fuzzy numbers) may be a more *natural* way for engineers to think about uncertainty, especially in early design phases. It is much easier to imagine an interval than a probability density function. Therefore, when decisions are made at the meeting table, hand calculation or even finite-element analysis, possibilistic and interval approaches allow for quick analysis. This is especially the case when no probabilistic data is available. Though the paradigm of probabilistic thought will not be altered by possibilistic methods, it may be a pragmatic "crutch" for the engineer to think about the problem in these terms.

10.2.2 *Computational effort of fuzzy analysis*

In this section, a rule of thumb is developed to approximate the computational effort for a fuzzy analysis. In a fuzzy analysis for each response, one must minimize and maximize on every α-level. Assuming the use of a gradient-based solver, for the first maximization and minimization, the algorithm of FUZZANPY needs typically between 5 and 10 iterations. As the starting value is then intelligently chosen for each subsequent maximization and minimization, typically only 1 to 3 iterations are needed.

For finite differencing response the algorithm then needs a number of evaluations equally

$$\begin{aligned} n_{\text{eval}} &= n_{\tilde{r}} \cdot 2[10\overbrace{\left(n_{\tilde{p}}+1\right)}^{\text{FD}} + \left(n_{\alpha}-1\right) 3 \left(n_{\tilde{p}}+1\right)] \\ &= 2n_{\tilde{r}} \left(n_{\alpha}+14\right) \left(n_{\tilde{p}}+1\right) \end{aligned} \tag{10.1}$$

for a direct fuzzy analysis.

When design sensitivities are available, the algorithm then needs depending on algorithm between zero to two further evaluations for step-length optimization

$$\begin{aligned} n_{\text{eval}} &= n_{\tilde{r}} \cdot 2\left[10\,(2) + (n_\alpha - 1)\,(3 \cdot 2)\right] \\ &= 2n_{\tilde{r}}\,(6n_\alpha + 14) \end{aligned} \tag{10.2}$$

For surrogate-based methods, a single sampling is carried out a priori. As the Gaussian process used here utilizes a quadratic regression function, this dictates the minimum number of samples necessary. In addition to this, an oversampling γ is chosen (here $\gamma \approx 3$) and when the number of uncertain parameters remains small the corners of the uncertain domain are included. This leads to a sampling size of

$$n_{\text{eval}} = \gamma \frac{\left(n_{\tilde{p}} + 1\right)\left(n_{\tilde{p}} + 2\right)}{2}$$

without the corners, and

$$n_{\text{eval}} = \gamma \frac{\left(n_{\tilde{p}} + 1\right)\left(n_{\tilde{p}} + 2\right)}{2} + 2^{n_{\tilde{p}}}$$

with corners.

From tab. 10.1 it can clearly be decided when which method is efficient to use. It should be further noted that the use in this work, the gradient-based algorithm NLPQLP greatly outperformed these forecasted number of evaluations, an example being the fuzzy analysis of § 7: Using the approximation and values for number of evaluations needed found above for $n_{\tilde{r}} = 4$, $n_{\tilde{p}} = 2$ and $n_\alpha = 6$ would result in 600 evaluations while only 248 are needed. This number greatly relies on the conditioning of the optimization problem. If the system response is noisy with respect to the uncertainty parameters, a smoothing response surface shall then be used, e.g. quadratic approximation.

Parallelization is possible for this type of analysis and the computation effort of the gradient-based algorithm methods as well as surrogate methods can be greatly reduced; this, though, was outside the scope of the present work.

10.3 OUTLOOK

Although efficient, integration of analytical sensitivity analysis—especially with adjoint methods—for uncertainty analysis via α-level optimization would enable a great deal of uncertain parameters to be investigated. It would especially be of interest to look into geometric uncertainties in stability analysis, e.g of an axially loaded cylinder. Geometric uncertainties may play a larger role as their uncertainty is perturbed when using iterative methods for temporal discretization.

Modern implementations of the finite-element method provide error estimations. The model error, an uncertain mapping, along with other parametric uncertainty

Table 10.1: Approximate number of evaluations needed for different problem sizes

$n_{\tilde{r}}$	$n_{\tilde{p}}$	n_{α}	Gradient-based using finite differencing	Gradient-based using analytical sensitivities	Surrogate-based without corners	Surrogate-based with corners
1	1	1	*40*	*20*	*9*	*11*
1	1	6	*100*	*50*	*9*	*11*
10	10	1	*2200*	*200*	*198*	*1222*
10	10	6	5500	*500*	*198*	*1222*
100	100	1	202000	*2000*	15453	*
100	100	6	505000	*5000*	15453	*
1	100	1	*2020*	*20*	15453	*
1	100	6	5050	*50*	15453	*
10	100	1	20200	*200*	15453	*
10	100	6	50500	*500*	15453	*
100	10	1	22000	*2000*	*198*	*1222*
100	10	6	55000	*5000*	*198*	*1222*
10	1000	1	200200	*200*	1504503	*
10	1000	6	500500	*500*	1504503	*

would give the engineer a confidence interval of the numerical simulation. This would especially be interesting to analyze deviations between simulation and experiment.

Other dynamic applications such as fluid dynamics may be of interest. Here, amongst other possibilities, efficient, gradient-based algorithms for the analysis of uncertainty could further help the design engineer in his pursuit of the optimal!

BIBLIOGRAPHY

Abramowicz, W. (2003). Thin-walled structures as impact energy absorbers. *Thin-Walled Structures 41*(2–3), 91–107.

Abramowicz, W. (2004). An alternative formulation of the FE method for arbitrary discrete/continuous models. *International Journal of Impact Engineering 30*(8–9), 1081–1098.

Abramowicz, W. and N. Jones (1984a). Dynamic axial crushing of circular tubes. *International Journal of Impact Engineering 2*(3), 263–281.

Abramowicz, W. and N. Jones (1984b). Dynamic axial crushing of square tubes. *International Journal of Impact Engineering 2*(2), 179–208.

Abramowicz, W. and N. Jones (1986). Dynamic progressive buckling of circular and square tubes. *International Journal of Impact Engineering 4*(4), 243–270.

Alexander, J. M. (1960). An approximate analysis of the collapse of thin cylindrical shells under axial loading. *The Quarterly Journal of Mechanics and Applied Mathematics 13*(1), 10–15.

Ayyub, B. and G. J. Klir (2006). *Uncertainty modeling and analysis in engineering and the sciences*. Chapman & Hall.

Banichuk, N. and P. Neittaanmäki (2010). *Structural optimization under uncertainties*. Springer.

Barlow, R. E. (1998). *Engineering reliability*. SIAM.

Barnett, R. L. (1966). Survey of optimum structural design. *Experimental Mechanics 6*(12), 19A–26A.

Beer, M. and M. Liebscher (2008). Designing robust structures – A nonlinear simulation based approach. *Computers & Structures 86*(10), 1102–1122.

Belytschko, T., W. K. Liu, and B. Moran (2000). *Nonlinear finite elements for continua and structures*. Wiley.

Belytschko, T. and K. Mish (2001). Computability in non-linear solid mechanics. *International Journal for Numerical Methods in Engineering 52*(1-2), 3–21.

Ben-Haim, Y. (1994). Convex models of uncertainty: Applications and implications. *Erkenntnis 41*, 139–156.

Ben-Tal, A., L. El Ghaoui, and A. Nemirovski. (2009). *Robust Optimization*. Princeton University Press.

Bendsøe, M. and O. Sigmund (2003). *Topology optimization: Theory, methods and applications*. Springer.

Bernardini, A. and F. Tonon (2010). *Bounding uncertainty in civil engineering*. Springer.

Black, M. (1937). Vagueness: An exercise in logical analysis. *Philosophy of Science 4*(4), 427–455.

Blockley, D. (1979). The role of fuzzy sets in civil engineering. *Fuzzy Sets and Systems 2*(4), 267–278.

Blumhardt, R. (2001). *Numerische Optimierung des Crashverhaltens von Fahrzeugstrukturen und -komponenten*. Dr.-Ing. diss., Lehrstuhl für Leichtbau, Technische Universität München.

Bonet, J. and R. D. Wood (1997). *Nonlinear continuum mechanics for finite element analysis*. Cambridge University Press.

Braun, S. (2014). Modellbildung und Entwurfsoptimierung von einer Gitterrohrrahmenstruktur für Elektrofahrzeuge. Semester thesis, Lehrstuhl für Leichtbau, Technische Universität München. Advisor: E. J. Wehrle.

Brown, C. B. and J. T. P. Yao (1983). Fuzzy Sets and Structural Engineering. *Journal of Structural Engineering 109*(5), 1211–1225.

Bucher, C. (2009). *Computational analysis of randomness in structural mechanics*. Taylor & Francis.

Cadete, R. N., J. P. Dias, and M. S. Pereira (2005). Optimization in vehicle crashworthiness design using surrogate models. In *6th World Congresses of Structural and Multidisciplinary Optimization*.

Chen, Q. (2000). *Comparing probabilistic and fuzzy set approaches for design in the presence of uncertainty*. Ph.D. diss., Virginia Polytechnic Institute and State University.

Choi, S.-K., R. V. Grandhi, and R. A. Canfield (2006). *Reliability-based structural design*. Springer.

Christensen, P. W. and A. Klabring (2009). *An introduction to structural optimization*. Springer.

Christlein, J. and L. Schüler (2000). Audi Space Frame 2. Generation: Realisierung eines zukunftsweisenden Leichtbau-Karosseriekonzepts mit Hilfe der Simulation. *VDI Berichte 1543*, 137–153.

Courant, R., K. Friedrichs, and H. Lewy (1928). Über die partiellen Differenzengleichungen der mathematischen Physik. *Mathematische Annalen 100*(1), 32–74.

Crisfield, M. (1996a). *Non-linear finite element analysis of solids and structures* (1st ed.), Volume 2: Advanced topics. Wiley.

Crisfield, M. (1996b). *Non-linear finite element analysis of solids and structures* (1st ed.), Volume 1: Essentials. Wiley.

Dai, Y.-H. and K. Schittkowski (2008). A sequential quadratic programming algorithm with non-monotone line search. *Pacific Journal of Optimization 4*, 335–351.

Dantzig, G. B. (1955). Linear programming under uncertainty. *Management Science 1*, 197–206.

de Borst, R., M. Crisfield, J. Remmers, and C. Verhoosel (2012). *Non-linear finite element analysis of solids and structures* (2nd ed.). Wiley.

Dubois, D. and H. Prade (1988). *Possibility theory*. Plenum Press, New York.

Duddeck, F. (2008). Multidisciplinary optimization of car bodies. *Structural and Multidisciplinary Optimization 35*(4), 375–389.

Elishakoff, I. (1999). *Probabilistic theory of structures* (2nd ed.). Dover.

Elishakoff, I. (2001). Interrelation between safety factors and reliability. Technical Report NASA CR-2001-211309, National Aeronautics and Space Administration.

Elishakoff, I. (2004). *Safety factors and reliability: friends or foes?* Kluwer.

Elishakoff, I., R. Haftka, and J. Fang (1994). Structural design under bounded uncertainty—Optimization with anti-optimization. *Computers & Structures 53*(6), 1401–1405.

Elishakoff, I. and M. Ohsaki (2010). *Optimization and anitoptimization of structures under uncertainty*. Imperial College Press.

Euler, L. (1744). *Methodus inveniendi lineas curvas maximi minimive proprietate gaudentes, sive solutio problematis isoperimetrici latissimo sensu accepti*.

Exler, O. and K. Schittkowski (2007). A trust region SQP algorithm for mixed-integer nonlinear programming. *Optimization Letters 1*(3), 269–280.

Fellner, F. (2013). Entwurfsoptimierung aufprallenergieabsorbierender Strukturen mithilfe vereinfachter Modellierung. Semester thesis, Lehrstuhl für Leichtbau, Technische Universität München. Advisor: E. J. Wehrle.

Fender, J. (2013). *Solution spaces for vehicle crash design*. Dr.-Ing. diss., Technische Universität München, Fachgebiet Computational Mechanics.

Fender, J., F. Duddeck, and M. Zimmermann (2014). On the calibration of simplified vehicle crash models. *Structural and Multidisciplinary Optimization 49*, 455–469.

Fleury, C. and V. Braibant (1986). Structural optimization: A new dual method using mixed variables. *International Journal for Numerical Methods in Engineering 23*(3), 409–428.

Ford, H. and S. Crowther (1922). *My life and work*. Doubleday, Page & Co.

Forrester, A. I. J., A. Sóbester, and A. J. Keane (2008). *Engineering design via surrogate modelling: A practical guide*. Wiley.

Forsberg, J. and L. Nilsson (2005). On polynomial response surfaces and Kriging for use in structural optimization of crashworthiness. *Structural and Multidisciplinary Optimization 29*(3), 232–243.

Freudenthal, A. M. (1947). The safety of structures. *Transactions of the American Society of Civil Engineers 112*(1), 125–159.

Ghanem, R. G. and P. D. Spanos (1991). *Stochastic finite elements: A spectral approach*. Springer.

Halgrin, J., G. Haugou, E. Markiewicz, and L. Rot (2008). Integrated simplified crash modelling approach dedicated to pre-design stage: evaluation on a front car part. *International Journal of Vehicle Safety 3*, 91–115.

Hammurabi (1750 BC). *Code of Hammurabi*. Translated: L. W. King (1910).

Hamza, K. and K. Saitou (2005). Design optimization of vehicle structures for crashworthiness using equivalent mechanism approximations. *Journal of Mechanical Design 127*(3), 485–492.

Hanss, M. (2005). *Applied fuzzy arithmetic: An introduction with engineering applications*. Springer.

Haug, E., T. Scharnhort, and B. Dubois (1986). FEM-Crash, Berechnung eines Fahrzeugfrontalaufpralls. *VDI Berichte 613*, 479–505.

Hilton, H. H. and M. Feigen (1960). Minimum weight analysis based on structural reliability. *Journal of the Aerospace Sciences 27*(9), 641–652.

Hockett, J. E. and O. D. Sherby (1975). Large strain deformations of polycrystalline metals at low homologous temperatures. *Journal of Mechanics and Physics of Solids 23*, 87–98.

Huang, X., Y. M. Xie, and G. Lu (2007). Topology optimization of energy-absorbing structures. *International Journal of Crashworthiness 12*(6), 663–675.

Huber, M. (2010). *Structural design optimization including quantitative manufacturing aspects derived from fuzzy knowledge*. Dr.-Ing. diss., Lehrstuhl für Leichtbau, Technische Universität München.

Huber, M., D. Neufeld, J. Chung, H. Baier, and K. Behdinan (2010). Data Mining based mutation function for engineering problems with mixed continuous-discrete design variables. *Structural and Multidisciplinary Optimization 41*, 589–604.

Hughes, T. (2000). *The Finite element method: Linear static and dynamic finite element analysis*. Dover Publications.

Johnson, W., P. Soden, and S. Al-Hassani (1977). Inextensional collapse of thin-walled tubes under axial compression. *The Journal of Strain Analysis for Engineering Design 12*(4), 317–330.

Jones, N. (1989). *Structural impact*. Cambridge University Press.

Jurecka, F. (2007). *Robust design optimization based on metamodeling techniques*. Dr.-Ing. diss., Lehrstuhl für Statik, Fakultät für Bauingenieur- und Vermessungswesen, Technische Universität München.

Karush, W. (1939). Minima of functions of several variables with inequalities as side constraints. Master's thesis, Department of Mathematics, University of Chicago.

Kim, C., A. Mijar, and J. Arora (2001). Development of simplified models for design and optimization of automotive structures for crashworthiness. *Structural and Multidisciplinary Optimization 22*, 307–321.

Kim, H.-S., S.-Y. Kang, I.-H. Lee, S.-H. Park, and D.-C. Han (1996). Vehicle frontal crashworthiness analysis by simplified structure modeling using nonlinear spring and beam elements. *International Journal of Crashworthiness 2*(1), 107–118.

Kleiner, M. and A. Klaus (2003). Flexible Fertigung leichter Tragwerke – der neue SFB/TR 10. In *Industriekolloquium des SFB 396*.

Klisinski, M. (1988). Plasticity theory based on fuzzy sets. *Journal of Engineering Mechanics 114*(4), 563–582.

Koiter, W. T. (1945). *Over de stabiliteit van het elastisch evenwicht*. Ph.D. diss., Technische Hogeschool van Delft. Translated as "The stability of elastic equilibrium" by E. Riks (1970).

Kuhn, H. W. and A. W. Tucker (1951). Nonlinear Programming. In *Proceedings of the Second Berkeley Symposium on Mathematical Statistics and Probability*, pp. 481–492.

Kurtaran, H., A. Eskandarian, D. Marzougui, and N. E. Bedewi (2002). Crashworthiness design optimization using successive response surface approximations. *Computational Mechanics 29*(4–5), 409–421.

Köylüoglu, H. U. and I. Elishakoff (1998). A comparison of stochastic and interval finite elements applied to shear frames with uncertain stiffness properties. *Computers & Structures 67*(1–3), 91–98.

Leitermann, W. and J. Christlein (2000). The 2nd generation Audi Space Frame of the A2: A trendsetting all-aluminium car body concept in a compact class car. In *Seoul 2000 FISITA World Automotive Congress*.

Lemaire, M. (2014). *Mechanics and uncertainty*. Wiley.

Liao, X., Q. Li, X. Yang, W. Li, and W. Zhang (2008). A two-stage multi-objective optimisation of vehicle crashworthiness under frontal impact. *International Journal of Crashworthiness 13*(3), 279–288.

Liu, Y. (2005). *Development of simplified models for crashworthiness analysis*. Ph.D. diss., University of Louisville, Department of Mechanical Engineering.

Liu, Y. (2010). Development of simplified truck chassis model for crash analysis in different impact scenarios. *International Journal of Crashworthiness 15*(5), 457–467.

Liu, Y. and M. L. Day (2007a). Development of simplified finite element models for straight thin-walled tubes with octagonal cross section. *International Journal of Crashworthiness 12*(5), 503–508.

Liu, Y. and M. L. Day (2007b). Development of simplified thin-walled beam models for crashworthiness analyses. *International Journal of Crashworthiness 12*(6), 597–608.

Liu, Y. and M. L. Day (2007c). Simplified modeling of thin-walled tubes with octagonal cross section – Axial crushing. In *6th European LS-DYNA Users' Conference*.

Liu, Y.-C. and M. L. Day (2006). Simplified modelling of thin-walled box section beam. *International Journal of Crashworthiness 11*(3), 263–272.

Lophaven, S. N., H. B. Nielsen, and J. Sondergaard (2002a). Aspects of the Matlab toolbox DACE. Technical Report IMM-REP-2002-13, Informatik og Matematisk Modellering, Danmarks Tekniske Universitet.

Lophaven, S. N., H. B. Nielsen, and J. Sondergaard (2002b). *DACE: A MATLAB Kriging toolbox*. Informatik og Matematisk Modellering, Danmarks Tekniske Universitet.

Martins, J. R. R. A. and J. T. Hwang (2013). Review and unification of methods for computing derivatives of multidisciplinary computational models. *AIAA Journal 51*(11), 2582–2599.

Mayer, H., F. Venier, and K. Koglin (2002). The ASF body of the Audi A8. *Automobiltechnische Zeitung 104*, 41–47.

Mayer, M. (1926). *Die Sicherheit der Bauwerke und ihre Berechnung nach Grenzkräften anstatt nach zulässigen Spannungen*. Springer.

Maymon, G. (2008). *Structural dynamics and probabilistic analysis for engineers*. Butterworth-Heinemann.

Menger, K. (1951). Ensembles flous et fonctions aléatoires. *Comptes rendus des séances de l'Académie des Sciences 232*, 2001–2003.

Mises, R. v. (1913). Mechanik der festen Körper im plastisch-deformablen Zustand. *Nachrichten von der königlichen Gesellschaft der Wissenschaften zu Göttingen 4*, 582–591.

Modarezadeh, M. (2005). *Dynamic analysis of structures with interval uncertainty*. Ph.D. diss., Case Western University.

Moens, D. and M. Hanss (2011). Non-probabilistic finite element analysis for parametric uncertainty treatment in applied mechanics: Recent advances. *Finite Elements in Analysis and Design 47*(1), 4–16.

Moens, D., D. Vandepitte, and W. Teichert (1998). Application of the fuzzy finite element method in structural dynamics. In *23rd International Conference on Noise and Vibration Engineering*, pp. 975–982.

Moore, R. E., R. B. Kearfott, and M. J. Cloud (2009). *Introduction to interval analysis*. Society for Industrial and Applied Mathematics.

Morasch, A., D. Matias, and H. Baier (2014). Material modelling for crash simulation of thin extruded aluminium sections. *International Journal of Crashworthiness 19*(5), 500–513.

Muhanna, R., H. Zhang, and R. Mullen (2007). Interval finite elements as a basis for generalized models of uncertainty in engineering mechanics. *Reliable Computing 13*, 173–194.

Muhanna, R. L. and R. L. Mullen (1999). Formulation of fuzzy finite-element methods for solid mechanics problems. *Computer-Aided Civil and Infrastructure Engineering 14*(2), 107–117.

Muhanna, R. L., R. L. Mullen, and H. Zhang (2004). Interval finite element as a basis for generalized models of uncertainty in engineering mechanics. In *NSF Workshop Reliable Engineering Computing*, pp. 353–370.

Möller, B. (1997). Fuzzy-Modellierung in der Baustatik. *Bauingenieur 72*(2), 75–84.

Möller, B. and M. Beer (2004). *Fuzzy randomness*. Springer.

Möller, B., W. Graf, and M. Beer (2000). Fuzzy structural analysis using α-level optimization. *Computational Mechanics 26*(6), 547–565.

Newmark, N. M. (1959). A method of computation for structural dynamics. *Journal of Engineering Mechanics 85*, 67–94.

Nikolaidis, E., S. Chen, H. Cudney, R. T. Haftka, and R. Rosca (2004). Comparison of probability and possibility for design against catastrophic failure under uncertainty. *Journal of Mechanical Design 126*(3), 386–394.

Paefgen, F.-J. and W. Leitermann (1994). Audi Space Frame – ASF: Ein neues PKW-Rohbaukonzept in Aluminium. *VDI Berichte 1134*, 23–70.

Panayirci, H. (2010). *Computational strategies for efficient stochastic finite element analysis of engineering structures*. Ph.D. diss., Leopold-Franzens-Universität Innsbruck.

Patel, N. (2007). *Crashworthiness design using topology optimization*. Ph.D. diss., University of Notre Dame.

Pedregosa, F., G. Varoquaux, A. Gramfort, V. Michel, B. Thirion, O. Grisel, M. Blondel, P. Prettenhofer, R. Weiss, V. Dubourg, J. Vanderplas, A. Passos, D. Cournapeau, M. Brucher, M. Perrot, and E. Duchesnay (2011). Scikit-learn: Machine learning in Python. *Journal of Machine Learning Research 12*, 2825–2830.

Perez, R., P. Jansen, and J. Martins (2012). pyOpt: A Python-based object-oriented framework for nonlinear constrained optimization. *Structural and Multidisciplinary Optimization 45*, 101–118.

Qiu, Z. and I. Elishakoff (1998). Antioptimization of structures with large uncertain-but-non-random parameters via interval analysis. *Computer Methods in Applied Mechanics and Engineering 152*(3–4), 361–372.

Rama Rao, M., R. Mullen, and R. Muhanna (2011). Interval finite elements for nonlinear material problems. In *Applications in Statistics and Probability in Civil Engineering*.

Ramberg, W. and W. Osgood (1943). Description of stress–strain curves by three parameters. Technical Note 902, National Advisory Committee For Aeronautics.

Rao, S. and J. P. Sawyer (1995). Fuzzy finite element approach for the analysis of imprecisely defined systems. *AIAA Journal 33*(12), 2364–2370.

Richter, M. (2014). Parallelization of numerical sensitivity analysis for large-scale structural design optimization. Semester thesis, Lehrstuhl für Leichtbau, Technische Universität München. Advisor: E. J. Wehrle.

Rosenblueth, A. and N. Wiener (1945). The role of models in science. *Philosophy of Science 12*(4), 316–321.

Rudolph, S. (2011). Konstruktion und Berechnung eines Spant-Leiterrahmen-Konzepts für das Elektrofahrzeug MU+E. Bachelor's thesis, Lehrstuhl für Leichtbau, Technische Universität München. Advisor: E. J. Wehrle.

Rudolph, S. (2013). Implementation of a Python-based structural optimization framework with pyOpt for engineering design. Semester thesis, Lehrstuhl für Leichtbau, Technische Universität München. Advisor: E. J. Wehrle.

Russell, B. (1923). Vagueness. *The Australasian Journal of Psychology and Philosophy, 1*, 84–92.

Sauerer, B., M. Schatz, E. Wehrle, and H. Baier (2014). Multistage structural optimization in the design of the lightweight electrical vehicle VisioM. In *European Altair Technology Conference*.

Schatz, M., E. Wehrle, and H. Baier (2014). Structural design optimization of lightweight structures considering material selection and sizing. In *International Conference on Engineering Optimization (EngOpt2014)*.

Schittkowski, K. (1985). NLPQL: A Fortran subroutine for solving constrained nonlinear programming problems. *Annals of Operations Research 5*, 485–500.

Schittkowski, K. (2013). NLPQLP: A Fortran implementation of a sequential quadratic programming algorithm with distributed and non-monotone line search. User's guide, version 4.0, Department of Computer Science, University of Bayreuth.

Schmit, L. A. (1960). Structural design by systematic synthesis. In *Proceedings of the Second Conference on Electronic Computation*, Volume 960. ASCE.

Schroll, M. (2013). Untersuchung analytischer Gradienten transienter nichtlinearer Strukturantworten nach Entwurfsvariablen anhand eines ebenen Fachwerkes. Bachelor's thesis, Lehrstuhl für Leichtbau, Technische Universität München. Advisors: E. J. Wehrle, M. Schatz.

Schulze Frenking, M. (2013). Profiloptimierung des Längsträgers des MUTE bezüglich Aufprallverhalten. Semester thesis, Lehrstuhl für Leichtbau, Technische Universität München. Advisor: E. J. Wehrle.

Schuëller, G. (2007). On the treatment of uncertainties in structural mechanics and analysis. *Computers & Structures 85*(5–6), 235–243.

Schuëller, G. I. (2006). Developments in stochastic structural mechanics. *Archive of Applied Mechanics 75*(10–12), 755–773.

Schöll, R., M. Holzapfel, and P. Steinle (2009). In sicherer, leichter Hülle – Die Fahrgastzelle der Zukunft: Strukturen in Spant- und Space-Frame-Bauweise. *DLR Nachrichten 123*, 34–37.

Seising, R. (2005). *Die Fuzzifizierung der Systeme: Die Entstehung der Fuzzy Set Theorie und ihrer ersten Anwendungen – Ihre Entwicklung bis in die 70er des 20. Jahrhunderts*. Habilitation, Ludwig-Maximilians-Universität München.

Seising, R. (2007). *The fuzzification of systems: The genesis of fuzzy Set theory and its initial applications – Developments up to the 1970s*. Springer.

Sobieszczanski-Sobieski, J., S. Kodiyalam, and R. Yang (2001). Optimization of car body under constraints of noise, vibration, and harshness (NVH), and crash. *Structural and Multidisciplinary Optimization 22*(4), 295–306.

Sudret, B., M. Berveiller, and M. Lemaire (2003). Application of a stochastic finite element procedure to reliability analysis. In *11th IFIP WG 7.5 Working Conference on Reliability and Optimization of Structural Systems*.

Sudret, B., M. Berveiller, and M. Lemaire (2006). A stochastic finite element procedure for moment and reliability. *European Journal of Computational Mechanics 15*, 825–866.

Sudret, B. and A. Der Kiureghian (2000). Stochastic finite elements and reliability: A state-of-the-art report. Technical Report UCB/SEMM-2000/08, Structural Engineering, Mechanics and Materials, Department of Civil & Environmental Engineering, University of California, Berkeley.

Svanberg, K. (1987). The method of moving asymptotes—A new method for structural optimization. *International Journal for Numerical Methods in Engineering 24*(2), 359–373.

Switzky, H. (1964). Minimum weight design with structural reliability. In *Fifth Annual Structures and Materials Conference*. AIAA.

Takada, K. and W. Abramowicz (2004). Fast crash analysis of 3D beam structures based on object oriented formulation. In *SAE 2004 World Congress & Exhibition*.

Takada, K. and W. Abramowicz (2007). Macro element fast crash analysis of 3D space frame. In *SAE World Congress & Exhibition*.

The Aluminum Association (1998). *Automotive aluminum crash energy management manual*. Washinton D.C., U.S.A.: The Aluminum Association.

Thiele, M., M. Liebscher, and W. Graf (2005). Fuzzy analysis as alternative to stochastic methods—A comparison by means of a crash analysis. In *4th German LS-DYNA Forum*.

Timoshenko, S. P. and J. M. Gere (1963). *Theory of elastic stability* (2nd ed.). McGraw-Hill.

Tischer, M. (2012). Untersuchung des Aufprallverhaltens eines Elektrokleinstfahrzeuges anhand eines parametrisierten Modells mit expliziter FEA. Diplomarbeit, Lehrstuhl für Leichtbau, Technische Universität München. Advisor: E. J. Wehrle.

Tonon, F., A. Bernardini, and I. Elishakoff (2001). Hybrid analysis of uncertainty: probability, fuzziness and anti-optimization. *Chaos, Solitons & Fractals 12*(8), 1403–1414.

Tovar, A. (2004). *Bone remodeling as a hybrid cellular automaton process*. Ph.D. diss., University of Notre Dame.

Turrin, S. and M. Hanss (2007). Uncertainty analysis in crash simulation with respect to structural design. In *Computational Uncertainty in Military Vehicle Design*.

Turrin, S., M. Hanss, and L. Gaul (2006). Fuzzy uncertainty analysis in automotive crash simulation. In *International Conference on Noise and Vibration Engineering ISMA2006*.

Urban, F. (2012). Strukturoptimierung und Robustheitsanalyse von Stauchrohren unter unscharfen Werkstoffgesetzen. Master's thesis, Lehrstuhl für Leichtbau, Technische Universität München. Advisor: E. J. Wehrle.

Wachter, F. (2014). Strukturoptimierung unter Aufpralllaster mittels Makroelemente. Bachelor's thesis, Lehrstuhl für Leichtbau, Technische Universität München. Advisor: E. J. Wehrle.

Wehrle, E. (2008). Robust structural optimization using possibility theory to model uncertainties. Master's thesis, Lehrstuhl für Leichtbau, Technische Universität München. Advisor: M. Huber.

Wehrle, E. (2013). Design optimization of lightweight structures for electrical vehicles including crashworthiness. In *6th Landshuter Leichtbau-Colloqium*.

Wehrle, E., J. Both, R. Wehrle, and H. Baier (2011). Development and design optimization of a space frame for an electric vehicle using hybrid materials. In *Landshuter Leichtbau-Colloquium*.

Wehrle, E., B. Sauerer, R. Wehrle, and H. Baier (2012). Ganzheitliche Strukturoptimierung von Fahrzeugkarosserien der Elektromobilität. In *Fakultätsseminar Mobilität*. Technische Universität München, Fakultät für Maschinenwesen.

Wehrle, E. J., Q. Xu, and H. Baier (2014a). Investigation, optimal design and uncertainty analysis of crash-absorbing extruded aluminium structures. *Procedia CIRP 18*, 27–32.

Wehrle, E. J., Q. Xu, and H. Baier (2014b). Investigation, optimal design and uncertainty analysis of crashabsorbing extruded aluminum structures. In *Conference on Manufacture of Lightweight Components (ManuLight2014)*.

Xu, Q. (2014). *Extended surrogate modeling techniques for large scale structural design optimization*. Dr.-Ing. diss., Lehrstuhl für Leichtbau, Technische Universität München.

Xu, Q., E. Wehrle, and H. Baier (2012). Adaptive surrogate-based design optimization with expected improvement used as infill criterion. *Optimization 61*(6), 661–684.

Yang, X.-S. (2010). *Engineering optimization: An introduction with metaheuristic applications*. John Wiley & Sons.

Zadeh, L. A. (1965). Fuzzy sets. *Information Control 8*, 338–353.

Zadeh, L. A. (1975a). The concept of a linguistic variable and its application to approximate reasoning–I. *Information Sciences 8*(3), 199–249.

Zadeh, L. A. (1975b). The concept of a linguistic variable and its application to approximate reasoning–II. *Information Sciences 8*(4), 301–357.

Zadeh, L. A. (1975c). The concept of a linguistic variable and its application to approximate reasoning–III. *Information Sciences 9*(1), 43–80.

Zadeh, L. A. (1978). Fuzzy sets as a basis for a theory of possibility. *Fuzzy Sets and Systems 1*, 3–28.

Zhang, H. (2005). *Nondeterministic linear static finite element analysis: An interval approach*. Ph.D. diss., Georgia Institute of Technology, School of Civil and Environmental Engineering.

Zhang, Y. and H. Baier (2011). Optimal parts allocation for structural systems via improved initial solution generation. In *VII. ALIO / EURO Workshop on Applied Combinatorial Optimization 2011, Porto, Portugal*.